CONTROL METHODS OF ASYNCHRONOUS INTRAFASCICULAR MULTI-ELECTRODE STIMULATION FOR NEUROMUSCULAR PROSTHESES

by

Mitchell Andrew Frankel

A dissertation submitted to the faculty of
The University of Utah
in partial fulfillment of the requirements for the degree of

Doctor of Philosophy

Department of Mechanical Engineering

The University of Utah

May 2013

The University of Utah Graduate School

STATEMENT OF DISSERTATION APPROVAL

The dissertation of **Mitchell Andrew Frankel**

has been approved by the following supervisory committee members:

Sanford G. Meek	, Chair	**Feb. 25, 2013** Date Approved
Richard A. Normann	, Member	**Feb. 25, 2013** Date Approved
Gregory A. Clark	, Member	**Feb. 25, 2013** Date Approved
V. John Mathews	, Member	**Feb. 25, 2013** Date Approved
Stacy J.M. Bamberg	, Member	**Feb. 25, 2013** Date Approved

and by **Tim Ameel**, Chair of the Department of **Mechanical Engineering**

and by Donna M. White, Interim Dean of The Graduate School.

ABSTRACT

Paralysis due to spinal cord injury or stroke can leave a person with intact peripheral nerves and muscles, but deficient volitional motor control, thereby reducing their health and quality of life. Functional neuromuscular stimulation (FNS) has been widely studied and employed in clinical devices to aid and restore lost or deficient motor function. Strong, selective, and fatigue-resistant muscle forces can be evoked by asynchronously stimulating small independent groups of motor neurons via multiple intrafascicular electrodes on an implanted Utah slanted electrode array (USEA). Determining the parameters of asynchronous intrafascicular multi-electrode stimulation (aIFMS), i.e., the per-electrode stimulus intensities and the interelectrode stimulus phasing, to evoke precise muscle force or joint motion presents unique challenges because this system has multiple-inputs, the n independently stimulated electrodes, but only one measurable output, the evoked endpoint isometric force or joint position. This dissertation presents three studies towards developing robust real-time control of aIFMS.

The first study developed an adaptive feedforward algorithm for selecting aIFMS per-electrode stimulus intensities and interelectrode stimulus phasing to evoke a variety of isometric ankle plantar-flexion force trajectories. In simulation and experiments, desired step, sinusoidal, and more-complex time-varying isometric forces were successfully evoked. The second study developed a closed-loop feedback control method for determining aIFMS per-electrode stimulus intensities to evoke precise single-muscle isometric ankle plantar-flexion force trajectories, in real-time. Using a proportional closed-loop force-feedback controller, desired step, sinusoid, and more complex time-varying forces were evoked with good response characteristics, even in the presence of nonlinear system dynamics, such as muscle fatigue. The third study adapted and extended the closed-loop feedback controller to the more demanding task of controlling joint position in the presence of opposing joint torques. A

proportional-plus-velocity-plus-integral (PIV) joint-angle feedback controller evoked and held desired steps in position with responses that were stable, consistent, and robust to disturbances. The controller evoked smooth ramp-up (concentric) and ramp-down (eccentric) motion, as well as precise slow moving sinusoidal motion.

The control methods developed in this dissertation provide a foundation for new lower-limb FNS-based neuroprostheses that can generate sustained and coordinated muscle forces and joint motions that will be desired by paralyzed individuals on a daily basis.

This dissertation is dedicated to everyone that strives to advance science and engineering for improving the quality of life of every living being.

CONTENTS

LIST OF FIGURES

LIST OF TABLES

ACKNOWLEDGMENTS

An enormous thank you goes to my parents Ken and Candy, and to my sweetheart Cindy, whose generosity, love, and encouragement kept me going through all the difficult days.

I would like to thank my entire Ph.D. committee for their trust, support, and guidance over the many years, in particular, Dr. Richard Normann and Dr. Gregory Clark for creating a diverse laboratory environment that inspires creativity and innovation, and Dr. Sanford Meek and Dr. V. John Mathews for help with the evolution of the controller designs and data analysis methods. I would also like to thank some of the numerous individuals who helped make this research successful: Dr. David Warren, Dr. Brett Dowden, Kiran Mathews, Andrew Wilder, David Hilgart, Dr. Noah Ledbetter, and Heather Wark.

This research was made possible by funding provided by the American taxpayers through the National Institutes of Health grants R01-NS039677 and R01-NS064318-01A1, USAMRMC W81XWH-10-1-0931, the Defense Advanced Research Projects Agency grant N66001-06-C-8005, the National Science Foundation IGERT grant 0654414, and The University of Utah.

CHAPTER 1

INTRODUCTION

Motivation

Our daily lives require us to perform hundreds of routine motions, from getting out of bed in the morning, to drinking a glass of water, to putting on our clothes. These movements are done without large conscious effort, even though they require strong activation and coordination of numerous muscle groups across multiple skeletal joints. These simple movements can become extremely time and energy consuming, or even physically impossible, for persons with motor deficits due to neuromuscular disease or injury, such as those living with paralysis due to a stroke or spinal cord injury (SCI).

In the United States, over 800,000 people suffer a stroke every year [1], and there are over 1.6 million people living with paralysis due to a stroke [2]. The National SCI Statistical Center reports that as of 2012, there are approximately 270,000 people in the United States living with paralysis due to SCI [3], but another report suggests this number to be much higher, over 1.2 million people [2]. Paralysis can cause secondary physical issues, such as pressure sores, bladder and bowel dysfunction, cardiovascular complications, and neurogenic pain, as well as mental health problems, such as depression and loss of self-identity [2, 3, 4, 5, 6, 7]. The life expectancy of a person living with paralysis can be greatly reduced and there are enormous costs associated with caring for these individuals [2, 3]. For many paralyzed individuals, the neuromuscular anatomy remains physically and functionally intact below the injury or insult. Because of this, researchers and clinicians have long investigated the ability to aid and restore the lost motor function by activating paralyzed muscles via stimulation of motor nerves, a field known as Functional Neuromuscular Stimulation (FNS).

Neuromuscular Electrophysiology

FNS relies on the electrochemical nature of the neuromuscular system, which has been studied for centuries [8], and the processes by which thoughts evoke skeletal movements are well understood [8, 9]. Motor commands in the form of neural action potentials are electrically transmitted from the central nervous system, through peripheral nerves, terminating at the neuromuscular junction [9]. The electrical transmission of action potentials occurs along myelinated motor nerve axons as described by the McNeal cable model [10] and the command signal is transmitted across the synapse between nerves via chemical neurotransmitters. Myelination along motor nerves acts as insulation, helping to increase the speed of signal transmission. When the neural action potential reaches the targeted muscle at the neuromuscular junction, the neurotransmitter acetylcholine is released, causing a muscle action potential to spread throughout the muscle fibers connected to the motor end-plate. This muscle action potential leads to muscle cellular changes that allow for ratcheting action between actin and myosin filaments within sarcomeres, causing forceful contraction of the associated muscle fibers [9]. The forceful muscle contractions generate joint torque by pulling the tendons that attach across skeletal joints, in turn creating movement.

The smallest functional grouping within a muscle is known as the motor unit and is comprised of a single alpha-motoneuron and the small group of innervated muscle fibers. Each motor unit within a muscle is activated in an all-or-nothing manner, i.e., all innervated muscle fibers are contracted when an action potential is transmitted to an alpha-motoneuron. More forceful contractions are evoked by higher frequency transmission of action potentials until a saturated state is reached [11], and the amount of force that can be generated by a motor unit is proportional to the size of the innervating alpha-motoneuron axon [12, 13]. Motor units are also distinguished by their type, which can range from slow-fatiguing Type-I, to moderate-fatiguing Type-IIa, to fast-fatiguing Type-IIb units [14]. In normal motor function, muscle forces are achieved by first activating smaller motor units, which are often slow-fatiguing Type-I. If more force is required, the firing rate of the activated units is increased and larger faster-fatiguing units are recruited [13, 15, 16]. This

recruitment order allows for sustained forces, which are necessary for stance and walking, saving the additional fast-fatiguing strength for emergency activities, such as running from predators.

FNS Technology

Researchers have utilized the electrochemical properties of motor nerve signal transmission to develop a variety of FNS methods that can evoke activation of paralyzed muscles. Some nonelectrical methods have been recently investigated, such as magnetic and optical neurostimulation [17, 18], but the majority of research and clinical FNS methods employ electrical stimulation of motor nerves [8, 19, 20]. Electrical FNS devices deliver a charge of current to a targeted efferent nerve fiber that in turn elicits a motor neuron action potential, leading to muscle fiber contraction as described above [21, 22]. There are relatively very short sections along motor nerves that are unmyelinated, known as Nodes of Ranvier [9]. Because Nodes of Ranvier are unmyelinated, they provide the locations for electrical stimulation to depolarize a nerve fiber and evoke a neural action potential. A multitude of motor nerve stimulating electrode technologies have been created and one distinguishing characteristic among them is the surgical invasiveness required, which is directly related to the required stimulation current and the ability to selectively activate individual muscles or independent groups of motor units within a single targeted muscle [19].

Surface Electrodes

Surface electrodes are the least invasive and generally consist of a small (1 cm) metal contact covered by a felt pad. The electrodes are attached to the shaved skin surface over the body of a targeted muscle via nonpermanent adhesive, and electrolytic gels are commonly used to ensure sufficient electrical contact between the skin surface and the electrode. Surface electrodes have been successfully used in clinical FNS devices for hemiplegic foot drop [23], for upper limb neuroprostheses evoking grasp [24], and for lower limb neuroprostheses evoking stance and gait [25]. Although clinically utilized, surface electrodes have a large number of limitations. A

relatively large current is required to evoke muscle activation, approximately 100 mA [26], which often results in ungraded and unselective muscle activation, i.e., the entire muscle is fully activated in an on/off manner, and additional unintended muscles may be activated. Because of this, deep muscles cannot be selectively activated. Rapid muscle fatigue is also common with surface stimulation because the entire muscle is strongly activated at a continuous high stimulation frequency [27]. Surface electrodes are not permanently adhered to the skin and replacement of the electrodes requires recalibration. To improve on these limitations, implantable electrode technologies have been created.

Epimysial and Intramuscular Electrodes

Epimysial and intramuscular electrodes have seen recent success in FNS devices for use in upper limb neuroprostheses evoking reaching and grasping [28, 29], and for use in a stance and gait lower limb neuroprosthesis [30]. Epimysial electrodes consist of a medical grade metallic contact, often made of Platinum, with wire leads encased in silicone, whereas intramuscular electrodes are often a straight or coiled piece of steel or platinum wire with an insulated wire lead [19]. Epimysial electrodes are sutured to the external fascia surrounding a muscle, often near the motor point of the muscle. This motor point is commonly found as the location that requires the least amount of stimulation current to evoke targeted muscle activation [19]. Intramuscular electrodes are placed deep inside the muscle body and are held in place by creating a hook at the end of the wire that attaches to muscle fibers when implanted. Stimulation current requirements for these electrodes, approximately 20 mA, are substantially less than what is required for surface electrode stimulation [30]. Although clinically utilized, there are considerable limitations to these electrodes. Though rare, intramuscular electrode tips can be broken or moved during strong muscle contractions [19]. Surgical placement of epimysial electrodes can be difficult and time consuming because the final position is empirically determined during placement. FNS devices using these electrodes are able to selectively activate largely separated targeted muscles. However, the electrode placements are still relatively far from the nerve that they innervate, which can lead to activation of unintended

muscles, especially in muscle compartments that have many small muscles in close proximity, such as the forearm. Also, because of the distance from electrode to nerve, the required currents are still relatively large, which can cause pain or tissue damage [31].

Peripheral Neural Interfaces

To reduce the stimulation current requirements, increase activated muscle selectivity, and increase the gradation of evoked forces, electrodes have been developed that make direct contact with peripheral neural tissue.

Peripheral Nerve Fascicular Organization

Large nerves that exit from the spinal column contain bundles of motor and sensory nerve axons that are grouped within structures known as fascicles. The nerves are surrounded by a connective tissue casing called the epineurium and individual fascicles are contained within a perineurium connective tissue, as shown in Fig. 1.1. These larger nerve bundles continually branch into smaller nerve bundles as they move distally toward their targeted skeletal muscles. Research has shown that motor nerve axons within proximal nerve bundles are fascicularly organized by the muscles that they innervate, e.g., the motor axons that activate muscles of the knee (rectus femoris, vastus lateralis, vastus intermedius, sartorius, etc.) are contained within individual or small groups of fascicles, even in very proximal nerve bundles, as shown in Fig. 1.2 [32]. In feline studies, muscles of the calf have also been shown to be fascicularly organized in nerve branches as high as the main sciatic nerve [33].

Because of the fascicular organization of motor axons, peripheral nerve electrode architectures have been developed that place the stimulating contact near or within targeted fascicles, allowing stimulation to selectively activate individual muscles and even grade the level of individual muscle activation [19], though very invasive surgery is required to implant these devices. There are a wide variety of peripheral nerve electrodes and these can be separated into two categories: extraneural electrodes where the electrode contact resides on the epineurium of the nerve, and intrafascicular electrodes where the electrode contact penetrates the epineurium and fascicle perineurium, and resides near motor axons within a fascicle.

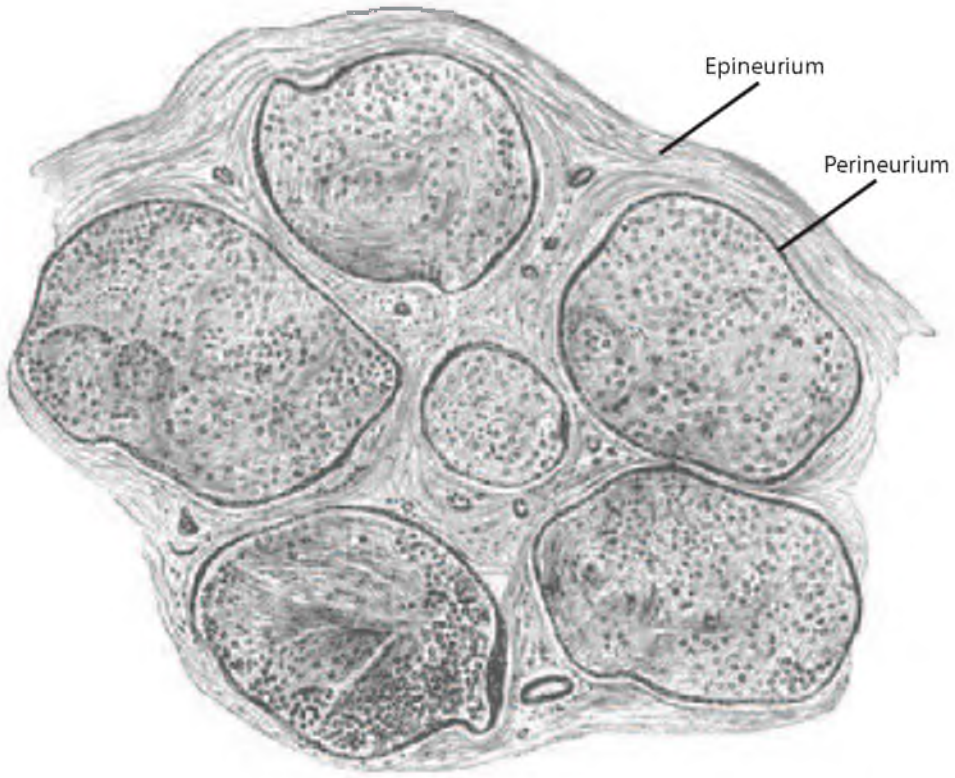

Figure 1.1: Cross Section of Peripheral Nerve.

Peripheral nerve cross section showing the epineurium surrounding the entire nerve bundle, the perineurium surrounding individual fascicles, and individual nerve axons within the fascicles (not labeled, but shown within the fascicles by the small dark circles that are the myelin sheath surrounding motor nerve axons) [34], public domain.

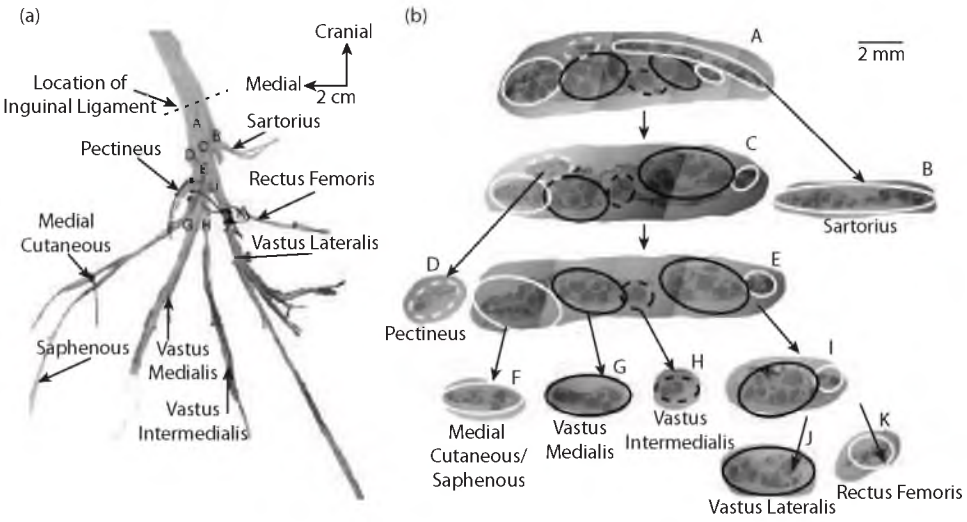

Figure 1.2: Fascicular Organization of the Human Femoral Nerve.

(a) Harvested (Femoral) nerve and (b) complete fascicle map of femoral nerve. The distal nerve branches of the femoral nerve were traced proximally to the compound femoral nerve. Nerve cross sections are shown ventral side up. A = nerve just proximal to branching, B = nerve branch to sartorius muscle, C = nerve just distal to sartorius nerve branching and just proximal to pectineus nerve branching, D = nerve branch to pectineus muscle, E = nerve just distal to pectineus nerve branching and just proximal to medial cutaneous/saphenous nerve branching, F = nerve to medial cutaneous and saphenous nerves, G = nerve branch to vastus medialis muscle, H = nerve branch to vastus intermedius muscle, I = nerve to vastus lateralis and rectus femoris muscles, J = nerve branch to vastus lateralis muscle, K = nerve branch to rectus femoris muscle [32], ©2009 JRRD.

Extraneural Electrodes

Extraneural electrodes can be as simple as two platinum wires sutured to the epineurium, but the most commonly used extraneural electrodes come in the form of a cuff of insulating material encircling the nerve, containing two or more exposed metallic contacts on the inner cuff surface [19]. Cuff electrodes require stimulation currents of approximately 500 µA [35, 36], and multicontact spiral cuffs have been used in recent clinical studies as an FNS neural interface for evoking stance in paralyzed individuals [37]. Selective activation of knee muscles was made possible because the multiple stimulation contact points within the cuff were spread around the entire nerve. One of the limitations of standard cuff electrodes is that stimulation of deeper fascicles within larger proximal nerves requires increased stimulation currents, which can reduce the selectivity of muscle activation [19]. To improve this, a recent variation of the cuff electrode has been designed that flattens the nerve within the cuff, altering the shape of fascicles to be more elliptical in shape and more spread out within the flattened nerve. This electrode design is known as the flat interface nerve electrode, or FINE [38], and it has been used to achieve graded and selective activation of knee extensors in a recent clinical study [39]. Although selectivity is improved with extraneural electrodes, selective activation of small groups of motor axons deep within a fascicle is not possible without also activating the more superficial motor axons, something that will be required of clinical FNS-based neuroprostheses because natural movements require coordinated and selective activation of hundreds of motor units within individual muscles.

Intrafascicular Electrodes

Intrafascicular electrodes and electrode arrays have been investigated as FNS delivery devices that can achieve improved selectivity and graded activation of small groups of motor units within individual targeted muscles [19]. Because these neural interfaces are intrafascicularly implanted, it is possible to place the stimulation contact closer to motor axon Nodes of Ranvier, which can decrease the required stimulation currents to approximately 10-100 µA [40]. The simplest of these electrodes is the longitudinal intrafascicular electrode, or LIFE, which contains a single

platinum-iridium wire that can be threaded and secured intrafascicularly [41]. LIFEs have been shown to evoke very selective and graded activation of small, independent groups of motor units within a single muscle [40]. A number of LIFE variations have been created to improve manufacturing and performance [19], and although LIFEs have yet to be clinically used in an FNS device for motor function, they have been clinically tested as a peripheral nerve interface to restore tactile and proprioceptive sensory information from artificial limbs worn by amputees, by stimulating sensory afferent nerve fibers [42]. The biggest limitations of LIFEs is the requirement of multiple electrodes to activate multiple muscles or motor unit groups and it can be difficult to surgically implant and secure these electrodes [19].

Arrays of intrafascicular electrodes have been developed that seek to provide activation of larger numbers of small independent groups of motor units, which would enable very selective and finely graded muscle activation. These microelectrode arrays (MEAs) have yet to be clinically used in FNS devices for restoration of motor function, but they have seen very successful clinical utility when used for recording of motor intent from the motor cortex of fully paralyzed individuals [43]. The motor intent is then decoded in real-time and used to control a cursor on a screen or even control a robotic arm, as has been accomplished very recently, allowing one quadriplegic individual the ability to feed herself [44].

The transverse intrafascicular multielectrode, or TIME, is similar in design to LIFEs, but has multiple electrical contacts that can activate independent groups of motor units when the TIME is implanted transversely through a peripheral nerve [45]. Researchers at multiple universities, in particular the University of Michigan, have been designing and testing flat flexible spear-like microprobes that can contain large numbers of electrode contacts [46]. These arrays have been tested for use in spinal cord stimulation but have not been fully tested as a peripheral nerve interface [19, 46, 47]. The Utah Electrode Array (UEA) is a slightly different MEA design that uses a grid of individual penetrating microelectrodes [48]. The original UEA was designed for intracortical recording and stimulation [49] where it has seen clinical success [43, 44], but a more recent version has been revised for use in the peripheral nerve of felines [50].

The Utah Slanted Electrode Array (USEA), shown in Fig. 1.3, is a 4x4 mm square grid of 100 silicon-based microelectrodes that have penetrating depths of 0.5-1.5 mm, with each electrode spaced 400 microns apart. Because of the lateral and axial spacing of the electrode, along with the varying depths of penetration, the USEA can be used as an FNS interface to independently activate very small groups of motor units in multiple fascicles throughout the entire nerve, as schematically shown in Fig. 1.4 [50]. Selective activation of multiple muscle groups, as well as multiple independent groups of motor units within a single muscle, was achieved with a single USEA implant in the main sciatic nerve of a feline [50], and long-term chronic stimulation has been possible [51, 52]. The gradation of single muscle force was shown to be improved over cuff electrodes when using stimulation via a USEA, i.e., the dynamic range of force-evoking stimulation was increased [50]. By having effective selective and graded access to a large number of skeletal muscles, including unique subsets of motor units within each muscle, researchers are hoping to now be able to evoke more coordinated and long-lasting motion in paralyzed individuals, but this requires investigation of stimulation paradigms and their associated control before intrafascicular multi-electrode stimulation (IFMS) can be used in a clinically viable FNS neuroprosthesis.

Stimulation Paradigms

Use of lower amplitude biphasic current stimulation via intrafascicular electrodes allows for safer neural stimulation due to the reduced stimulation currents required [21, 40, 50]. However, electrical stimulation of a motor nerve activates motor units in a manner that is inverse to the natural recruitment of motor fibers, i.e., larger fast-fatiguing Type-II motor units are activated first and slower-fatiguing Type-I motor units are recruited as the stimulation level is increased. This is because the larger Type-II motor axons have Nodes of Ranvier that are spaced farther apart, which creates a larger electrical gradient along the axon, in turn allowing for lower action potential evoking stimulation thresholds [53]. Electrical activation of Type-II motor units results in a 'twitch' response in muscle force that is substantially faster in kinetics than the slower Type-I motor units [54]. Because the twitch-response

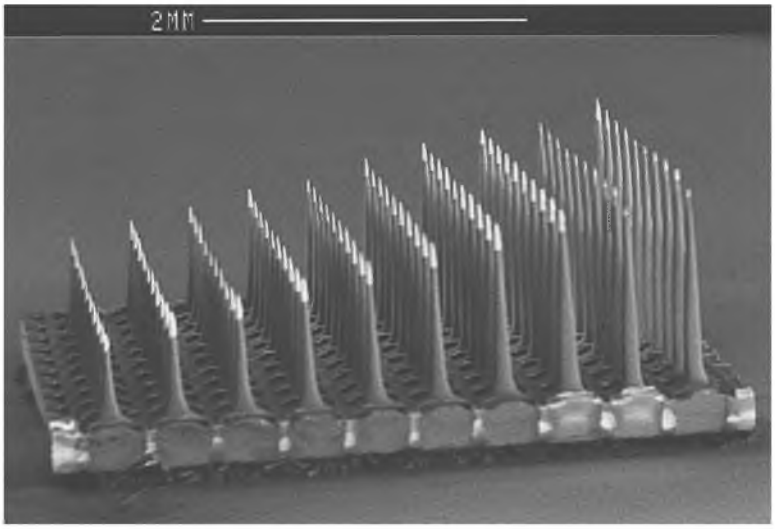

Figure 1.3: Scanning Electron Microscope Picture of a USEA.

The USEA is a 4x4 mm square grid of 100 microelectrodes with penetrating depths of 0.5-1.5mm [50], ©2011 JNP.

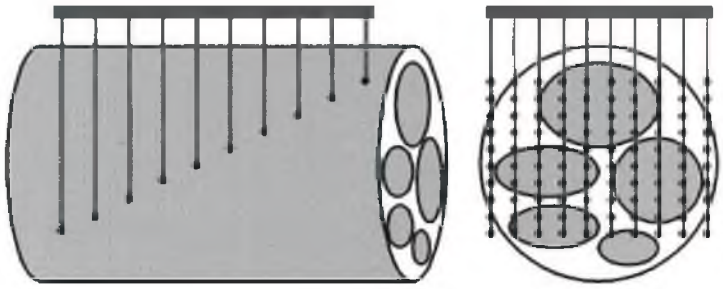

Figure 1.4: Schematic of Fascicular Depth and Cross-Sectional Coverage of the USEA.

The 400-micron lateral and axial spacing of the electrodes, along with varying penetration depths, allows stimulation via the USEA to activate small groups of independent motor units within multiple fascicles throughout the entire peripheral nerve [50], ©2011 JNP.

kinetics of Type-II motor units are faster (they are often called fast-twitch motor units), relatively high-frequency stimulation is required to achieve a fused tetanic muscle force output, which leads to rapid muscle fiber fatigue and the inability to sustain strong muscle forces [53].

Researchers have investigated a variety of stimulation paradigms to reduce the level of fatigue associated with FNS, including changing the shape of the commonly used biphasic square pulse stimulation waveform [55]. Other methods have tried to be more biomimetic to normal neuromuscular physiology by stimulating independent groups of motor units via multiple stimulating electrodes in an asynchronous manner [56, 57, 58, 59, 60]. In these studies, fused tetanic forces were achieved by using a relatively high composite stimulation frequency but a low per-electrode stimulation frequency that proved to be fatigue-resistant. The researchers in [56] were able to show a significant decrease in associated fatigue when using asynchronous IFMS (aIFMS), while still being able to evoke forceful tetanic muscle contractions, using a USEA implanted in the sciatic nerve of feline. One of the few remaining obstacles for an aIFMS neuroprosthesis is the need for control methods to evoke precise muscle forces and joint movements that are necessary for coordinated motion.

FNS Control Methods

Numerous open-loop and closed-loop control methods have been developed for FNS. Predictive feedforward controllers rely on having a good model of the system dynamics. For isometric force control, where the muscle does not change length, a relationship between the stimulation intensity and muscle force output can be determined, commonly known as the recruitment curve [61]. However, the nonisometric force generation during motion has muscle fiber length and velocity dependencies [62]. A variety of static and dynamic models have been created to understand the relationship between electrical stimulation parameters, i.e., the stimulus intensity and rate, and the muscle force or joint torque output [63, 64, 65, 66, 67, 68]. Open-loop [69], adaptive feedback [70], and nonlinear [71] FNS controllers have been designed around these models. Other closed-loop methods using classical, adaptive, optimal, and nonlinear controllers have been designed that use muscle force, joint torque, or

even muscle-spindle activity as feedback to alter the stimulation intensity of FNS [72, 73, 74, 75, 76, 77, 78].

These control methods have been clinically tested and show promise for FNS, but they have limitations in their present form for use with more advanced FNS methods, such as fatigue-resistant aIFMS. With regards to model-based controllers, there are many unmodeled, time-varying, nonlinear system dynamics involved with FNS that are poorly modeled, such as motor unit potentiation [79], muscle fiber fatigue [80], as well as the nonlinear summation of muscle contractions and axonal activation overlap associated with IFMS [81, 50]. All of the current open-loop and closed-loop FNS control methods were developed for single electrode activation of individual muscles, and they do not adapt well to the multiple-input system of aIFMS, where there are multiple stimulating electrodes that evoke forces in a single muscle. It is from this starting point that the research presented herein aimed to design and evaluate novel aIFMS control methods that could be used as a foundation for the next generation of FNS-based neuroprostheses that may be able to evoke coordinated and fatigue-resistant motion in paralyzed individuals.

Research Outline

The focus of this dissertation was the design and experimental evaluation of feedforward and feedback control strategies for determining the parameters of aIFMS, i.e., the per-electrode stimulus intensities and the interelectrode stimulus phasing, to evoke precise fatigue-resistant isometric muscle forces and dynamic joint motions. This was achieved using aIFMS, via a USEA that was implanted either acutely or chronically in the sciatic nerve of an anesthetized feline, and evoking physiologically relevant forces [82] in fast-twitch ankle plantar-flexion muscles.

Model-Based Feedforward Isometric Force Control

The research presented in Chapter 2 discusses the development and evaluation of an adaptive feedforward algorithm for selecting aIFMS per-electrode stimulus intensities and interelectrode stimulus phasing to evoke a variety of time-varying isometric ankle plantar-flexion force trajectories. The algorithm employed a linear model of aIFMS evoked forces and a gradient descent approach for updating the

stimulation parameters. In simulation and experiments, desired step, sinusoidal, and more complex time-varying isometric plantar-flexion forces were successfully evoked for short stimulation periods. The results of this work were published as a conference paper in the *Proceedings of the 2012 IEEE International Conference on Acoustics, Speech and Signal Processing.*

Closed-loop Control of Isometric Forces Using Force Feedback

The research presented in Chapter 3 develops a closed-loop feedback control method for determining aIFMS per-electrode stimulus intensities to evoke precise single-muscle isometric ankle plantar-flexion force trajectories, in real-time. Using a proportional closed-loop force-feedback controller, desired step, sinusoid, and more-complex time-varying isometric plantar-flexion forces were evoked over stimulation periods up to seven minutes with good response characteristics, even in presence of muscle potentiation and fatigue. The results of this study were published as a journal article in the *IEEE Transactions on Neural Systems and Rehabilitation Engineering.*

Closed-loop Control of Limb Motion Using Joint Angle Feedback

The research presented in Chapter 4 adapts and extends the closed-loop feedback controller from Chapter 3 to the more demanding task of controlling joint position in the presence of opposing joint torques. Generating joint motion requires evoking nonisometric muscle force, which is additionally complicated by nonlinear dependencies of muscle force on muscle length and velocity. A proportional-plus-velocity-plus-integral (PIV) joint-angle feedback controller with integrator antiwindup was created to determine the per-electrode stimulus intensities of aIFMS in real-time, to evoke precise joint motion. The closed-loop controller evoked and held desired steps in position with good response characteristics that were robust to changes in loading torque, stable against an externally applied torque, and consistent during an experimental session and over experimental days. The controller evoked smooth ramp-up (concentric) and ramp-down (eccentric) motion, as well as precise slow moving sinusoidal motion. This research is currently in submission as a journal article to the *IEEE Transactions on Biomedical Engineering.*

References

[1] A. S. Go, D. Mozaffarian, V. L. Roger, E. J. Benjamin, J. D. Berry, W. B. Borden, D. M. Bravata, S. Dai, E. S. Ford, C. S. Fox, S. Franco, H. J. Fullerton, C. Gillespie, S. M. Hailpern, J. A. Heit, V. J. Howard, M. D. Huffman, B. M. Kissela, S. J. Kittner, D. T. Lackland, J. H. Lichtman, L. D. Lisabeth, D. Magid, G. M. Marcus, A. Marelli, D. B. Matchar, D. K. McGuire, E. R. Mohler, C. S. Moy, M. E. Mussolino, G. Nichol, N. P. Paynter, P. J. Schreiner, P. D. Sorlie, J. Stein, T. N. Turan, S. S. Virani, N. D. Wong, D. Woo, and M. B. Turner, "Heart disease and stroke statistics, 2013 update: A report from the american heart association," *Circulation*, vol. 127, no. 1, pp. e6–e245, 2013.

[2] "One degree of separation: Paralysis and spinal cord injury in the united states," Christopher and Dana Reeve Foundation Paralysis Task Force, Tech. Rep., 2009.

[3] "Spinal cord injury facts and figures at a glance," National Spinal Cord Injury Statistical Center, Tech. Rep., 2012.

[4] J. Kemp and J. S. K. Bryan, "Depression and life satisfaction among people ageing with post-polio and spinal cord injury," *Disability and Rehabilitation*, vol. 21, no. 5-6, pp. 241–249, Jan. 1999.

[5] L. Weaver and C. Pohsa, "The clinical problems in cardiovascular control following spinal cord injury: an overview," *Autonomic Dysfunction After Spinal Cord Injury*, vol. 152, p. 223, 2005.

[6] J. S. Walter, J. Sacks, R. Othman, A. Z. Rankin, B. Nemchausky, R. Chintam, and J. S. Wheeler, "A database of self-reported secondary medical problems among va spinal cord injury patients: its role in clinical care and management," *Journal of Rehabilitation Research and Development*, vol. 39, no. 1, pp. 53–62, 2002.

[7] N. Westgren and R. Levi, "Quality of life and traumatic spinal cord injury," *Archives of Physical Medicine and Rehabilitation*, vol. 79, no. 11, pp. 1433–1439, 1998.

[8] D. Prodanov, E. Marani, and J. Holsheimer, "Functional electrical stimulation for sensory and motor functions: Progress and problems," *Biomedical Reviews*, vol. 14, pp. 23–50, 2003.

[9] E. R. Kandel, J. H. Schwartz, and T. M. Jessell, *Principles of Neural Science*, 4th ed. McGraw-Hill New York, 2000.

[10] D. R. McNeal, "Analysis of a model for excitation of myelinated nerve," *IEEE Transactions on Biomedical Engineering*, vol. BME-23, no. 4, pp. 329–337, 1976.

[11] G. R. Mines, "On the summation of contractions," *The Journal of Physiology*, vol. 46, no. 1, pp. 1–27, 1913.

[12] R. B. Wuerker, A. M. McPhedran, and E. Henneman, "Properties of motor units in a heterogeneous pale muscle (m. gastrocnemius) of the cat," *Journal of Neurophysiology*, vol. 28, no. 1, pp. 85–99, 1965.

[13] E. Henneman and L. M. Mendell, "Functional organization of motoneuron pool and its inputs," *Comprehensive Physiology*, Jan. 2011.

[14] R. E. Burke, D. N. Levine, I. Zajac, F. E., P. Tsairis, and W. K. Engel, "Mammalian motor units: Physiological-histochemical correlation in three types in cat gastrocnemius," *Science*, vol. 174, no. 4010, pp. 709–712, 1971.

[15] E. Henneman, G. Somjen, and D. O. Carpenter, "Functional significance of cell size in spinal motoneurons," *Journal of Neurophysiology*, vol. 28, no. 3, pp. 560–580, 1965.

[16] A. W. Monster and H. Chan, "Isometric force production by motor units of extensor digitorum communis muscle in man," *Journal of Neurophysiology*, vol. 40, no. 6, pp. 1432–1443, Nov. 1977.

[17] M. Polson, A. Barker, and I. Freeston, "Stimulation of nerve trunks with time-varying magnetic fields," *Medical and Biological Engineering and Computing*, vol. 20, no. 2, pp. 243–244, 1982.

[18] G. A. Clark, S. L. Schister, N. M. Ledbetter, D. J. Warren, F. Solzbacher, J. D. Wells, M. D. Keller, S. M. Blair, L. W. Rieth, and P. R. Tathireddy, "Selective, high-optrode-count, artifact-free stimulation with infrared light via intrafascicular utah slanted optrode arrays," *Proceedings of SPIE 8207 - Photonic Therapeutics and Diagnostics VIII*, p. 82075I, 2012.

[19] X. Navarro, T. B. Krueger, N. Lago, S. Micera, T. Stieglitz, and P. Dario, "A critical review of interfaces with the peripheral nervous system for the control of neuroprostheses and hybrid bionic systems," *Journal of the Peripheral Nervous System*, vol. 10, no. 3, pp. 229–258, Sep. 2005.

[20] P. H. Peckham and J. S. Knutson, "Functional electrical stimulation for neuromuscular applications," *Annual Review of Biomedical Engineering*, vol. 7, pp. 327–360, Aug. 2005.

[21] D. R. Merrill, M. Bikson, and J. G. R. Jefferys, "Electrical stimulation of excitable tissue: design of efficacious and safe protocols," *Journal of Neuroscience Methods*, vol. 141, no. 2, pp. 171–198, 2005.

[22] B. J. Roth, "Mechanisms for electrical stimulation of excitable tissue," *Critical Reviews in Biomedical Engineering*, vol. 22, no. 3-4, pp. 253–305, 1994.

[23] R. B. Stein, D. G. Everaert, A. K. Thompson, S. L. Chong, M. Whittaker, J. Robertson, and G. Kuether, "Long-term therapeutic and orthotic effects of a foot drop stimulator on walking performance in progressive and nonprogressive neurological disorders," *Neurorehabilitation and Neural Repair*, vol. 24, no. 2, pp. 152–167, 2010.

[24] D. Popovic, A. Stojanovic, A. Pjanovic, S. Radosavljevic, M. Popovic, S. Jovic, and D. Vulovic, "Clinical evaluation of the bionic glove," *Archives of Physical Medicine and Rehabilitation*, vol. 80, no. 3, pp. 299–304, 1999.

[25] K. J. Klose, P. L. Jacobs, J. G. Broton, R. S. Guest, B. M. Needham-Shropshire, N. Lebwohl, M. S. Nash, and B. A. Green, "Evaluation of a training program for persons with sci paraplegia using the parastep1 ambulation system: Part 1. ambulation performance and anthropometric measures," *Archives of Physical Medicine and Rehabilitation*, vol. 78, no. 8, pp. 789–793, 1997.

[26] M. R. Popovic, T. Keller, I. P. I. Pappas, V. Dietz, and M. Morari, "Surface-stimulation technology for grasping and walking neuroprosthesis," *IEEE Engineering in Medicine and Biology Magazine*, vol. 20, no. 1, pp. 82–93, Jan.-Feb. 2001.

[27] J. T. Mortimer, "Motor prostheses," *Comprehensive Physiology*, pp. 155–187, 1981.

[28] S. Carroll, C. Cooper, D. Brown, G. Sormann, S. Flood, and M. Denison, "Australian experience with the freehand system for restoring grasp in quadriplegia," *The Australian and New Zealand Journal of Surgery*, vol. 70, no. 8, p. 563, 2000.

[29] K. L. Kilgore, H. A. Hoyen, A. M. Bryden, R. L. Hart, M. W. Keith, and P. H. Peckham, "An implanted upper-extremity neuroprosthesis using myoelectric control," *The Journal of Hand Surgery*, vol. 33, no. 4, p. 539, 2008.

[30] R. Kobetic, R. J. Triolo, J. P. Uhlir, C. Bieri, M. Wibowo, G. Polando, E. B. Marsolais, J. Davis, J. A., K. A. Ferguson, and M. Sharma, "Implanted functional electrical stimulation system for mobility in paraplegia: a follow-up case report," *EEE Transactions on Rehabilitation Engineering*, vol. 7, no. 4, pp. 390–398, 1999.

[31] J. Chae and R. Hart, "Comparison of discomfort associated with surface and percutaneous intramuscular electrical stimulation for persons with chronic hemiplegia1," *American Journal of Physical Medicine and Rehabilitation*, vol. 77, no. 6, 1998.

[32] K. J. Gustafson, G. C. J. Pinault, J. J. Neville, I. Syed, J. A. Davis Jr, J. Jean-Claude, and R. J. Triolo, "Fascicular anatomy of human femoral nerve: implications for neural prostheses using nerve cuff electrodes," *Journal of Rehabilitation Research and Development*, vol. 46, no. 7, p. 973, 2009.

[33] W. M. Grill and J. T. Mortimer, "Quantification of recruitment properties of multiple contact cuff electrodes," *IEEE Transactions on Rehabilitation Engineering*, vol. 4, no. 2, pp. 49–62, 1996.

[34] H. Gray, *Anatomy of the human body.* Philadelphia, PA: Lea & Febiger, 1918.

[35] G. E. Loeb and R. A. Peck, "Cuff electrodes for chronic stimulation and recording of peripheral nerve activity," *Journal of Neuroscience Methods*, vol. 64, no. 1, pp. 95–103, 1996.

[36] J. D. Sweeney, D. A. Ksienski, and J. T. Mortimer, "A nerve cuff technique for selective excitation of peripheral nerve trunk regions," *IEEE Transactions on Biomedical Engineering*, vol. 37, no. 7, pp. 706–715, 1990.

[37] L. E. Fisher, M. E. Miller, S. N. Bailey, J. A. Davis, J. S. Anderson, L. Rhode, D. J. Tyler, and R. J. Triolo, "Standing after spinal cord injury with four-contact nerve-cuff electrodes for quadriceps stimulation," *IEEE Transactions on Neural Systems and Rehabilitation Engineering*, vol. 16, no. 5, pp. 473–478, 2008.

[38] D. J. Tyler and D. M. Durand, "Functionally selective peripheral nerve stimulation with a flat interface nerve electrode," *IEEE Transactions on Neural Systems and Rehabilitation Engineering*, vol. 10, no. 4, pp. 294–303, 2002.

[39] M. A. Schiefer, K. H. Polasek, R. J. Triolo, G. C. J. Pinault, and D. J. Tyler, "Selective stimulation of the human femoral nerve with a flat interface nerve electrode," *Journal of Neural Engineering*, vol. 7, no. 2, p. 026006, 2010.

[40] K. Yoshida and K. Horch, "Reduced fatigue in electrically stimulated muscle using dual channel intrafascicular electrodes with interleaved stimulation," *Annual Review of Biomedical Engineering*, vol. 21, pp. 709–714, Nov. 1993.

[41] N. Nannini and K. Horch, "Muscle recruitment with intrafascicular electrodes," *IEEE Transactions on Biomedical Engineering*, vol. 38, no. 8, pp. 769–776, 1991.

[42] K. Horch, S. Meek, T. G. Taylor, and D. T. Hutchinson, "Object discrimination with an artificial hand using electrical stimulation of peripheral tactile and proprioceptive pathways with intrafascicular electrodes," *IEEE Transactions on Neural Systems and Rehabilitation Engineering*, vol. 19, no. 5, pp. 483–489, 2011.

[43] L. R. Hochberg, M. D. Serruya, G. M. Friehs, J. A. Mukand, M. Saleh, A. H. Caplan, A. Branner, D. Chen, R. D. Penn, and J. P. Donoghue, "Neuronal ensemble control of prosthetic devices by a human with tetraplegia," *Nature*, vol. 442, no. 7099, pp. 164–171, Jul. 2006.

[44] J. L. Collinger, B. Wodlinger, J. E. Downey, W. Wang, E. C. Tyler-Kabara, D. J. Weber, A. J. C. McMorland, M. Velliste, M. L. Boninger, and A. B. Schwartz, "High-performance neuroprosthetic control by an individual with tetraplegia," *The Lancet*, 2012.

[45] B. Jordi, B. Tim, A. David, A.-C. Christine, S. Thomas, and N. Xavier, "Comparative analysis of transverse intrafascicular multichannel, longitudinal intrafascicular and multipolar cuff electrodes for the selective stimulation of nerve fascicles," *Journal of Neural Engineering*, vol. 8, no. 3, p. 036023, 2011.

[46] D. C. Rodger, A. J. Fong, W. Li, H. Ameri, A. K. Ahuja, C. Gutierrez, I. Lavrov, H. Zhong, P. R. Menon, E. Meng, J. W. Burdick, R. R. Roy, V. R. Edgerton, J. D. Weiland, M. S. Humayun, and Y.-C. Tai, "Flexible parylene-based multielectrode array technology for high-density neural stimulation and recording," *Sensors and Actuators B: Chemical*, vol. 132, no. 2, pp. 449–460, 2008.

[47] D. R. Kipke, W. Shain, G. Buzski, E. Fetz, J. M. Henderson, J. F. Hetke, and G. Schalk, "Advanced neurotechnologies for chronic neural interfaces: new horizons and clinical opportunities," *The Journal of Neuroscience*, vol. 28, no. 46, pp. 11 830–11 838, 2008.

[48] P. K. Campbell, K. E. Jones, R. J. Huber, K. W. Horch, and R. A. Normann, "A silicon-based, three-dimensional neural interface: manufacturing processes for an intracortical electrode array," *IEEE Transactions on Biomedical Engineering*, vol. 38, no. 8, pp. 758–768, 1991.

[49] P. K. Campbell, R. A. Normann, K. W. Horch, and S. S. Stensaas, "A chronic intracortical electrode array: preliminary results," *Journal of Biomedical Materials Research*, vol. 23, no. A2, pp. 245–259, 1989.

[50] A. Branner, R. B. Stein, and R. A. Normann, "Selective stimulation of cat sciatic nerve using an array of varying-length microelectrodes," *Journal of Neurophysiology*, vol. 85, no. 4, pp. 1585–1594, Apr. 2001.

[51] A. Branner, R. B. Stein, E. Fernandez, Y. Aoyagi, and R. A. Normann, "Long-term stimulation and recording with a penetrating microelectrode array in cat sciatic nerve," *IEEE Transactions on Biomedical Engineering*, vol. 51, no. 1, pp. 146–157, Jan. 2004.

[52] R. A. Normann, D. McDonnall, G. A. Clark, R. B. Stein, and A. Branner, "Physiological activation of the hind limb muscles of the anesthetized cat using the utah slanted electrode array," *Proceedings of the 2005 IEEE IJCNN*, vol. 5, pp. 3101–3108, Aug. 2005.

[53] N. Bhadra and P. H. Peckham, "Peripheral nerve stimulation for restoration of motor function," *Journal of Clinical Neurophysiology*, vol. 14, no. 5, 1997.

[54] A. J. Buller, J. C. Eccles, and R. M. Eccles, "Interactions between motoneurones and muscles in respect of the characteristic speeds of their responses," *The Journal of Physiology*, vol. 150, no. 2, p. 417, 1960.

[55] Z. P. Fang and J. T. Mortimer, "A method to effect physiological recruitment order in electrically activated muscle," *IEEE Transactions on Biomedical Engineering*, vol. 38, no. 2, pp. 175–179, 1991.

[56] D. McDonnall, G. Clark, and R. A. Normann, "Interleaved, multisite electrical stimulation of cat sciatic nerve produces fatigue-resistant, ripple-free motor responses," *IEEE Transactions on Neural Systems and Rehabilitation Engineering*, vol. 12, no. 2, pp. 208–215, Jun. 2004.

[57] P. M. H. Rack and D. R. Westbury, "The effect of length and stimulus rate on tension in the isometric cat soleus muscle," *The Journal of Physiology*, vol. 204, no. 2, pp. 443–460, Oct. 1969.

[58] A. K. Wise, D. L. Morgan, J. E. Gregory, and U. Proske, "Fatigue in mammalian skeletal muscle stimulated under computer control," *Journal of Applied Physiology*, vol. 90, no. 1, pp. 189–197, Jan. 2001.

[59] K. Yoshida and K. Horch, "Selective stimulation of peripheral nerve fibers using dual intrafascicular electrodes," *IEEE Transactions on Biomedical Engineering*, vol. 40, no. 5, pp. 492–494, w 1993.

[60] T. I. H. Brown, Y. Huang, D. L. Morgan, U. Proske, and A. Wise, "A new strategy for controlling the level of activation in artificially stimulated muscle," *IEEE Transactions on Rehabilitation Engineering*, vol. 7, no. 2, pp. 167–173, 1999.

[61] P. E. Crago, P. H. Peckham, and G. B. Thorpe, "Modulation of muscle force by recruitment during intramuscular stimulation," *IEEE Transactions on Biomedical Engineering*, vol. 27, no. 12, pp. 679–684, Dec. 1980.

[62] W. K. Durfee and K. I. Palmer, "Estimation of force-activation, force-length, and force-velocity properties in isolated, electrically stimulated muscle," *IEEE Transactions on Biomedical Engineering*, vol. 41, no. 3, pp. 205–216, Mar. 1994.

[63] L. A. Bernotas, P. E. Crago, and H. J. Chizeck, "A discrete-time model of electrically stimulated muscle," *IEEE Transactions on Biomedical Engineering*, vol. 33, no. 9, pp. 829–838, Sep. 1986.

[64] J. Bobet, R. B. Stein, and M. N. Oguztoreli, "A linear time-varying model of force generation in skeletal muscle," *IEEE Transactions on Biomedical Engineering*, vol. 40, no. 10, pp. 1000–1006, Oct. 1993.

[65] M. Ferrarin and A. Pedotti, "The relationship between electrical stimulus and joint torque: a dynamic model," *IEEE Transactions on Rehabilitation Engineering*, vol. 8, no. 3, pp. 342–352, Sep. 2000.

[66] H. Gollee, D. Murray-Smith, and J. Jarvis, "A nonlinear approach to modeling of electrically stimulated skeletal muscle," *IEEE Transactions on Biomedical Engineering*, vol. 48, no. 4, pp. 405–415, Apr. 2001.

[67] R. Riener, J. Quintern, and G. Schmidt, "Biomechanical model of the human knee evaluated by neuromuscular stimulation," *Journal of Biomechanics*, vol. 29, no. 9, pp. 1157–1167, Sep. 1996.

[68] H. S. Gasser and A. V. Hill, "The dynamics of muscular contraction," *Proceedings of the Royal Society of London. Series B, Containing Papers of a Biological Character*, vol. 96, no. 678, pp. 398–437, Aug. 1924.

[69] J. M. Hausdorff and W. K. Durfee, "Open-loop position control of the knee joint using electrical stimulation of the quadriceps and hamstrings," *Medical and Biological Engineering and Computing*, vol. 29, no. 3, pp. 269–280, May 1991.

[70] L. A. Bernotas, P. E. Crago, and H. J. Chizeck, "Adaptive control of electrically stimulated muscle," *IEEE Transactions on Biomedical Engineering*, vol. 34, no. 2, pp. 140–147, Feb. 1987.

[71] T. Schauer, O. Negard, F. Previdi, K. J. Hunt, M. H. Fraser, E. Ferchland, and J. Raisch, "Online identification and nonlinear control of the electrically stimulated quadriceps muscle," *Control Engineering Practice*, vol. 13, pp. 1207–1219, Sep. 2005.

[72] H. J. Chizeck, P. E. Crago, and L. S. Kofman, "Robust closed-loop control of isometric muscle force using pulsewidth modulation," *IEEE Transactions on Biomedical Engineering*, vol. 35, no. 7, pp. 510–517, Jul. 1988.

[73] S. Jezernik, R. G. V. Wassinik, and T. Keller, "Sliding mode closed-loop control of fes: controlling the shank movement," *IEEE Transactions on Biomedical Engineering*, vol. 51, no. 2, pp. 263–272, Feb. 2004.

[74] B. Lau, L. Guevremont, and V. Muschawar, "Strategies for generating prolonged functional standing using intramuscular or intraspinal microstimulation," *IEEE Transactions on Neural Systems and Rehabilitation Engineering*, vol. 15, no. 2, pp. 273–285, Jun. 2007.

[75] V. Nekoukar and A. Erfanian, "Adaptive terminal sliding mode control of ankle movement using functional electrical stimulation of agonist-antagonist muscles," *Proceedings of IEEE EMBS 2010, Beunos Aires, Argentina*, pp. 5448–5451, 2010.

[76] D. B. Popovic, R. B. Stein, R. Jovanovic, R. Dai, A. Kostov, and W. W. Armstrong, "Sensory nerve recording for closed-loop control to restore motor function," *IEEE Transactions on Biomedical Engineering*, vol. 40, no. 10, pp. 1024–1031, Oct. 1993.

[77] P. H. Veltink, H. J. Chizeck, P. E. Crago, and A. El-Bialy, "Nonlinear joint angle control for artificially stimulated muscle," *IEEE Transactions on Biomedical Engineering*, vol. 39, no. 4, pp. 368–380, Apr. 1992.

[78] K. Yoshida and K. Horch, "Closed-loop control of ankle position using muscle afferent feedback with functional neuromuscular stimulation," *IEEE Transactions on Biomedical Engineering*, vol. 43, no. 2, pp. 167–176, Feb. 1996.

[79] D. A. Gordon, R. M. Enoka, and D. G. Stuart, "Motor-unit force potentiation in adult cats during a standard fatigue test," *The Journal of Physiology*, vol. 421, pp. 569–582, Feb. 1990.

[80] Y. Giat, J. Mizrahi, and M. Levy, "A musculotendon model of the fatigue profiles of paralyzed quadriceps muscle under fes," *IEEE Transactions on Biomedical Engineering*, vol. 40, no. 7, pp. 664–674, Jul. 1993.

[81] F. Parmiggiani and R. B. Stein, "Nonlinear summation of contractions in cat muscles," *Journal of General Physiology*, vol. 78, no. 3, pp. 277–311, Sep. 1981.

[82] M. Kaya, A. Jinha, T. R. Leonard, and W. Herzog, "Multi-functionality of the cat medical gastrocnemius during locomotion," *Journal of Biomechanics*, vol. 38, no. 6, pp. 1291–1301, 2005.

CHAPTER 2

ADAPTIVE PARAMETER SELECTION FOR ASYNCHRONOUS INTRAFASCICULAR MULTI-ELECTRODE STIMULATION

This chapter is a published conference paper in the *Proceedings of the 2012 IEEE International Conference on Acoustics, Speech and Signal Processing*, pp. 753-756, 2012. Authors of this chapter are M.A. Frankel, G.A. Clark, S.G. Meek, R.A. Normann, and V.J. Mathews.

Abstract

This paper describes an adaptive algorithm for selecting per-electrode stimulus intensities and interelectrode stimulation phasing to achieve desired isometric plantar-flexion forces via asynchronous, intrafascicular multi-electrode stimulation. The algorithm employed a linear model of force production and a gradient descent approach for updating the parameters of the model. The adaptively selected model stimulation parameters were validated in experiments in which stimulation was delivered via a Utah Slanted Electrode Array that was acutely implanted in the sciatic nerve of an anesthetized feline. In simulations and experiments, desired steps in force were evoked, and exhibited short time-to-peak (< 0.5 s), low overshoot (< 10 %), low steady-state error (< 4 %), and low steady-state ripple (< 12 %), with rapid convergence of stimulation parameters. For periodic desired forces, the algorithm was able to quickly converge and experimental trials showed low amplitude error (mean error < 10 % of maximum force), and short time delay (< 250 ms).

Introduction

Functional Electrical Stimulation (FES) has been clinically employed to restore lost neuromuscular function due to spinal cord injury or other neural deficits. Elec-

trical stimulation applied to nerves can evoke forceful contractions of paralyzed muscle, resulting in functional movement. However, current clinical FES methods to control muscle function rely on high-frequency, single-electrode surface or extraneural stimulation, which has limited force scalability and can lead to rapid fatigue [1].

Recent advances in high-channel-count peripheral nerve interfaces, such as the Utah Slanted Electrode Array (USEA), allow for selective activation of large numbers of motor-unit groups within a single muscle [2]. Graded force production can be achieved by modulating the stimulus intensity delivered to an implanted electrode, thus activating more or less motor-unit groups. Relatively high-frequency muscle contractions are required to evoke smooth tetanic forces [3]. When stimulating via only one electrode, this high-frequency stimulation leads to rapid muscle fatigue. Because multi-electrode arrays allow for selective access to unique populations of motor-unit groups within a single muscle, asynchronous stimulation via multiple independent electrodes at a low per-electrode frequency, but high composite frequency, can evoke smooth, fatigue-resistant muscle contractions [1, 4].

Asynchronous Multi-Electrode Stimulation (AMES) poses unique challenges, especially in the determination of stimulation parameters-per-electrode stimulus intensities and interelectrode stimulation phasing that will evoke smooth, precise motor function. Algorithms have been developed that can predict the dynamic muscle response to single-electrode stimulation [5], but these models have not been extended to AMES. Adaptive algorithms have been used to determine optimal interelectrode phasing for AMES that can evoke smooth static isometric forces [4, 6], and other algorithms have been designed to determine per-electrode stimulus intensities to evoke precise periodic joint torques [7]. Recently, we have investigated closed-loop force-feedback control that modulates per-electrode stimulus intensities to evoke any desired force trajectory, using asynchronous IntraFascicular Multi-electrode Stimulation (aIFMS) [8]. However, we are unaware of any method that can adaptively determine both per-electrode stimulus intensities and interelectrode stimulation phasing to evoke smooth, precise, arbitrary force trajectories.

Here we present a gradient descent adaptive filtering method that can determine per-electrode stimulus intensities and interelectrode stimulation phasing by mini-

mizing the difference (error) between any desired force trajectory and an estimate of aIFMS-evoked forces. Stimulation parameters were adaptively determined in open-loop simulation and then validated with experimental stimulation, as a first step towards developing a real-time closed-loop method. The simulations and subsequent experimental results show successful production of desired isometric force trajectories.

Adaptive Parameter Selection

Single-pulse stimulation via a single USEA electrode evokes a twitch response in force, Figure 2.1a, and graded force production can be achieved by modulating the stimulus intensity (i.e., the stimulus duration), Figure 2.1b. For stimulation via each utilized electrode, there is a known normalized, characteristic twitch-force response to a single stimulus, $x_i(t)$. Our algorithm uses these characteristic responses in a linear summation model of aIFMS force production:

$$F_e(t) = \sum_{i=1}^{M} \sum_{j=1}^{K} a_{i,j} \cdot x_i(t - \tau_{i,j}), \tag{2.1}$$

where $a_{i,j}$ is the stimulation intensity for electrode i during stimulation cycle j, $\tau_{i,j}$ is the stimulation time, M is the total number of stimulating electrodes, and K is the total number of stimulation cycles.

For each electrode, we want to determine the stimulation parameters, a and τ, that will minimize the difference (error) between a desired force trajectory, $F_d(t)$, and the estimated evoked forces, $F_e(t)$, where

$$e(t) = F_d(t) - F_e(t). \tag{2.2}$$

For each stimulation, the cost function to be minimized is set as

$$L(t) = \int_{T_1}^{T_2} [e(\lambda)]^2 d\lambda, \tag{2.3}$$

where the interval of interest is between the time when the twitch-force response initially rises above 25 % of the maximum response, T_1, and the time when the

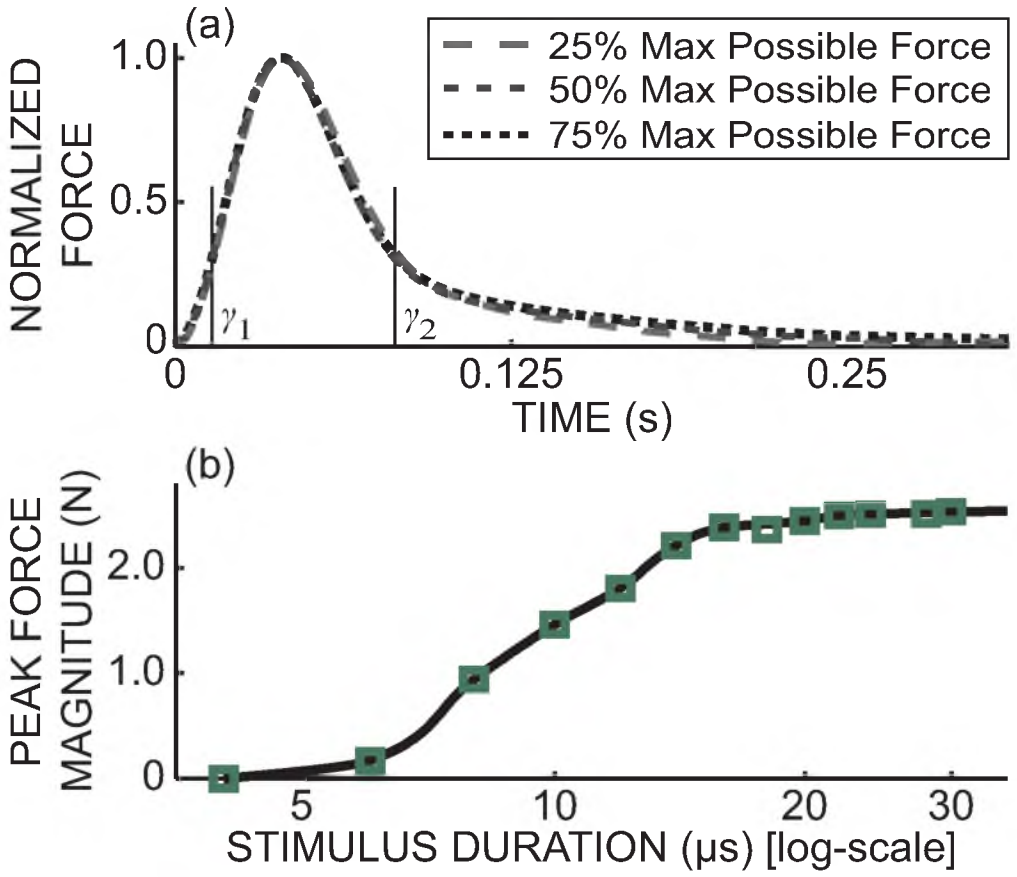

Figure 2.1: Electrode Characterization.

(a) Stimulation was delivered to a single USEA electrode at a stimulus duration that would evoke 25%, 50%, and 75% of the maximum possible twitch-force, as determined from (b). The normalized twitch-force responses show stimulus duration invariant kinetics, which is desirable for this study. γ_1 and γ_2, the cost function bounds, are marked for this characteristic twitch-force response. (b) Typical twitch-force recruitment map, showing the relationship between delivered stimulus duration and evoked peak twitch-force, and the bounds of useable stimulus durations.

twitch-force response drops below 25 % of the maximum response, T_2. These bounds are used because this is the time window when the majority of the twitch-force response occurs, and when the majority of changes in $F_e(t)$ are due to stimulation via the corresponding electrode, Figure 2.1a. For each stimulation, T_1 andT_2 are set as

$$T_1 = \tau_{i,j} + \gamma_{i,1} \text{ and } T_2 = \tau_{i,j} + \gamma_{i,2}, \tag{2.4}$$

where γ_1 and γ_2 are as shown in Figure 2.1a.

Gradients of the cost function based on stimulation intensity, a, and stimulation time, τ, are determined:

$$\nabla_{a_{i,j}}[L(t)] = \int_{T_1}^{T_2} [-2 \cdot e(\lambda) \cdot x_i(\lambda - \tau_{i,j})] d\lambda \tag{2.5}$$

$$\nabla_{\tau_{i,j}}[L(t)] = \int_{T_1}^{T_2} \Big[2 \cdot e(\lambda) \cdot a_{i,j} \cdot \frac{d}{d\tau}[x_i(\lambda - \tau_{i,j})]\Big] d\lambda. \tag{2.6}$$

The parameters for the subsequent cycle of stimulation are updated as

$$a_{i,j+1} = a_{i,j} - \eta_a \cdot \nabla_{a_{i,j}}[L(t)] \tag{2.7}$$

$$o_{i,j+1} = o_{i,j} - \eta_\tau \cdot \nabla_{\tau_{i,j}}[L(t)] \tag{2.8}$$

$$\tau_{i,j+1} = \tau_{i-1,j+1} + o_{i,j+1}, \tag{2.9}$$

where $o_{i,j}$ is the offset time between stimulation via the prior electrode $(i-1)$ and the current electrode (i), and η is the rate of adaptation, independently set for each stimulation parameter, a and τ. The stimulation parameters for each electrode are iteratively determined for each subsequent cycle of stimulation by looking backwards in time at the bounded estimated force response during the previous cycle of stimulation, Figure 2.2. After the subsequent cycle of stimulation parameters are updated for each stimulating electrode, the force estimation model is updated, Figure 2.2.

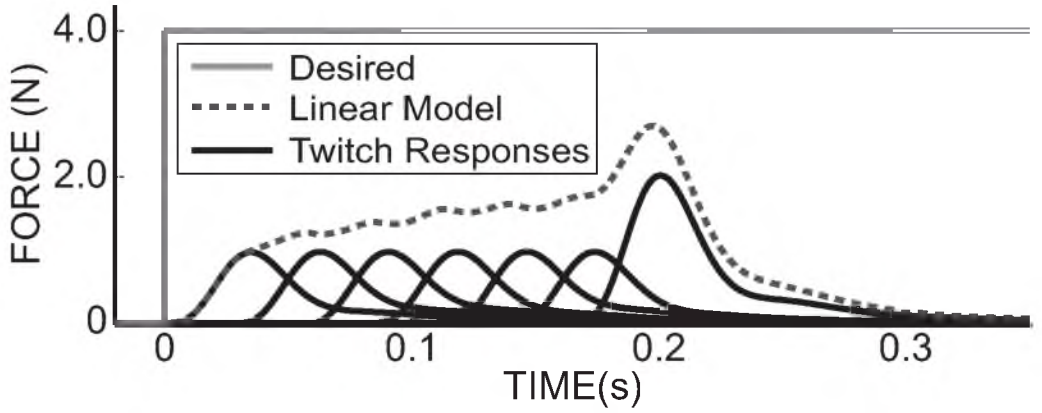

Figure 2.2: First Cycle Iteration of Algorithmic Parameter Determination.

The first cycle of algorithmic parameter determination is shown for a simulation of 6-electrode, 36-Hz asynchronous stimulation, where all twitch-response kinetics are similar. The desired force was a 4-N step function. The initial cycle of stimulation was estimated. The algorithm then determined the stimulation intensity (increase) and timing (decreased offset) for the second cycle of stimulation via the first electrode by looking backwards in time at the linear model of estimated force during the first stimulation cycle. The second cycle of stimulation via the first electrode with adapted parameters is shown by the larger twitch-response due to stimulation at $t = 0.161$ s.

Methods

Animal Preparation and Surgery

Experiments were conducted on an adult male feline using procedures approved by the University of Utah Institutional Animal Care and Use Committee. The initial experimental methods are fully described in [8], and are briefly described below. The feline was anesthetized and mechanically ventilated. Vital signs were monitored and recorded to assess the depth of anesthesia and animal status.

A 100-electrode USEA was implanted in the left sciatic nerve. The animal was placed in a prone position in a rigid trough with its hind limbs suspended. The metatarsal-phalangeal joint of the animal's left foot was secured to a six degree-of-freedom load cell (model Gamma-US-15, ATI, Apex, USA) via plastic ties. Bone pins were inserted in the left tibia and fixed to the surgical table, to ensure that all forces generated by plantar-flexor muscles were isometric. The magnitude of the evoked ground reaction force vector was used as the force response for all experiments.

Electrode Characterization

Monophasic electrical stimulation was delivered using a custom-built, multichannel, constant-voltage stimulation unit [9] at a voltage of -4 V, using stimulus durations between 0.2 µs and 512 µs with 0.2-µs resolution. Twitch-force recruitment maps were generated for all electrodes that generated a peak force greater than 0.5 N in response to a single 256-µs stimulus, Figure 2.1b [10]. The pair-wise level of axonal activation overlap was measured for all electrodes whose stimulation evoked fast-twitch plantar-flexion [1].

Simulations

Six electrodes were chosen for simulation and experimental stimulation from those having the smallest pair-wise overlap, low activation thresholds, and strong maximum peak twitch-force as determined from recruitment maps (Figure 2.1b), and from those having similar normalized force response kinetics at all possible stimulus durations (Figure 2.1a). For each of these six electrodes, the normalized, characteristic twitch-force response, $x_i(t)$, was determined as the normalized twitch-force response to the stimulus duration that evoked 50% of maximal twitch-force.

Simulations were performed using MATLAB software (The Mathworks, Natick, USA). Initial stimulation intensities were set to $F_d(0)/M$, where M was the total number of stimulation electrodes, and initial interelectrode timing offsets were set to $1/f_c$, where f_c was the desired composite frequency in Hertz. Both intensity and offset were bounded. The minimum allowable stimulation intensity was zero, and the maximum allowable stimulation intensity via each electrode was determined from initial twitch-force recruitment mapping, Figure 2.1b. The minimum and maximum allowable offset times were set as 0.5 times and 1.5 times the initial offset ($1/f_c$). The derivative in (2.6) was numerically determined from a smoothed model of the characteristic twitch-response, $x_i(t)$.

Adaptation Tuning and Data Analysis

Adaptation gains, η_a and η_τ, were tuned through iterative simulations to find the gains that produced steps in force with adequate response characteristics (short time-to-peak, low overshoot, low steady-state error, and low steady-state ripple), which are defined as follows. Time-to-peak, T_p, is the time from force step onset to peak evoked force. Percent overshoot, $\%OS$, is the percent difference between the peak evoked force and the mean evoked steady-state force, measured during the last 0.25 s of stimulation. Steady-state error, SSE, is the difference between the desired force and the mean evoked steady-state force. Steady-state ripple, SSR, is the difference between the peak-to-peak evoked force during the last 0.25 s of stimulation and the mean evoked steady-state force. The SSR metric is important for multi-electrode stimulation because it is a characteristic of the smoothness of the evoked forces.

For periodic desired forces, the adaptation gains were tuned to produce forces with minimal amplitude error, E_A. To determine E_A, the evoked forces were shifted backwards in time until the sum of the squared per-sample difference between the time-shifted forces and desired force trajectory was a minimum. E_A is the square-root of this squared per-sample difference. The time shift was also measured as a time delay metric of the response, T_d.

Experimental Verification

After parameter sets were determined in simulation, stimulus intensities were converted to useable stimulus durations via recruitment maps (Figure 2.1b). This was necessary because the recruitment map for each electrode is a nonlinear function with varying characteristics. Because stimulation via the chosen electrodes did not activate completely independent motor-unit groups, and because muscle contractions do not combine linearly [11], an additional gain factor of 0.6 (determined experimentally) was applied to the stimulus intensities prior to stimulus duration conversion (see Discussion). Electrical stimulation was delivered via the six chosen USEA electrodes through custom MATLAB software.

Results

All experimental stimulations were conducted using six electrodes with an initial composite frequency of $f_c = 36$ Hz. In simulation, desired steps in force were achieved with short T_p (425 ms), low $\%OS$ (7.5 %), low SSE (-1 %), and low SSR (10 %), Figure 2.3. Experiments, using the stimulation parameters determined in simulation, evoked similar results ($T_p = 445$ ms, $\%OS = 7.6$ %, $SSE = 3$ %, $SSR = 11$ %), Figure 2.3. The maximum instantaneous per-electrode stimulation frequency was 6.9 Hz, and the steady-state converged composite frequency was 40.2 Hz.

Periodic force trajectories were achieved in simulation with low amplitude error ($E_A = 0.06 \pm 0.04$ N, mean $\pm$ SD) and short time delay ($T_d = 215$ ms), Figure 2.4. Experimental stimulation evoked periodic forces with slightly larger amplitude error than simulation ($E_A = 0.28 \pm 0.21$ N), but similar time delay ($T_d = 224$ ms), Figure 2.4. The maximum instantaneous per-electrode stimulation frequency was 7.2 Hz. Higher frequency desired force trajectories were achieved with similar amplitude errors and time delays (data not shown).

More complex time-varying force trajectories were also achieved in simulation with low amplitude error ($E_A = 0.11 \pm 0.08$ N) and short time delay ($T_d = 208$ ms), Figure 2.5. Experimental stimulation evoked forces with slightly larger amplitude error ($E_A = 0.34 \pm 0.22$ N), but similar time delay ($T_d = 222$ ms), Figure 2.5. The maximum instantaneous per-electrode stimulation frequency was 7.1 Hz.

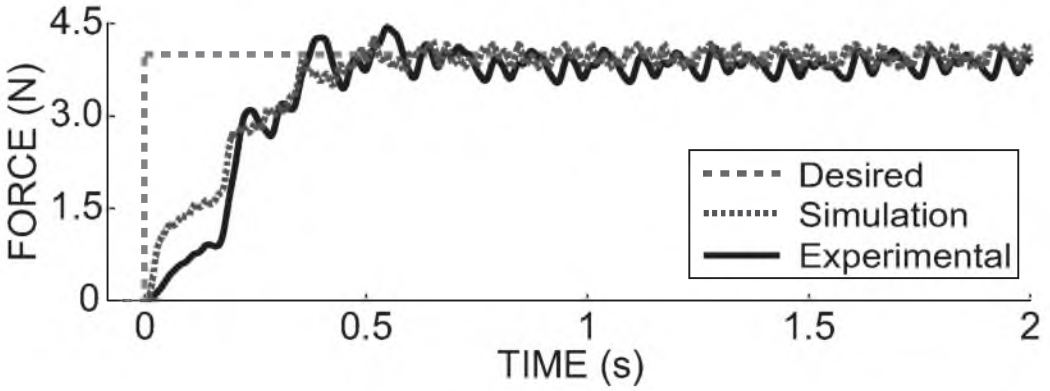

Figure 2.3: Isometric Force Tracking - Step Function.

A 4-N desired step in force was successfully evoked in simulation and with experimental stimulation.

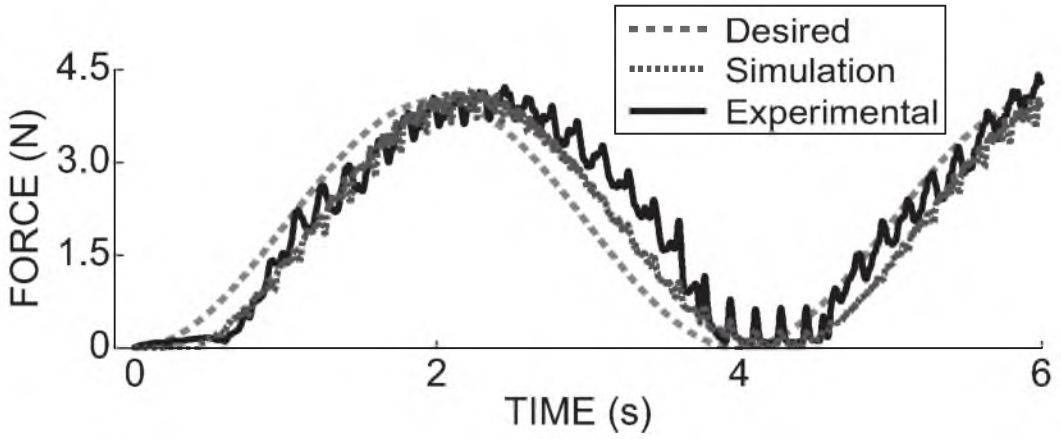

Figure 2.4: Isometric Force Tracking - Sine Function.

A 4-N, 0.25-Hz sinusoidal desired force trajectory was successfully evoked in simulation and with experimental stimulation. Experimental results had slightly larger amplitude error than simulation results.

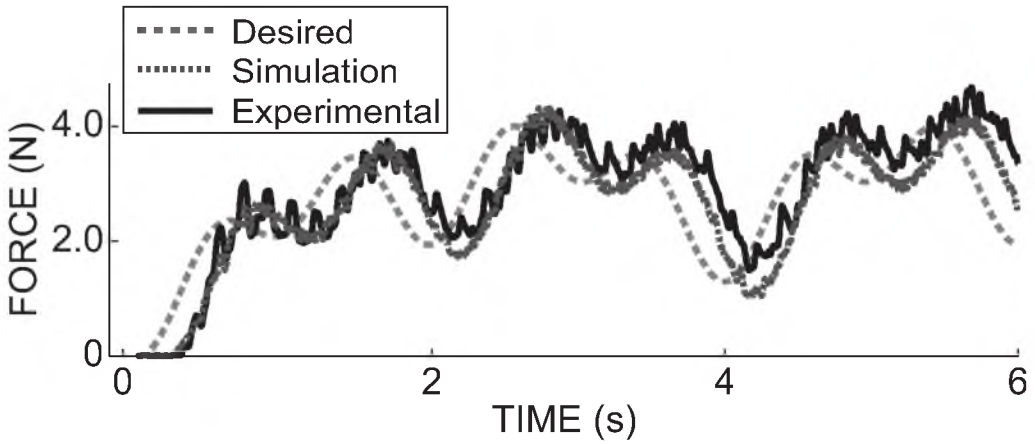

Figure 2.5: Isometric Force Tracking - Composite Function.

A 4-N composite of sinusoids, desired force trajectory was successfully evoked in simulation and with experimental stimulation. Again, experimental results had slightly larger amplitude errors than simulation results.

Discussion

Experiments described in this paper demonstrated that complex isometric force trajectories can be successfully achieved with aIFMS. Other algorithms may be able to evoke smooth static muscle forces or periodic joint torques [4, 6, 7], but our approach has the benefit of being able to determine all stimulation parameters for any desired forces, including completely arbitrary trajectories.

One difficulty with this method is the offline tuning of adaptation gains, η_a and η_τ. It would be beneficial to have automated gain parameterization to determine optimal stimulation parameters. Experimental stimulation required an additional stimulation intensity gain factor of 0.6, which was determined experimentally. Contractions of multiple motor-unit groups do not combine in a completely linear manner [11], and we are unaware of a good model for the specific interaction of stimulation via multiple intrafascicular electrodes. Although aIFMS can evoke fatigue-resistant force, fatigue will eventually occur in muscle fibers even at low stimulation frequencies [1]. Long-term stability of the algorithm has not yet been experimentally evaluated. Real-time implementation of the algorithm with closed-loop feedback of the force error signals [8] should enhance the ability of the algorithm to compensate for modeling errors and time-variations in the force generation mechanism. Future work will investigate better force generation models as well as closed-loop adaptation of the stimulation parameters in the experiments.

References

[1] D. McDonnall, G. Clark, and R. A. Normann, "Interleaved, multisite electrical stimulation of cat sciatic nerve produces fatigue-resistant, ripple-free motor responses," *IEEE Transactions on Neural Systems and Rehabilitation Engineering*, vol. 12, no. 2, pp. 208–215, Jun. 2004.

[2] A. Branner, R. B. Stein, and R. A. Normann, "Selective stimulation of cat sciatic nerve using an array of varying-length microelectrodes," *Journal of Neurophysiology*, vol. 85, no. 4, pp. 1585–1594, Apr. 2001.

[3] P. M. H. Rack and D. R. Westbury, "The effect of length and stimulus rate on tension in the isometric cat soleus muscle," *The Journal of Physiology*, vol. 204. no. 2, pp. 443–460, Oct. 1969.

[4] A. K. Wise, D. L. Morgan, J. E. Gregory, and U. Proske, "Fatigue in mammalian skeletal muscle stimulated under computer control," *Journal of Applied Physiology*, vol. 90, no. 1, pp. 189–197, Jan. 2001.

[5] T. Schauer, O. Negard, F. Previdi, K. J. Hunt, M. H. Fraser, E. Ferchland, and J. Raisch, "Online identification and nonlinear control of the electrically stimulated quadriceps muscle," *Control Engineering Practice*, vol. 13, pp. 1207–1219, Sep. 2005.

[6] A. M. Wilder, R. A. Normann, and G. A. Clark, "Optimization of a tremor-reducing algorithm for asynchronous stimulation of independent motor-unit groups," *Proceedings of IFESS 2010 in Artificial Organs*, vol. 34, no. 8, Aug. 2010.

[7] J. J. Abbas and R. J. Triolo, "Experimental evaluation of an adaptive feedforward controller for use in functional neuromuscular stimulation systems," *IEEE Transactions on Rehabilitation Engineering*, vol. 5, no. 1, pp. 12–22, Mar. 1997.

[8] M. A. Frankel, B. R. Dowden, V. J. Mathews, R. A. Normann, G. A. Clark, and S. G. Meek, "Multiple-input single-output closed-loop isometric force control using asynchronous intrafascicular multi-electrode stimulation," *IEEE Transactions on Neural Systems and Rehabilitation Engineering*, vol. 19, no. 3, pp. 325–332, Jun. 2011.

[9] S. D. Hiatt, A. M. Wilder, K. S. Guillory, B. R. Dowden, R. A. Normann, and G. A. Clark, "1100-channel neural stimulator for functional electrical stimulation using high-electrode-count neural interfaces," *Proceedings of IFESS 2010 in Artificial Organs*, vol. 34, no. 8, Aug. 2010.

[10] A. M. Wilder, S. D. Hiatt, B. R. Dowden, N. A. T. Brown, R. A. Normann, and G. A. Clark, "Automated stimulus-response mapping of high-electrode-count neural implants," *IEEE Transactions on Neural Systems and Rehabilitation Engineering*, vol. 17, no. 5, pp. 504–511, Aug. 2009.

[11] F. Parmiggiani and R. B. Stein, "Nonlinear summation of contractions in cat muscles," *Journal of General Physiology*, vol. 78, no. 3, pp. 277–311, Sep. 1981.

CHAPTER 3

MULTIPLE-INPUT SINGLE-OUTPUT CLOSED-LOOP ISOMETRIC FORCE CONTROL USING ASYNCHRONOUS INTRAFASCICULAR MULTI-ELECTRODE STIMULATION

This chapter is a published journal article in the *IEEE Transactions on Neural Systems and Rehabilitation Engineering*, Vol. 19, No. 3, pp. 325-332, Jun. 2011. Authors of this chapter are M.A. Frankel, B.R. Dowden, V.J. Mathews, R.A. Normann, G.A. Clark, and S.G. Meek.

Abstract

Although asynchronous, intrafascicular, multi-electrode stimulation (IFMS) can evoke fatigue-resistant muscle force, *a priori* determination of the necessary stimulation parameters for precise force production is not possible. This paper presents a proportionally-modulated, multiple-input, single-output (MISO) controller that was designed and experimentally validated for real-time, closed-loop, force-feedback control of asynchronous IFMS. Experiments were conducted on anesthetized felines with a Utah Slanted Electrode Array implanted in the sciatic nerve, either acutely or chronically ($n = 1$ for each). Isometric forces were evoked in plantar-flexor muscles, and target forces consisted of up to seven minutes of step, sinusoidal, and more complex time-varying trajectories. The controller was successful in evoking steps in force with time-to-peak of less than 0.45 s, steady-state ripple of less than 7 % of the mean steady-state force, and near-zero steady-state error even in the presence of muscle fatigue, but with transient overshoot of near 20 %. The controller was also successful in evoking target sinusoidal and complex time-varying force trajectories with amplitude error of less than 0.5 N and time delay of approximately 300 ms. This

MISO control strategy can potentially be used to develop closed-loop asynchronous IFMS controllers for a wide variety of multi-electrode stimulation applications to restore lost motor function.

Introduction

Clinically viable motor neuroprostheses using functional electrical stimulation (FES) must be able to produce precise limb movements in a controllable and predictable manner. However, existing FES-based motor neuroprostheses commonly suffer from two important difficulties: 1) rapid muscle fatigue from aggressive electrical stimulation, and 2) large variability in muscle force generation for given stimulation parameters. This paper presents a novel closed-loop force-feedback control strategy that utilizes asynchronous, intrafascicular, multi-electrode stimulation (IFMS) to evoke precise, fatigue-resistant, isometric muscle force in the hind limb of an anesthetized feline.

Our stimulation approach is to use asynchronous, low-frequency electrical stimulation of multiple independent motor-unit groups within a targeted skeletal muscle, which can evoke smooth fatigue-resistant force that closely resembles normal motor function [1, 2, 3, 4, 5]. This approach has been made possible because of recently developed high-electrode-count neural interfaces, such as the 96-electrode Utah Slanted Electrode Array (USEA) [6, 7, 8, 9].

The goal of the present work was to develop a real-time closed-loop control system suitable for asynchronous IFMS. The muscle response of FES-based motor neuroprostheses has been well studied [10, 11, 12, 13, 14, 15], but these stimulator-nerve-muscle systems contain nonlinear time-varying processes that are difficult to model, such as potentiation and fatigue [16, 17]. Asynchronous IFMS-based motor neuroprostheses contain additional complexities that have not been well characterized, such as axonal excitation overlap between stimulating electrodes and nonlinear combination of forces produced by multiple stimulating electrodes [18, 19, 20]. Because such system complexities are difficult to model, open-loop production of precise muscle force via asynchronous IFMS is not possible, and a closed-loop control strategy is necessary to accurately produce fatigue-resistant, time-varying, muscle force. However, cur-

rent closed-loop FES-based motor control methods typically rely on a single-input, single-output (SISO) system, where the single input is typically stimulation via a single epimysial, intraspinal, extraneural, or intrafascicular electrode, and the single output is either muscle force, joint angle or torque, or muscle-spindle activity [21, 22, 23, 24, 25, 26, 27, 28]. In contrast, the asynchronous IFMS approach that we employ has the additional complexity of being a multiple-input (n stimulating electrodes), single-output (MISO) system, and no suitable closed-loop control strategy exists. One of the main challenges in developing a closed-loop MISO controller for asynchronous IFMS is determining how to update stimulation parameters for individual electrodes based on the error between the desired force and the evoked force. Our control approach was to update the stimulation strength delivered via an electrode during the next cycle of stimulation, based on the error between the desired and evoked muscle force during a time frame containing the expected time of the peak force response due to the current cycle of stimulation via that electrode.

In this paper, we first describe the development of a simple proportional closed-loop MISO controller for precise isometric force production via asynchronous IFMS of plantar-flexor muscles in an anesthetized feline using an implanted USEA. Subsequently, we present physiological results demonstrating successful implementation of this control system. Up to seven minutes of step, sinusoidal, or arbitrary-shaped force trajectories were used as the target forces because these force trajectories would be necessary for normal human motor function. Desired steps in force were evoked with short response time-to-peak, large overshoot, near-zero steady-state error, and moderate steady-state ripple, where ripple in this case is the variability in force due primarily to the differences in responses evoked by the multiple electrodes used in IFMS. Our results also show that time-varying isometric force trajectories can be produced with low amplitude error and short time delay.

Methods

Surgical Preparation and Electrode Array Implantation

Experiments were conducted on two adult felines using procedures approved by the University of Utah Institutional Animal Care and Use Committee. Each animal

was initially anesthetized with an intramuscular injection of Telazol (Fort Dodge Animal Health, Fort Dodge, USA) at a dosage of 10 mg/kg. The animal was then intubated and mechanically ventilated. Anesthesia was maintained with Isoflorane (Hospira, Lake Forest, USA) at a level of 1.25-2.5 %. Fluid and blood sugar levels were maintained via an intravenous drip of lactated Ringer's solution at a rate of 10 ml/kg/hr. Vital signs were monitored and recorded every 15 minutes to assess the depth of anesthesia and animal status.

Experiments to verify the efficacy of the control system were conducted on a feline with an USEA acutely implanted in the left sciatic nerve, whereas all other experiments were conducted on a feline with a USEA chronically implanted in the left sciatic nerve during two different experimental sessions at 37 and 65 days after implantation. An earlier, but similar, version of the USEA is described in detail elsewhere [29]. The animal was placed in a prone position in a rigid trough with its hind limbs suspended from the rear of the trough. The metatarsal-phalangeal joint of the animal's left foot was secured via plastic ties to the top surface of a six degree-of-freedom (6-DoF) load cell (model Gamma-US-15, ATI, Apex, USA), which was attached to the surgical table. In the acute preparation, two bone pins were inserted mid-tibia in the left leg and rigidly fixed to the surgical table, whereas in the chronic experiments, the left hind limb was constrained from movement via noninvasive clamps at the left knee. The trough was elevated above the table, and the bone pins or clamps were secured at a position that set the ankle joint angle at approximately 90 degrees. This system of fixation was used to ensure that all forces generated by plantar-flexor muscles were isometric and were transmitted to the 6-DoF load cell. The magnitude of the evoked ground reaction force vector was used as the force response for all experiments.

Stimulation and Recording Setup

Monophasic electrical stimulation was delivered using a custom-built, multichannel, constant-voltage stimulation unit [30]. Voltage amplitude was held constant throughout each experiment at a value between -2.4 V and -4.0 V. Stimulus strength was modulated by varying the stimulus duration between 0.2 µs and 1024 µs, with

0.2-µs steps, and were controlled via custom C++ software [31] for twitch-force recruitment mapping and axonal activation overlap determination (described below), and via custom MATLAB (The Mathworks, Natick, USA) routines for all other studies. The 6-DoF load cell output was sampled at 10 kHz using either a Cerebus data acquisition system (Blackrock Microsystems, Salt Lake City, USA) or custom MATLAB software, via an NI PCI-6040E data acquisition card (National Instruments, Austin, USA). To reduce sensor noise, all forces were filtered in MATLAB using a forward and backward 4th-order Butterworth low-pass filter with a 50-Hz cutoff frequency, which provides near-zero amplitude distortion and zero phase distortion. This was accomplished in the real-time control system because the controller uses forces recorded during a previous cycle of stimulation, and thus is able to accommodate the delays caused by the backward filtering process.

USEA Calibration

Twitch-force recruitment curves were generated for all electrodes that generated a peak force greater than 0.5 N in response to a single 256-µs stimulus. Electrodes whose stimulation activated plantar-flexor muscles were identified by analyzing the direction of the evoked force vector [32]. Fatigue-reducing effects of asynchronous IFMS can be maximized by utilizing electrodes that activate unique nonoverlapping populations of motor neurons [1, 2]. The level of axonal activation overlap was measured for all pairs of electrodes using the refractory technique described in [1, 32] for electrodes that activated plantar-flexor muscles. 60-Hz asynchronous stimulation was used for the closed-loop experiments because this composite frequency is sufficient to produce a fused muscle contraction in cat hind limb muscles that consist of both slow-twitch and fast-twitch motor fibers [33]. Six electrodes activating plantar-flexor muscles with the least amount of overlap were chosen so that the per-electrode stimulation frequency would be 10 Hz, which is advantageous for fatigue reduction relative to the 60-Hz composite stimulation frequency [1].

Twitch-Force Time-to-Peak Determination

The control strategy used by the controller for updating per-electrode stimulation strengths requires reasonably accurate knowledge of the time from stimulation via each USEA electrode to the peak of the evoked twitch-force response, denoted as T_{pf} in further discussion. Consequently, this control strategy could fail if there is substantial variability in T_{pf} during a train of stimulation.

To evaluate T_{pf} variability across different stimulation frequencies, three minutes of open-loop stimulation at 2 Hz, 4 Hz, and 8 Hz was delivered via each electrode as chosen above, using a stimulus duration that would evoke half-maximal twitch-force, as determined from twitch-force recruitment curves. Even though closed-loop studies were performed at 10-Hz per-electrode stimulation frequencies, 8-Hz stimulation was set as the maximal stimulation frequency for T_{pf} studies because of the difficulty in extracting single-twitch waveforms from higher-frequency stimulation trains. Evoked forces were recorded, and T_{pf} was determined for responses to the stimuli delivered at each second.

Next, to evaluate T_{pf} variability across different stimulation strengths, three minutes of 8-Hz, open-loop stimulation was delivered via each electrode using stimulus durations that would evoke 20%, 40%, 60%, and 80% of maximal twitch-force, as determined from twitch-force recruitment curves. Evoked forces were recorded, and T_{pf} was determined for responses to the stimuli delivered at each second.

Statistical analyses of variance and covariance were performed with alpha equal to 0.05, using MATLAB and SigmaPlot software (Systat Software Inc., San Jose, USA). A lookup table of mean T_{pf} for each electrode at 8-Hz stimulation frequency, using a stimulus duration that evoked half-maximal twitch-force, was created for use by the closed-loop controller.

Closed-Loop Studies

Six electrodes with the least amount of axonal activation overlap were chosen as described above. 10-Hz asynchronous stimulation via each of the six electrodes was performed to produce 60-Hz composite stimulation. As a basic means to help reduce steady-state ripple, the phasing of time between stimulation via each electrode was

chosen such that the predicted T_{pf} due to stimulation via each electrode would be evenly spaced over the 100-ms cycle of stimulation via all six electrodes.

SD_{min}, the stimulus duration that was just below the force producing threshold, along with SD_{max}, the minimum stimulus duration to evoke maximal twitch-force, were determined from the twitch-force recruitment curves of each electrode utilized. These were set as the minimum and maximum allowable stimulus durations for each electrode, creating a bounded input system. The slope of the twitch-force recruitment curve between 20-80% of maximal twitch-force was also determined for each electrode, and this slope was used by the controller as a per-electrode gain to normalize for different recruitment curve slopes amongst the six electrodes in use.

A proportionally-modulated, real-time, closed-loop controller was designed to evoke step, sinusoidal, and more complex, time-varying, isometric force trajectories of varying amplitudes and frequencies. For desired force step trajectories, the closed-loop system was experimentally evaluated for the overall evoked force time-to-peak, percent overshoot, steady-state error, and steady-state ripple. Time-to-peak (T_p) was measured as the time from the step onset to the peak evoked force. Percent overshoot ($\%OS$) was measured as the percent difference between the peak evoked force and the mean steady-state evoked force during the last half-second of stimulation. Steady-state error (SSE) was measured as the difference between the mean evoked force during the last half-second of stimulation and the desired force step value. Steady-state ripple (SSR) was measured as the difference between the peak-to-peak evoked force during the last half-second of stimulation and the mean evoked force during the last half-second of stimulation.

For desired sinusoidal force trajectories, the closed-loop system was experimentally evaluated for evoked force amplitude error, time delay, and phase delay for 0.1-Hz to 2.0-Hz trajectories, because these frequencies are within the bounds of normal cyclical human lower limb movements [34]. After each trial, the complete evoked force output was shifted backward in time until the sum of the squared per-sample difference between the time-shifted evoked forces and the desired force trajectory was a minimum. This time shift was evaluated as a time delay parameter of the closed-loop system, T_d, along with the associated phase delay, Φ_d. Amplitude

error, E_A, was determined as the difference between the time-shifted evoked force and the desired force. More complex, time-varying force trajectories were created by combining harmonics of sinusoids to create relatively arbitrary-shaped waveforms that were repetitive within trial. These arbitrary-shaped force trajectories were analyzed for amplitude error and time delay using the same method employed for sinusoidal target forces.

Controller Design

A substantial difficulty in designing a MISO controller for IFMS is how to update the stimulation strength delivered to individual electrodes based on the error between the desired force and overall evoked force. During tetanic IFMS, the forces evoked by individual electrodes are not directly measureable, and there are many unmodeled, nonlinear, time-varying processes involved. A proportionally-modulated, real-time, closed-loop controller was designed for this series of experiments.

The force evoked by stimulation delivered to the ith electrode during the jth cycle of stimulation is a function of the stimulus duration, $SD_{i,j}$ (measured in µs), and the overall produced force, F_e, is a nonlinear combination of the forces evoked by all electrodes. The stimulus duration for the jth + 1 cycle of stimulation for the ith electrode in the proportionally-modulated controller is written as

$$SD_{i,j+1} = SD_{i,j} + k_p \cdot E_{i,j}, \tag{3.1}$$

where k_p is the proportional gain of the controller and $E_{i,j}$ is the error used for the ith electrode during the jth cycle of stimulation.

Although the evoked force due to stimulation via each electrode cannot be extracted from the overall produced force, the time from stimulation to peak twitch-force, T_{pf}, can be experimentally measured. On the basis of the conjecture that the time of peak response would be the most meaningful for per-electrode error measurement, the controller used the sum of the error between the desired force and the overall evoked force during a small window of time around the experimentally determined T_{pf} due to stimulation via the ith electrode. That is, the error measure in this discretely sampled system is written as

$$E_{i,j} = \sum_{k=T_{pf_{i,j}}-w}^{k=T_{pf_{i,j}}+w} [F_d(k) - F_e(k)], \tag{3.2}$$

where F_d is the desired force, Fe is the evoked force, $2w+1$ is the length of the sampling window over which the error function is evaluated, and $T_{pf_{i,j}}$ is the predicted time of peak twitch-force for the ith electrode during the jth cycle of stimulation (expressed in samples).

Because stimulation via each electrode will likely evoke a different twitch-force recruitment curve slope, an additional per-electrode gain factor was necessary so that all electrodes would recruit force in a similar manner. This additional gain factor, g_i, was based on experimentally determined recruitment-curve slopes for each electrode, s_i, and was determined as

$$g_i = \frac{log_{10}(1/s_i)}{2}, \tag{3.3}$$

which has a value ranging from 0.5 for steeper curves to 1.2 for flatter curves, based on analysis of plantar-flexor recruitment-curve slopes due to IFMS. The overall closed-loop control equation used in these experiments was

$$SD_{i,j+1} = SD_{i,j} + k_p \cdot g_i \cdot E_{i,j}. \tag{3.4}$$

The initial value of the stimulus duration for stimulation via each electrode, $SD_{i,1}$, was set as the peri-threshold stimulus duration, $SD_{i,min}$, as determined during twitch-force recruitment mapping.

This controller was designed for real-time application. T_{pf} due to stimulation via an electrode was typically in the neighborhood of 25 ms after stimulation. Because stimulation via each electrode is delivered every 100 ms (10 Hz), and w was chosen to be 5 ms (50 samples based on 10 kHz sampling), there is a maximum of 70 ms to acquire evoked forces, extract and filter the forces during the $T_{pf_{i,j}} \pm w$ window, calculate the error $E_{i,j}$, determine the next stimulus duration $SD_{i,j+1}$, and prepare the necessary outputs to the stimulator for the next stimulation cycle of electrode i. This was easily accomplished in our custom MATLAB software.

Results

Analysis of Twitch-Force Time-to-Peak

Because the controller uses the experimentally determined time from stimulation to peak twitch-force, T_{pf}, it is important that T_{pf} does not vary substantially to changes in stimulation strength or during an individual train of stimulation. A constant stimulation frequency was used in all closed-loop tests; therefore, any possible variation in T_{pf} across stimulation frequencies would not have affected the control strategy in our experiments, but it could pose concerns for future use where the stimulation frequency may become a control parameter. From a functional perspective, T_{pf} was sufficiently stable across stimulation frequency, stimulus strength, and time, thus allowing our control strategy to use this parameter.

The value of T_{pf} was determined for responses to the stimuli delivered every second for three-minute trains of open-loop stimulation delivered to each of six electrodes at 2-Hz, 4-Hz, and 8-Hz stimulation frequency. The mean value of T_{pf} was determined for each electrode at each tested stimulation frequency (27.1 $\pm$ 0.90 ms at 2-Hz stimulation, 26.5 $\pm$ 0.96 ms at 4-Hz stimulation, 25.4 $\pm$ 0.76 ms at 8-Hz stimulation, mean $\pm$ SD). For all six tested electrodes, a repeated-measures ANOVA and a Tukey multiple-comparison test showed that there were significant differences between the mean values of T_{pf} among all pair-wise combinations of the three tested frequencies ($F_{2,5} = 35.6$, $p < 0.05$). However, these small differences were not expected to affect the current control strategy.

The value of T_{pf} was determined for responses to the stimuli delivered every second for three-minute trains of open-loop stimulation delivered to each of four electrodes at 8-Hz stimulation frequency using stimulus durations that would evoke 20%, 40%, 60%, and 80% of the maximal twitch-force. The mean value of T_{pf} was determined for each electrode at each tested stimulation strength (24.4 $\pm$ 1.58 ms at 20%, 25.2 $\pm$ 1.45 ms at 40%, 24.9 $\pm$ 1.16 ms at 60%, 24.8 $\pm$ 1.33 ms at 80% of maximal twitch-force). For all four tested electrodes, a repeated-measures ANOVA showed that there were no significant differences between the mean values of T_{pf} among the four tested stimulation strengths ($F_{3,3} = 3.23$, $p = 0.075$).

In other experimental sessions, the value of T_{pf} was determined for responses to the stimuli delivered every second for one minute trains of open-loop stimulation delivered to each of 17 electrodes at 8-Hz stimulation frequency using stimulus durations that would evoke half-maximal twitch-force. An analysis of covariance was performed on all trains of stimulation to determine if there was a linear trend to changes in T_{pf} over the duration of the stimulus train. 46 of the 51 tested electrodes showed slopes that were not significantly different from zero ($p > 0.05$). The maximum absolute slope was 1.3-ms change in T_{pf} per minute of stimulation. This deviation was minor enough to not affect the closed-loop control strategy implemented in this study, given that the mean value of T_{pf} was used for the closed-loop experimentation, and w, the window of error analysis around T_{pf}, was set at 5 ms.

Step in Force: Closed-Loop Studies

The closed-loop controller was successful in producing target steps in force. Evoked steps in force were evaluated for (a) time-to-peak of the overall force, T_p, (b) percent overshoot, $\%OS$, (c) steady-state error, SSE, and (d) steady-state ripple, SSR, all calculated as described in Methods. Figure 3.1 shows representative closed-loop results for a 4-N desired step in force as the proportional controller gain, k_p, is adjusted from the minimum possible value to the largest tested value. When the system was just beyond critically damped (Figure 3.1b), $\%OS$ was nearly zero, Tp was approximately 1.0 s, SSE was equal to 0.1 N or 2.5 % of the desired force, and SSR was equal to 0.4 N or 9.8 % of the mean steady-state force. As the proportional gain was increased, T_p decreased to 0.4 s, SSE decreased to nearly zero, and SSR decreased to 5 % (Figure 3.1c). However, the underdamped response also exhibited relatively large overshoot of approximately 25 %. The controller was tested for longer trains of asynchronous IFMS (up to seven minutes) with steps in force ranging from 2 N to 7 N, and the critically dampened system response was consistent across all force step sizes ($T_p = 0.93 \pm 0.3$ s, $SSE = 4.3 \pm 1.4$ % of the desired force, and $SSR = 11.4 \pm 3.3$ % of the mean steady-state evoked force, $n = 7$ trials). There was at least 15 % overshoot in force during the transient response for underdamped

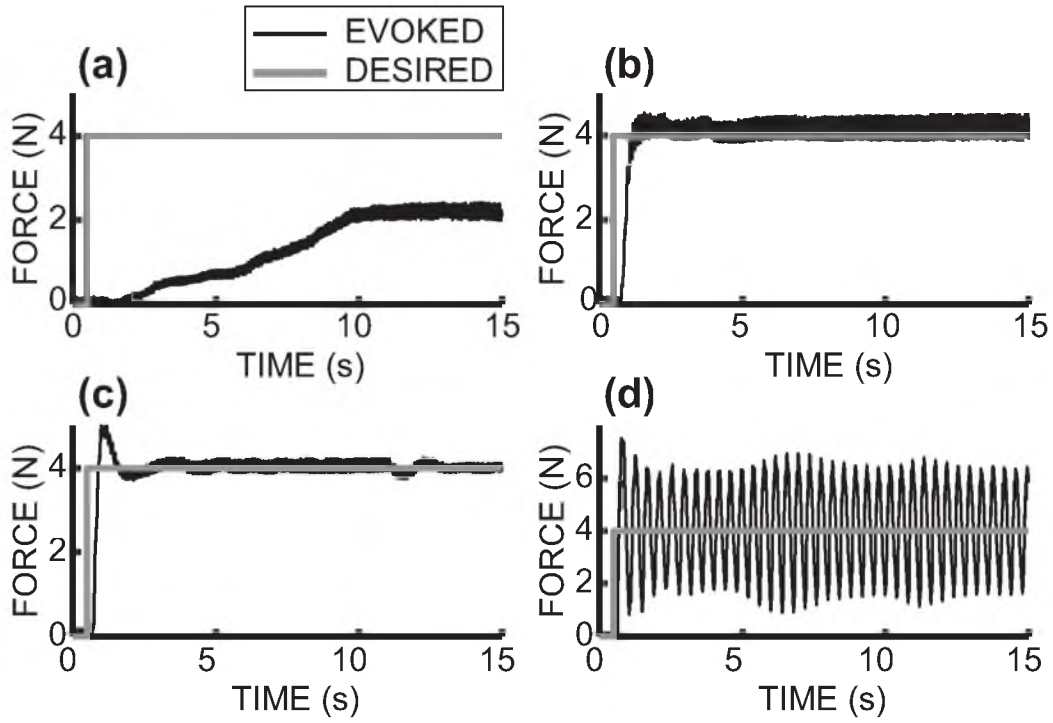

Figure 3.1: Proportional Isometric Force Controller Gain Tuning.

(a) The closed-loop controller successfully evoked desired steps in force. The first 15 seconds of results are depicted for different controller gain values (a-d), for a 4-N desired step in force beginning at $t = 0.5$ s, with 30 seconds of 6-electrode, 60-Hz, asynchronous IFMS. (a) The proportional gain, k_p, was set at the minimum, which produced a highly overdamped response. (b) Critically damped response demonstrating successful closed-loop control. (c) Underdamped response with steady-state error near 0 %. (d) The proportional gain was set at the highest tested value, and the system was completely oscillatory (marginally stable), but not unstable because the controller has saturation limits.

closed-loop system responses with SSE of less than 1 % and Tp of less than 0.45 s (n = 9 trials).

The control system was also tested to the limit where the activated muscle fibers showed strong fatigue (Figure 3.2). The controller was able to rapidly increase stimulus durations delivered to electrodes when the activated muscle fibers showed decreased force production (increased error) and then maintain the desired force until the muscle fibers were no longer able to produce the desired force even with maximal stimulation. As a comparison with a closed-loop trial, a 60-s, 60-Hz, open-loop asynchronous IFMS train was delivered to electrodes (Figure 3.3). The open-loop trial was performed using constant stimulus durations that were extracted from the closed-loop trial during the stimulation cycle at t = 40 s, when there was near-zero error. The open-loop system achieved a slightly larger force than desired, but then showed a slow decline in force due to fatigue, whereas the closed-loop system showed a large initial force overshoot, but then near-constant force close to the desired force throughout the rest of the trial.

Time-Varying Force Trajectories: Closed-Loop Studies

The closed-loop controller also successfully evoked up to seven minutes of sinusoidal and more complex, time-varying force trajectories. The frequencies of sinusoidal target force trajectories ranged from 0.1 Hz to 2.0 Hz. For each target force frequency, the controller gain was experimentally optimized to a value that produced a system with minimal amplitude error, E_A. Figure 3.4 shows a five-minute trial for a 0.1-Hz target sinusoidal force trajectory, where the controller accurately evoked target forces with $E_A = 0.24 \pm 0.16$ N over the entire trial.

Time delays for all six tested sinusoidal target force trajectories were approximately 300 ms and ranged from 240 ms to 440 ms (Table 3.1). However, the associated phase delay became quite large for desired frequencies above 0.2 Hz ($\Phi_d >$ 45 degrees). This is expected because there will always be a minimum time delay of 0.1 s between the desired and evoked forces as the controller is sampling one stimulation cycle backwards in time.

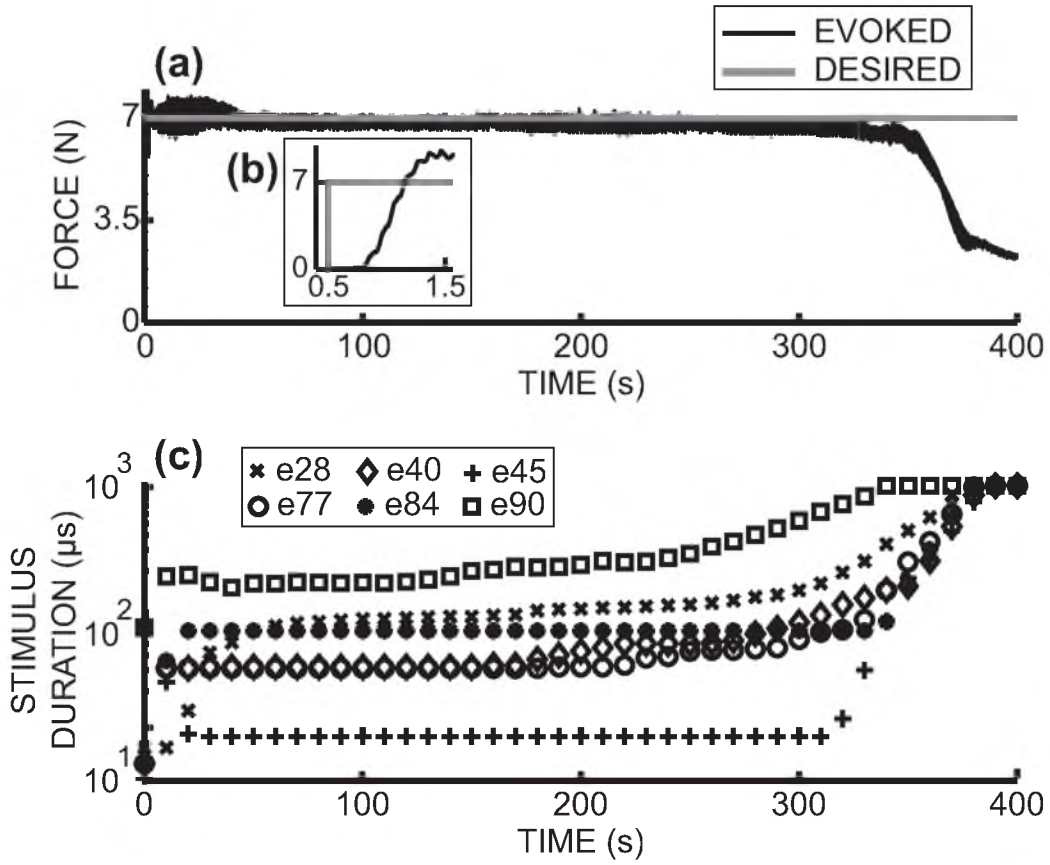

Figure 3.2: Modulation of Electrode Stimuli to Achieve and Hold a Desired Isometric Force.

The closed-loop controller successfully modulated stimulus durations to compensate for fatigue effects. Results are shown for a 7-N target step in force, with seven minutes of 6-electrode, 60-Hz asynchronous IFMS. (a) As the activated muscle fibers began to fatigue at approximately $t = 150$ s, the overall evoked force began to decrease, and the controller compensated by increasing the stimulus durations for all electrodes (c). Eventually, the activated muscle fibers were unable to produce the desired force even with maximal stimulus durations delivered to all electrodes. e28, e40, and e90 showed larger increases in stimulus duration as fatigue began to occur because of their larger per-electrode gain, g_i. Inset (b) shows the first 1.5 s of stimulation and the initial transient response of the closed-loop system.

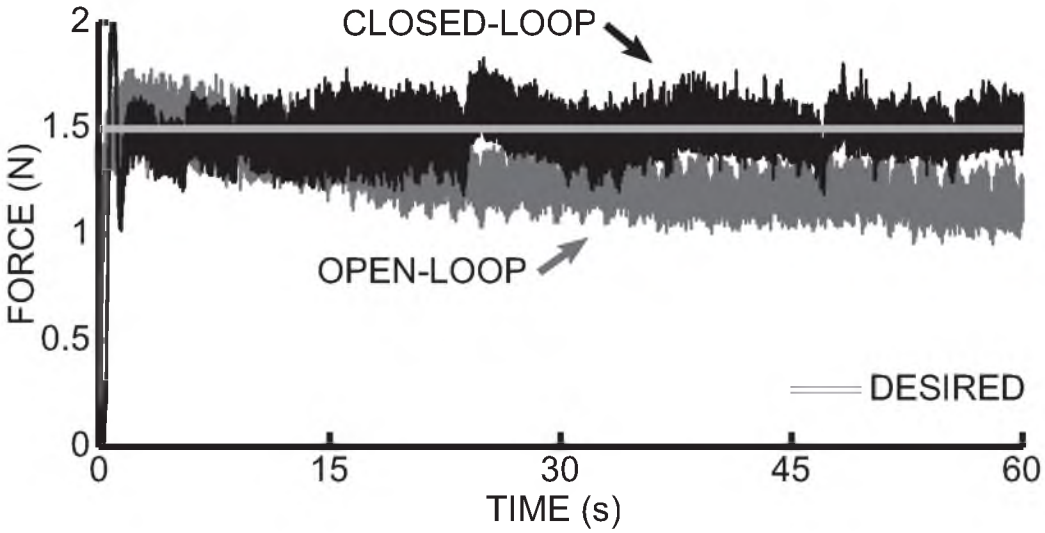

Figure 3.3: Open-Loop vs. Closed-Loop Isometric Force Control.

Closed-loop control successfully compensated for fatigue, keeping evoked forces relatively constant, compared with declining forces under open-loop control of 6-electrode, 60-Hz, asynchronous IFMS.

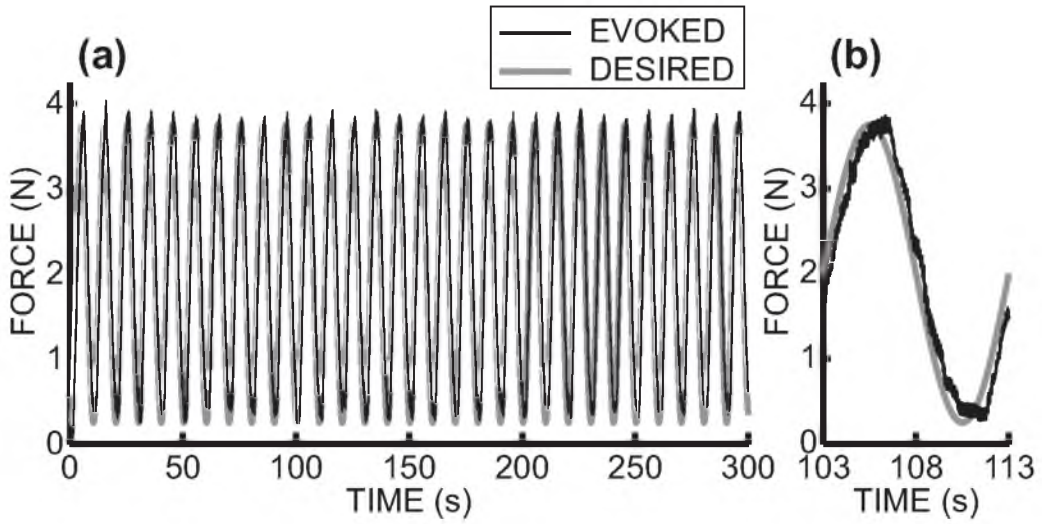

Figure 3.4: Closed-Loop Isometric Force Tracking - Sine Function.

(a) Closed-loop control successfully evoked a 0.1-Hz sinusoidal target force trajectory with five minutes of 6-electrode, 60-Hz, asynchronous IFMS. (b) One cycle of results extracted from (a). The evoked force showed a smooth profile except near peaks and valleys, where the transitions were more abrupt.

Table 3.1: Time and Phase Delay Across Sinusoidal Target Force Trials

Desired Force Frequency (Hz)	Time Delay (s)	Phase Delay (degrees)
0.1	0.30	10.8
0.2	0.24	17.3
0.4	0.44	63.4
0.8	0.38	108.0
1.4	0.28	138.6
2.0	0.25	180.0

More complex, time-varying, target force trajectories were created by combining harmonic sinusoids to create arbitrary-shaped waveforms that were repetitive within a trial. Figure 3.5 shows a 0-N to 4-N, two-minute long, target force trajectory. Over the entire trial, the amplitude error was less than 0.35 N ($E_A = 0.19 \pm 0.8$ N) and the time delay was 0.27 s. Other tests involving complex, time-varying, target force trajectories showed similar results.

Discussion

This paper demonstrated the first successful use of a MISO closed-loop control strategy for asynchronous IFMS to produce precise, time-varying, fatigue-resistant isometric muscle force. This demonstration is important because although asynchronous IFMS has the ability to evoke smooth fatigue-resistant force, *a priori* determination of the necessary stimulation parameters for precise force production is not possible due to many unmodeled, time-varying system properties.

The proportionally-modulated, real-time controller designed for these experiments was able to accurately evoke desired steps in isometric force with reasonable system performance. By increasing the controller gain, the closed-loop system was driven from being highly overdamped to critically damped to highly underdamped, as would be expected from the proportionally-modulated control strategy (Figure 3.1). The value of T_p was approximately 1.0 s when the experimental closed-loop system was critically damped, but this may not be a fast enough response for ballistic movements, such as the swing phase of running which takes approximately 300 ms [35]. Critically damped responses also showed small SSE of approximately 4.5 %. To reduce SSE and T_p, the closed-loop system was driven to an underdamped state, which also resulted in potentially undesirable force overshoot (Figure 3.1c).

After the system achieved a steady-state force, the controller was able to react to changes in muscular force production, due to potentiation, fatigue, or other factors, by adjusting the stimulus durations delivered via USEA electrodes (Figure 3.2). Eventually, all activated muscle fibers will show strong fatigue that cannot be compensated for by increasing stimulus strengths, and the overall evoked force will not reach the target level. This could create problems for continued stimulation during

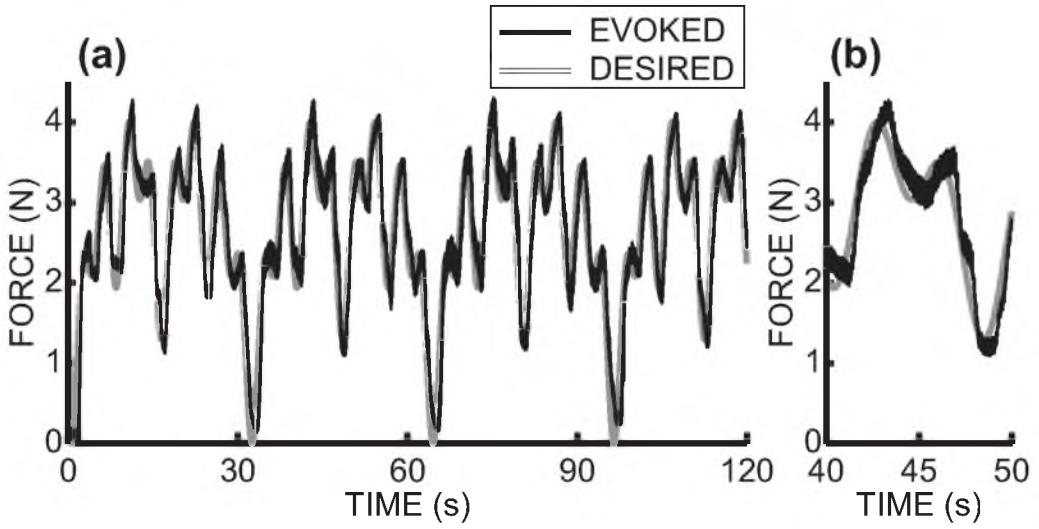

Figure 3.5: Closed-Loop Isometric Force Tracking - Composite Function.

(a) Closed-loop control successfully evoked a 0-N to 4-N, time-varying, target force trajectory with two minutes of 6-electrode, 60-Hz, asynchronous IFMS. (b) One cycle of results extracted from (a).

an experimental session. Near this point of system failure due to fatigue, there was a rapid increase in all stimulus durations delivered, even though the desired force remained constant (Figure 3.2, at $t \approx 300$ s). This information could be useful in designing online safety measures. After the initial transient response, one may be able to compare the derivative of the desired force with the derivative of delivered stimulus durations and make a judgment as to the safety of continued stimulation. The results from the open-loop comparison test (Figure 3.3) reinforce the conclusion that static stimulation strengths will not produce a constant force over long periods of time, and that a closed-loop strategy is required to evoke precise steps in muscle force.

Sinusoidal target force trajectories up to 2 Hz were evoked with low amplitude error after optimization of the proportional controller gain (Figure 3.4). These amplitude optimized responses did show a consistent time lag of approximately 300 ms across all tested sinusoidal target trajectories, which is not substantially different from normal human reaction rates of 200 ms [36]. Arbitrary-shaped, isometric, target forces were also evoked with small amplitude error and time delay similar to those found for the sinusoidal target trajectories. This type of control will be particularly important for upper limb motions such as reaching and grasping, which are often more arbitrary than lower limb movements, as well as for arbitrary movements of the lower limbs themselves.

The control strategy developed here relied on accurate knowledge of the time from stimulation to the peak evoked twitch-force, T_{pf}, for each electrode in use. Although there was some statistically significant variability in T_{pf} during a stimulation train, the overall variability was quite low when compared to mean values, and this variability did not appear to affect the closed-loop results. Closed-loop stimulation was performed at 10 Hz, but the controller used T_{pf} values determined from initial 8-Hz stimulation tests because of the difficulty in extracting single-stimuli responses from higher-frequency stimulation. Although statistically significant differences were found for mean T_{pf} values across the three tested stimulation frequencies, the differences were quite small and did not appear to affect the closed-loop results.

Improvements to closed-loop system responses, such as a reduction in time and phase delay for time-varying desired force trajectories, may be achievable by using more sophisticated nonlinear, adaptive, and optimal control strategies, which have been extensively studied for SISO control of FES-based motor neuroprostheses [21, 25, 26, 27, 28]. Adding some level of predictive feedforward control [37, 38] would also likely add improvements to the system response because there is an inherent response delay due to the fact that the controller is always sampling one cycle of stimulation backward in time. Methods of modulating the phasing of time between stimulations via multiple electrodes to reduce steady-state ripple have been proposed and tested [3, 39], but would present additional challenges in creating a closed-loop controller that modulates both the stimulus durations and stimulation phasing of asynchronous IFMS. A sliding mode asynchronous IFMS controller is currently in development, and future controllers will be examined for closed-loop, lower limb, joint angle control with varied loading conditions and disturbances. These controllers will then be extended to more complex multiple muscle and multiple joint control.

The ability to obtain meaningful results using an animal with a chronically implanted USEA is an important outcome of these experiments confirming and extending the successful chronic use of USEAs for single-electrode stimulation and recording [40, 41]. All prior IFMS studies using a USEA have been performed on animals immediately after array implantation. Many of the electrodes whose stimulation activated plantar-flexor muscles during the experiments 37 days post-USEA implantation also activated plantar-flexor muscles during the experiments 28 days later, and four electrodes (out of six) were used during both closed-loop experimental sessions. Minimizing the time required for initialization processes (twitch-force recruitment curve mapping, axonal activation overlap, T_{pf} determination, and controller gain optimization) is of critical importance to making a clinically viable, closed-loop, IFMS-based, motor neuroprosthesis, and future work will investigate how much of this lengthy initialization is required for each experimental session on a single chronic animal preparation.

Conclusion

This paper demonstrated the first successful implementation of a closed-loop MISO controller for asynchronous IFMS delivered via a chronically implanted USEA. Although this study only looked at isometric force trajectories, the ability to evoke target force trajectories with high accuracy and short time delay suggests that our control strategy can provide a basis for designing future robust IFMS controllers for complex limb movements. This work is an important step towards creating a clinically viable, fatigue-resistant, IFMS-based, motor neuroprosthesis for patients who have lost motor function due to stroke or spinal cord injury.

References

[1] D. McDonnall, G. Clark, and R. A. Normann, "Interleaved, multisite electrical stimulation of cat sciatic nerve produces fatigue-resistant, ripple-free motor responses," *IEEE Transactions on Neural Systems and Rehabilitation Engineering*, vol. 12, no. 2, pp. 208–215, Jun. 2004.

[2] K. Yoshida and K. Horch, "Reduced fatigue in electrically stimulated muscle using dual channel intrafascicular electrodes with interleaved stimulation," *Annual Review of Biomedical Engineering*, vol. 21, pp. 709–714, Nov. 1993.

[3] A. K. Wise, D. L. Morgan, J. E. Gregory, and U. Proske, "Fatigue in mammalian skeletal muscle stimulated under computer control," *Journal of Applied Physiology*, vol. 90, no. 1, pp. 189–197, Jan. 2001.

[4] N. M. Malesevic, L. Z. Popovic, L. Schwirtlich, and D. B. Popovic, "Distributed low-frequency functional electrical stimulation delays muscle fatigue compared to conventional stimulation," *Muscle and Nerve*, vol. 42, no. 4, pp. 556–562, Jul. 2010.

[5] M. Thomsen and P. H. Veltink, "Influence of synchronous and sequential stimulation on muscle fatigue," *Medical and Biological Engineering and Computing*, vol. 35, no. 3, pp. 186–192, May 1997.

[6] A. Branner, R. B. Stein, and R. A. Normann, "Selective stimulation of cat sciatic nerve using an array of varying-length microelectrodes," *Journal of Neurophysiology*, vol. 85, no. 4, pp. 1585–1594, Apr. 2001.

[7] W. L. C. Rutten, "Selective electrical interfaces with the nervous system," *Annual Review of Biomedical Engineering*, vol. 4, pp. 407–452, Aug. 2002.

[8] X. Navarro, T. B. Krueger, N. Lago, S. Micera, T. Stieglitz, and P. Dario, "A critical review of interfaces with the peripheral nervous system for the control of neuroprostheses and hybrid bionic systems," *Journal of the Peripheral Nervous System*, vol. 10, no. 3, pp. 229–258, Sep. 2005.

[9] T. Boretius, J. Badia, A. Pascual-Font, M. Schuettler, X. Navarro, K. Yoshida, and T. Stieglitz, "A transverse intrafascicular multichannel electrode (time) to interface with the peripheral nerve," *Biosensors and Bioelectronics*, vol. 26, no. 1, pp. 62–69, Sep. 2010.

[10] R. Riener, J. Quintern, and G. Schmidt, "Biomechanical model of the human knee evaluated by neuromuscular stimulation," *Journal of Biomechanics*, vol. 29, no. 9, pp. 1157–1167, Sep. 1996.

[11] F. E. Zajac, "Muscle and tendon: properties, models, scaling, and application to biomechanics and motor control," *CRC Critical Reviews in Bioengineering*, vol. 17, no. 4, pp. 359–411, 1989.

[12] J. M. Hausdorff and W. K. Durfee, "Open-loop position control of the knee joint using electrical stimulation of the quadriceps and hamstrings," *Medical and Biological Engineering and Computing*, vol. 29, no. 3, pp. 269–280, May 1991.

[13] J. Bobet, R. B. Stein, and M. N. Oguztoreli, "A linear time-varying model of force generation in skeletal muscle," *IEEE Transactions on Biomedical Engineering*, vol. 40, no. 10, pp. 1000–1006, Oct. 1993.

[14] L. A. Bernotas, P. E. Crago, and H. J. Chizeck, "A discrete-time model of electrically stimulated muscle," *IEEE Transactions on Biomedical Engineering*, vol. 33, no. 9, pp. 829–838, Sep. 1986.

[15] P. M. H. Rack and D. R. Westbury, "The effect of length and stimulus rate on tension in the isometric cat soleus muscle," *The Journal of Physiology*, vol. 204, no. 2, pp. 443–460, Oct. 1969.

[16] Y. Giat, J. Mizrahi, and M. Levy, "A musculotendon model of the fatigue profiles of paralyzed quadriceps muscle under fes," *IEEE Transactions on Biomedical Engineering*, vol. 40, no. 7, pp. 664–674, Jul. 1993.

[17] D. A. Gordon, R. M. Enoka, and D. G. Stuart, "Motor-unit force potentiation in adult cats during a standard fatigue test," *The Journal of Physiology*, vol. 421, pp. 569–582, Feb. 1990.

[18] Z. Z. Karu, W. K. Durfee, and A. M. Barzilai, "Reducing muscle fatigue in fes applications by stimulating n-let pulse trains," *IEEE Transactions on Biomedical Engineering*, vol. 42, no. 8, pp. 809–817, Aug. 1995.

[19] F. Parmiggiani and R. B. Stein, "Nonlinear summation of contractions in cat muscles," *Journal of General Physiology*, vol. 78, no. 3, pp. 277–311, Sep. 1981.

[20] T. G. Sandercock, "Nonlinear summation of force in cat soleus muscle results primarily from stretch of the common-elastic elements," *Journal of Applied Physiology*, vol. 89, no. 6, pp. 2206–2214, Dec. 2000.

[21] S. Jezernik, R. G. V. Wassinik, and T. Keller, "Sliding mode closed-loop control of fes: controlling the shank movement," *IEEE Transactions on Biomedical Engineering*, vol. 51, no. 2, pp. 263–272, Feb. 2004.

[22] B. Lau, L. Guevremont, and V. Muschawar, "Strategies for generating prolonged functional standing using intramuscular or intraspinal microstimulation," *IEEE Transactions on Neural Systems and Rehabilitation Engineering*, vol. 15, no. 2, pp. 273–285, Jun. 2007.

[23] D. B. Popovic, R. B. Stein, R. Jovanovic, R. Dai, A. Kostov, and W. W. Armstrong, "Sensory nerve recording for closed-loop control to restore motor function," *IEEE Transactions on Biomedical Engineering*, vol. 40, no. 10, pp. 1024–1031, Oct. 1993.

[24] K. Yoshida and K. Horch, "Closed-loop control of ankle position using muscle afferent feedback with functional neuromuscular stimulation," *IEEE Transactions on Biomedical Engineering*, vol. 43, no. 2, pp. 167–176, Feb. 1996.

[25] H. J. Chizeck, P. E. Crago, and L. S. Kofman, "Robust closed-loop control of isometric muscle force using pulsewidth modulation," *IEEE Transactions on Biomedical Engineering*, vol. 35, no. 7, pp. 510–517, Jul. 1988.

[26] L. A. Bernotas, P. E. Crago, and H. J. Chizeck, "Adaptive control of electrically stimulated muscle," *IEEE Transactions on Biomedical Engineering*, vol. 34, no. 2, pp. 140–147, Feb. 1987.

[27] P. H. Veltink, H. J. Chizeck, P. E. Crago, and A. El-Bialy, "Nonlinear joint angle control for artificially stimulated muscle," *IEEE Transactions on Biomedical Engineering*, vol. 39, no. 4, pp. 368–380, Apr. 1992.

[28] V. Nekoukar and A. Erfanian, "Adaptive terminal sliding mode control of ankle movement using functional electrical stimulation of agonist-antagonist muscles," *Proceedings of IEEE EMBS 2010, Beunos Aires, Argentina*, pp. 5448–5451, 2010.

[29] R. A. Normann, D. McDonnall, G. A. Clark, R. B. Stein, and A. Branner, "Physiological activation of the hind limb muscles of the anesthetized cat using the utah slanted electrode array," *Proceedings of the 2005 IEEE IJCNN*, vol. 5, pp. 3101–3108, Aug. 2005.

[30] S. D. Hiatt, A. M. Wilder, K. S. Guillory, B. R. Dowden, R. A. Normann, and G. A. Clark, "1100-channel neural stimulator for functional electrical stimulation using high-electrode-count neural interfaces," *Proceedings of IFESS 2010 in Artificial Organs*, vol. 34, no. 8, Aug. 2010.

[31] A. M. Wilder, S. D. Hiatt, B. R. Dowden, N. A. T. Brown, R. A. Normann, and G. A. Clark, "Automated stimulus-response mapping of high-electrode-count neural implants," *IEEE Transactions on Neural Systems and Rehabilitation Engineering*, vol. 17, no. 5, pp. 504–511, Aug. 2009.

[32] B. R. Dowden, M. A. Frankel, R. A. Normann, and G. A. Clark, "Non-invasive method for selection of electrodes and stimulus parameters for fes applications with intrafascicular arrays," *Journal of Neural Engineering*, vol. 9, no. 1, p. 016006, 2012.

[33] D. Kernell, O. Eerbeek, and B. A. Verhey, "Relation between isometric force and stimulus rate in cat's hindlimb motor units of different twitch contraction time," *Experimental Brain Research*, vol. 50, no. 2-3, pp. 220–227, May 1983.

[34] M. P. Murray, "Gait as a pattern of movement," *American Journal of Physical Medicine and Rehabilitation*, vol. 46, no. 1, pp. 290–333, Feb. 1976.

[35] R. A. Mann, G. T. Moran, and S. E. Dougherty, "Comparative electromyography of the lower extremity in jogging, running, and sprinting," *American Journal of Sports Medicine*, vol. 14, no. 6, pp. 501–510, Dec. 1986.

[36] A. T. Welford, *Reaction times*. New York, NY: Academic Press, 1980.

[37] P. E. Crago, N. Lan, P. H. Veltink, J. J. Abbas, and C. Kantor, "New control strategies for neuroprosthetic systems," *Journal of Rehabilitation Research and Development*, vol. 33, no. 2, pp. 158–172, Apr. 1996.

[38] J. J. Abbas and R. J. Triolo, "Experimental evaluation of an adaptive feedforward controller for use in functional neuromuscular stimulation systems," *IEEE Transactions on Rehabilitation Engineering*, vol. 5, no. 1, pp. 12–22, Mar. 1997.

[39] A. M. Wilder, R. A. Normann, and G. A. Clark, "Optimization of a tremor-reducing algorithm for asynchronous stimulation of independent motor-unit groups," *Proceedings of IFESS 2010 in Artificial Organs*, vol. 34, no. 8, Aug. 2010.

[40] G. A. Clark, N. Ledbetter, D. J. Warren, S. Towns, and R. A. Normann, "Chronic, emg-free unit recordings from utah slanted electrode arrays in cat sciatic nerve," *Society for Neuroscience Meeting Planner, Washington, D.C.*, p. 673.611, 2008.

[41] A. Branner, R. B. Stein, E. Fernandez, Y. Aoyagi, and R. A. Normann, "Long-term stimulation and recording with a penetrating microelectrode array in cat sciatic nerve," *IEEE Transactions on Biomedical Engineering*, vol. 51, no. 1, pp. 146–157, Jan. 2004.

CHAPTER 4

CLOSED-LOOP CONTROL OF PARALYZED LIMB MOTION USING ASYNCHRONOUS INTRAFASCICULAR MULTI-ELECTRODE STIMULATION

This chapter is a journal article in submission to the *IEEE Transactions on Biomedical Engineering*. Authors of this chapter are M.A. Frankel, V.J. Mathews, G.A. Clark, R.A. Normann, and S.G. Meek.

Abstract

Closed-loop control of asynchronous intrafascicular multi-electrode stimulation (aIFMS) of small independent populations of peripheral nerve motor axons can evoke selective, fatigue-resistant muscle forces. However, *a priori* determination of aIFMS parameters to generate precise muscle forces or limb motion is currently not possible and closed-loop feedback control methods are required. We previously developed a real-time proportional closed-loop control method for aIFMS generation of isometric muscle force. The present work extends and adapts this closed-loop controller to the more demanding task of dynamically controlling joint position in the presence of opposing joint torques. A proportional-integral-velocity controller, with integrator antiwindup strategies, was experimentally validated as a means to evoke precise joint-angle trajectories against various imposed joint torques. Experiments were conducted on an anesthetized feline with a Utah Slanted Electrode Array chronically implanted in the sciatic nerve. Motion about the hind-limb ankle joint was generated by activating fast-twitch plantar-flexor muscles. The controller was successful in evoking steps in joint position with 2.4 % overshoot, 2.3-s rise time, 4.5-s settling time, and near-zero steady-state error. Controlled step responses were consistent across changes in step size, stable against external disturbances, and reliable over

time. The controller was able to evoke smooth eccentric motion at joint velocities less than 16 deg./s, as well as sinusoidal trajectories with frequencies of less 0.1 Hz, with time delays less than 1.5 s. These experiments provide important insights towards creating a robust closed-loop aIFMS controller that can evoke precise fatigue-resistant motion in paralyzed individuals.

Introduction

There are more than one million people in the U.S. living with some level of spinal cord injury (SCI) [1]. Most SCIs result in at least partial paralysis, and many paralyzed individuals consider restoration of lost basic motor functions like grasping and walking as important behaviors that could improve their quality of life [2]. Functional neuromuscular stimulation (FNS) has been extensively investigated as a means to aid and restore lost motor function to paralyzed individuals, and clinical FNS-based devices have been in use for over 50 years [3, 4]. These clinical devices have provided benefit to paralyzed individuals [5], but their use has been limited by rapid muscle fatigue and poorly evoked movement kinematics [6, 7]. Most of the limitations can be attributed to the surface or intramuscular stimulating electrodes used, which achieve poor muscle selectivity and a low ability to grade muscle force output, making current clinical FNS-based systems behave like on/off stimulators [8].

Advances in high-electrode-count peripheral neural interfaces, such as the Utah Slanted Electrode Array (USEA) used in this study, have enabled the selective activation of small groups of motor-units within a single targeted muscle [9, 10]. Smoothly graded muscle forces can be generated by modulating the stimulus intensity delivered via a subset of selected implanted electrodes, which proportionally activate groups of motor-units within the targeted muscle. Relatively high-frequency electrical stimulation is required to evoke smooth tetanic muscle forces [11, 12, 13], and this leads to rapid muscle fatigue when the stimulation is delivered via a surface, epimysial, or extraneural electrode, or via a single stimulating intraneural electrode. However, smooth fatigue-resistant muscle forces can be evoked by asynchronously activating multiple small populations of motor unit groups within a single muscle

by stimulating via multiple intrafascicularly implanted microelectrodes at a low per-electrode frequency, but at a high composite stimulation frequency [12, 14, 15, 16]. This method of asynchronous intrafascicular multi-electrode stimulation (aIFMS) has been successfully accomplished using USEAs in acute and chronic studies [14, 17, 18] and provides a more biomimetic form of muscle activation than the stimulation strategies used in current clinical FNS-based neuroprostheses.

However, before an aIFMS system can become clinically viable for evoking coordinated movements, one must be able to control the stimulation parameters delivered via multiple selected electrodes. The dynamic muscle response to single electrode stimulation has been well studied, modeled, and used to create control algorithms [11, 19, 20, 21, 22, 23]. Unfortunately, these models do not extend well to multi-electrode stimulation because of currently unmodeled dynamics, such as axonal activation overlap between stimulating electrodes and the nonlinear combination of muscle forces evoked by the multiple stimulating electrodes [24]. FNS-based neuroprostheses also contain poorly modeled, nonlinear, time-varying processes such as potentiation and fatigue [25, 26]. Because of these issues, a priori determination of aIFMS parameters to evoke precise muscle forces or limb motion is currently not possible; hence, closed-loop control methods are required.

Recently, we developed a multiple-input, single-ouput (MISO) real-time closed-loop control method for determining aIFMS per-electrode stimulation intensities (stimulus pulse durations) to evoke precise, fatigue-resistant, isometric muscle forces in an anesthetized feline [17], a commonly used model of human paralysis. Because this work was successful in evoking isometric forces, it presented a foundation for extending the aIFMS control strategy to the necessary nonisometric muscle forces required for many real-world desired movements that involve dynamic limb motion.

In this study, we extend the force-feedback proportional control strategy to a proportional plus integral plus velocity controller (PIV) for joint-angle feedback control that includes integrator antiwindup strategies. To evaluate the controller used in this study, we selected desired trajectories (steps, ramps, and sinusoids) that were physiologically relevant to normal human lower-limb movements. Steps in desired position are relevant to the ability to hold a stance. Ramp trajectories are relevant

for controlled sit-to-stand and stand-to-sit (eccentric) motions. Periodic trajectories are relevant to gait movements. Physiological results are presented demonstrating the successful use of the controller to evoke steps in joint position of varying size and against varying oppositional torques, to produce smooth evoked ramped motion, and to track sinusoidal joint trajectories.

Methods

Surgical Preparation and Electrode Array Implantation

Experiments were conducted on an adult female feline using procedures approved by the University of Utah Institutional Animal Care and Use Committee. The animal was anesthetically induced with an intramuscular injection of Telazol (Fort Dodge Animal Health, Fort Dodge, USA) at a dosage of 10 mg/kg. The animal was then intubated and mechanically ventilated. Anesthesia was maintained with Isoflorane (Hospira, Lake Forest, USA) at a level of 0.5-1.5%. Fluid and blood sugar levels were maintained via an intravenous drip of lactated Ringer's solution at a rate of 10 ml/kg/hr. Vital signs were monitored and recorded every 15 minutes to assess the depth of anesthesia and animal status.

A 100-electrode USEA was chronically implanted in the left sciatic nerve [27, 28], and experiments were conducted 3.5 and 4 months post-implantation. Details of an earlier version of the USEA are described elsewhere [29]. The animal was placed on its right side on a heated foam pad and secured, schematically shown in Fig. 4.1. Because the animal was horizontal, there were no joint loading effects due to gravity. The only motion-resistive joint torque was provided by the ankle torque and angle control system, as schematically shown in Fig. 4.1. The left foot was secured via plastic zip ties to the rotating foot mounting plate so that the center of rotation of the ankle was concentric with the center of rotation of the foot mounting plate. The left knee was secured in a soft foam clamp to prevent knee rotation, and the animal was positioned so that the left knee was at 90 deg.

Stimulation and Recording Setup

Monophasic constant-voltage (-5 V) stimulation was delivered via USEA electrodes using a custom-built, multichannel stimulator, using stimulus pulse durations

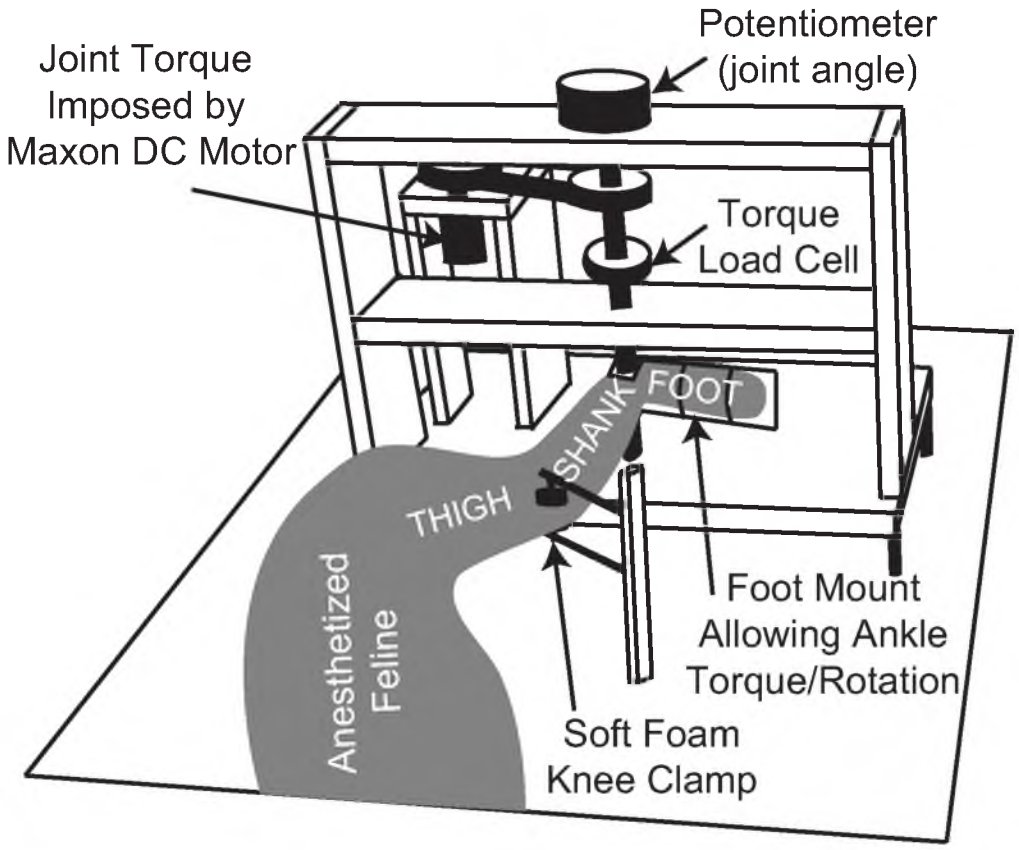

Figure 4.1: Ankle Torque and Angle Control System.

The animal's foot is secured to the rotating foot mounting plate, ensuring that the ankle joint is concentric with the plate's center of rotation. The system electronics and an Arduino microcontroller (not shown) are mounted in the back of the setup near the DC motor. The animal's right leg slides underneath the base of the apparatus, between this base and the main surgical table (not shown).

between 0.2 µs and 1024 µs with 0.2-µs resolution [30]. Stimulus pulse durations were controlled via custom MATLAB routines (The Mathworks, Natick, USA). Ankle joint torque was measured by an inline torque loadcell (TQ201-50, Omegadyne, Stamford, USA), and ankle angular position was measured by a high-precision potentiometer. For initial twitch-force recruitment mapping and axonal activation overlap determination (described below), the torque loadcell output was sampled at 10 kHz using a Cerebus multichannel data acquisition system (Blackrock Microsystems, Salt Lake City, USA).

For closed-loop tests, the joint-angle potentiometer output was sampled at 2 kHz using custom MATLAB software, via an NI PCI-6040E data acquisition card (National Instruments, Austin, USA). All presented data were postprocessed in MATLAB using a forward and backward 4th-order Butterworth low-pass filter with a 50-Hz cutoff frequency.

USEA Calibration

For initial USEA calibration [31, 32], the foot mounting plate was locked to ensure that all evoked muscle forces were isometric. The ankle angle was set at approximately 90 deg., which sets the fast-twitch ankle-plantar flexion calf muscles near an optimal force-generation length. Twitch-torque recruitment maps were generated for all electrodes that evoked a peak torque greater than 0.01 Nm in response to a single 512-µs stimulus. The pair-wise level of axonal activation overlap was then measured for all electrodes whose stimulation activated fast-twitch ankle plantar-flexion calf muscles [14, 31]. Six electrodes activating fast-twitch ankle plantar-flexion muscles with the least amount of axonal overlap were chosen for further experiments.

The control strategy used in this experiment required knowledge of the time from stimulation via each USEA electrode to the peak of the evoked twitch-torque response, and this time to peak response metric (T_{pr}) was measured for each of the six electrodes with the ankle joint-angle fixed at 90 deg. [17]. Because the closed-loop experiment involved nonisometric contractions, and because T_{pr} changes as the muscle length changes [33], the relationship between T_{pr} and ankle joint-angle was determined in early studies by measuring the T_{pr} for fast-twitch plantar-flexion

muscle fibers when the ankle was held fixed at different joint angles. Although the relationship found in [33] was nonlinear, our closed-loop controller used a linear equation that adjusted the expected T_{pr} for each stimulation from T_{pr} +5 ms when the joint-angle was 20 deg. to T_{pr} -5 ms when the joint-angle was 160 deg.

Controller Design and Closed-Loop Studies

For closed-loop experiments, the foot mounting plate was released, and a plantar-flexion resistive torque was generated by a geared DC motor (A-max 26, Maxon Precision Motors, Fall River, USA) controlled by a microcontroller (Arduino Uno, Smart Projects, Italy), schematically shown in Fig. 4.1. Asynchronous stimulation of six electrodes at a composite 60-Hz stimulation frequency was used for all closed-loop tests (10 Hz per electrode), and the stimulation phasing was set such that the predicted T_{pr} due to stimulation via each electrode would be 1/60 s after the predicted T_{pr} due to the stimulation via the prior electrode, thus equally spacing the predicted peak responses across each period of six-electrode stimulation.

The stimulus pulse duration that was just below the torque producing threshold, along with the lowest stimulus pulse duration that evoked the maximal twitch-torque, were determined from twitch-torque recruitment curves measured for each electrode. These were set as the minimum and maximum allowable stimulus pulse durations for each electrode, creating a bounded input system [17]. Twitch-torque recruitment curves are sigmoidal in shape and the maximal twitch-torque was determined as the point at which continued increases in stimulus pulse duration evoked no substantial increase in torque, denoted as the torque plateau in [31]. The slope of the twitch-torque recruitment curve between 20-80% of maximal twitch-torque (the 'linear' range) was also determined for each electrode, and this slope was used by the controller as a per-electrode gain (4.2) to normalize for different recruitment curve slopes amongst the six electrodes in use.

A real-time closed-loop aIFMS control strategy and system was previously created for evoking precise desired isometric forces [17]. This system was extended and adapted for these experiments to a dynamic motion PIV controller, schematically shown in Fig. 4.2.

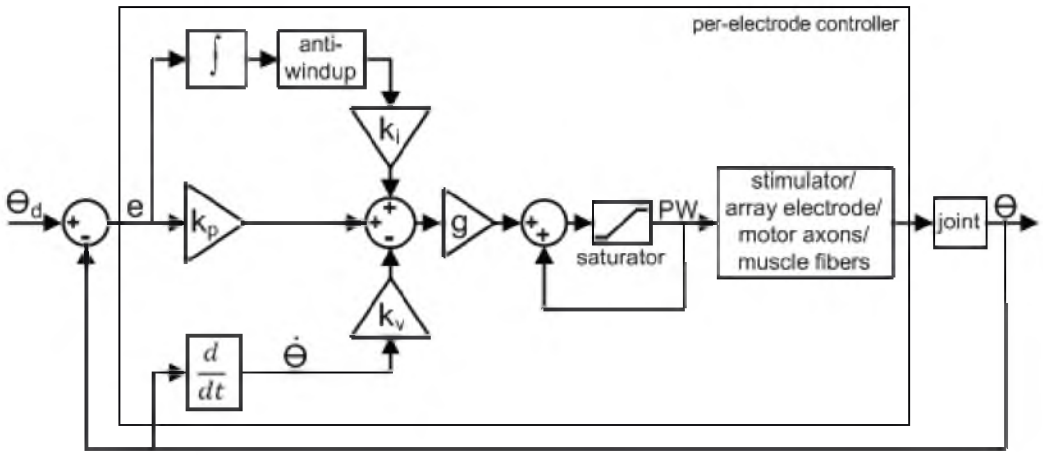

Figure 4.2: Block Diagram of Per-Electrode PIV Controller.

The proportional error gain, k_p, the joint velocity gain, k_v, and the integral of the error gain, k_i, are all constant linear terms. The per-electrode stimulus level, determined by the stimulus pulsewidth (PW), used during the previous cycle of stimulation is added to the controller regulated change in pulsewidth to determine the stimulus level delivered via that electrode during the subsequent stimulation cycle. The saturator is used to bound the system between a prethreshold stimulus level and a maximum allowable stimulus level.

The overall control law used for these experiments was

$$SD_{e,j+1} = SD_{e,j} + g_e \cdot \left[(k_p \cdot E_{e,j}) + \left(k_i \cdot \sum_{l=0}^{n} E_{e,j-l} \cdot \Delta t \right) - \left[k_v \cdot (\theta_{e,j} - \theta_{e,j-1}) / \Delta t \right] \right], \quad (4.1)$$

where $SD_{e,j}$ is the stimulus pulse duration for the eth electrode during the jth stimulation cycle, k_p is the proportional gain, k_i is the integral gain, k_v is the velocity gain, $E_{e,j}$ is the joint-angle error determined by (4.3), $\theta_{e,j}$ is the joint-angle position, g_e is an additional gain factor based on experimentally determined recruitment-curve slopes for each electrode determined by (4.2), and Δt is the time step between per-electrode stimulations (100 ms). The limit of summation, n, was initially set to j-1, which allows for complete integration across all error samples. Adjustments to this limit, which provided closed-loop response improvements, will be described below.

Similarly to what was done for force-feedback control in [17], the additional per-electrode gain was determined as

$$g_e = log_{10}(1/s_e), \quad (4.2)$$

where s_e is the slope of the per-electrode twitch-torque recruitment curve over 20-80% of maximal twitch-torque. After g_e was determined for all electrodes, the values were normalized to the largest value, giving g_e values of 0.5-1.0. Also similar to what was done in [17], the per-electrode error was determined as

$$E_{e,j} = \left(\sum_{k=T_{pr_{e,j}}-w}^{k=T_{pr_{e,j}}+w} [\theta_d(k) - \theta_m(k)] \right) / (2w+1), \quad (4.3)$$

where θ_d is the desired joint-angle position, θ_m is the measured joint-angle position, $2w$+1 is the length of the sampling window over which the error function is evaluated, where w was set to 5 ms of samples in all experiments, and $T_{pr_{e,j}}$ is the predicted time of peak twitch-torque for the eth electrode during the jth cycle of stimulation (expressed in samples). The joint-angle position in (4.1), $\theta_{e,j}$, was determined as the mean of θ_m, determined over the same sampling window used in (4.3).

To tune the PIV controller, i.e., to determine the controller gains k_p, k_v, and k_i, a 30-deg. step in ankle angle was used as the desired joint-angle trajectory with an oppositional torque of 0.4 Nm and a 25-deg. ankle joint-angle starting position. First, using only proportional control, the proportional gain was slowly increased to drive the system from overdamped to highly underdamped kinetics with a fast, but stable, transient response. Second, using proportional-plus-velocity control (PV), the velocity gain was slowly increased until the system was near critically damped. This reduced the transient overshoot and decreased the settling time. The velocity term in (4.1) is made negative because the dampening is created by opposing the speed of the motion; thus, increased velocity results in decreased stimulus intensity. Finally, using proportional-plus-velocity-plus-integral control (PIV), the integrator gain was slowly increased to speed up the initial transient response until the overshoot reached 10%. In these experiments, the integrator was used to speed up the initial transient response and drive the steady-state error toward zero for desired step motions, but the increased response speed can come at the cost of large overshoot due to integrator windup.

Integrator windup often occurs when there is a large rapid change in a desired response, e.g., during a stepped change in the desired response, and the integral of the error accumulates substantially during the rising phase of the closed-loop system response, often causing large overshoot that is not released until the integrator is unwound by error in the opposite direction. In our system, additional integrator windup occurred because of the inherent delay in the system due to the controller looking one full cycle backward in time, and because the initial stimulus intensity was prethreshold, requiring time for the controller to increase the stimulus intensity high enough to overcome the oppositional loading torque.

To reduce the integrator windup, the integrator was then made leaky, in effect turning the integrator into a lag compensator. This was done by dropping out early acquired error values from the numerical integration, i.e., only the N most recently acquired error values were summed; $n = N-1$ in (4.1). The value of N was empirically determined to be 8 error samples (800 ms) because this created a near critically-damped response. Also, because reduction in joint position was based solely on the

relaxation of muscle fibers against the joint loading torque, the integrator tended to cause an oscillatory response, which was reduced by removing the integrator for error values less than zero, i.e., when the evoked response was greater than the desired response. These improvements were implemented by modifying the control law of (4.1) so that the limit of summation, n, was set to 7, and by setting $k_i = 0$ when $E_{e,j} < 0$.

Various step sizes from 15 deg. to 75 deg. were tested along with various loading torques ranging from 0.2 Nm to 0.8 Nm, using the tuned PIV closed-loop controller gains and the adapted control law of (4.1) as described above. For these desired step responses, the closed-loop system was experimentally evaluated for the overall evoked joint position percent overshoot, rise time, time-to-peak, settling time, and steady-state error. Percent overshoot ($\%OS$) was measured as the percent difference between the peak evoked position and the mean position during the last half-second of stimulation (steady-state position). Rise time (T_r) was measured as the time from step onset to when the system reached 90% of the steady-state position. Time-to-peak (T_p) was measured as the time from the step onset to when the system reached the peak evoked position. Settling time (T_s) was measured as the time from the step onset to when the system settled to within $\pm 2\%$ of the steady-state position. Steady-state error (SSE) was measured as the difference between the steady-state position and the desired step position.

The controller was additionally tested for time-varying joint-angle trajectories. For desired ramp-up, hold, then ramp-down joint trajectories ranging from 2 deg./s to 64 deg./s, the closed-loop system was experimentally evaluated for time delay and amplitude error. After each trial, both the evoked ramp-up phase and the evoked ramp-down phase were shifted backward in time until the sum of the squared per-sample difference between the time-shifted evoked response and the desired joint-angle trajectory was a minimum. This time shift was evaluated as a time delay parameter (T_d) of the closed-loop system. Amplitude error (E_a) was also used as a performance metric and was determined as the per-sample difference between the time-shifted evoked response and the desired joint position [17].

For desired sinusoidal joint trajectories, the closed-loop system was experimentally evaluated for time delay (T_d), phase delay (Φ_d), and peak-to-peak response amplitude for 0.05-Hz to 0.4-Hz trajectories, which are well within the bounds of normal periodic human lower limb movements [34]. The analysis was done by estimating the components of the evoked response waveform that was correlated with the desired trajectory using a least-squares method.

Results

PIV Gain Tuning

The performance of the joint-angle feedback control system was first studied using proportional-only control. Although proportional-only control had previously proved successful for controlling isometric contractions [17], it was insufficient for the more demanding kinematic behavior here. The proportional control (P control) closed-loop system response for several values of the proportional gain, k_p, is displayed in Fig. 4.3. Using a loading torque of 0.4 Nm, the P-gain was tuned until the system showed a highly underdamped response with $T_r = 1.18$ s, $T_p = 2.4$ s, and $\%OS = 55$ %. Because the response never fully reached a steady-state, the steady-state position was estimated to calculate rise time. This steady-state estimate was determined as the middle position between the last two evoked response peaks.

Velocity control was then added to the controller (PV control) to reduce the transient overshoot and oscillatory behavior caused by the large proportional gain. The PV closed-loop system response for various values of the velocity gain, k_v, is shown in Fig. 4.4, with k_p held constant at 8.0 µs/deg. The velocity gain was tuned until the system was nearly critically damped, yielding a response with $T_r = 2.95$ s, $T_p = 6.13$ s, $\%OS = 0.3$ %, and $SSE = 0.63$ % or 0.19 deg.

Integral control was then added to the controller (PIV control) to speed up the transient response and ensure that the steady-state error stays near zero. The PIV closed-loop system response for increasing values of the integrator gain, k_i, is presented in Fig. 4.5, with k_p held constant at 8.0 µs/deg. and k_v held constant at 10 µs/(deg./s). The integrator gain was tuned to produce a faster system response, $T_r = 1.95$ s, but with transient overshoot of 11.4 %. To reduce settling time, the integrator

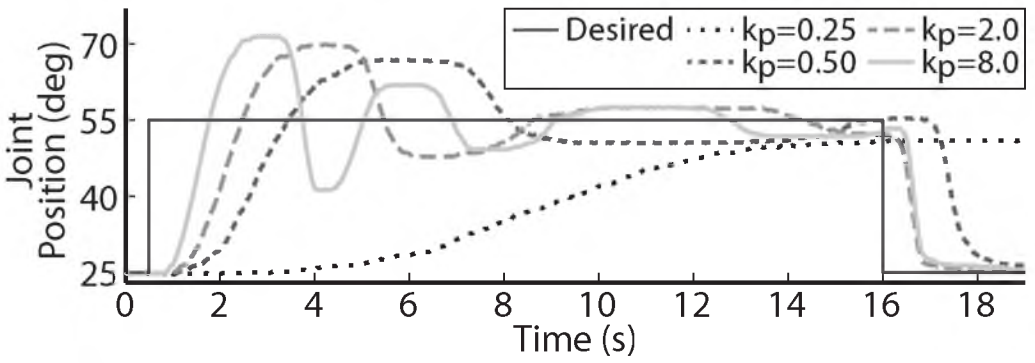

Figure 4.3: P-Controller Gain Tuning.

The joint position response to proportional-only control with a 0.4-Nm loading torque. Changes in the closed-loop system response are shown for increases in the proportional gain, k_p (µs/deg.). At very low values of k_p, the system was under-damped. As k_p was increased to a maximum value of 8.0 µs/deg., the closed-loop response became faster, $T_r = 1.18$ s, $T_p = 2.4$ s, but with substantial overshoot, $\%OS = 55$ %.

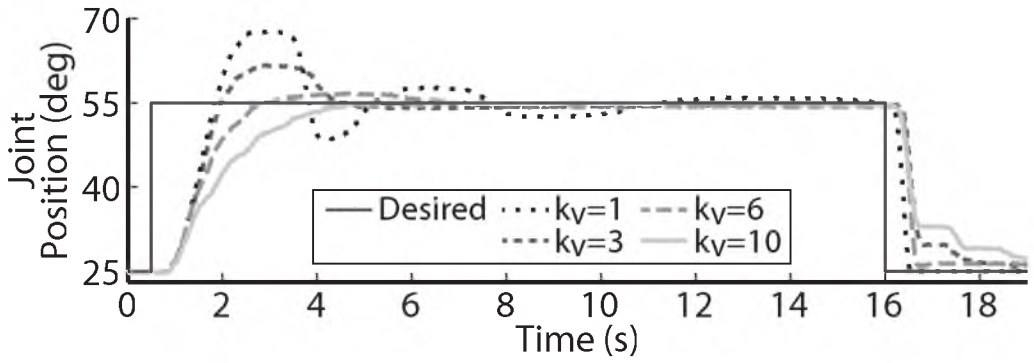

Figure 4.4: PV-Controller Gain Tuning.

The joint position response to proportional-plus-velocity (PV) control with a 0.4-Nm loading torque. Changes in the closed-loop system response are shown for increases in the velocity gain, k_v [µs/(deg./s)], with the proportional gain set at $k_p = 8.0$ µs/deg. As the velocity gain was increased, the transient overshoot and oscillatory behavior were reduced, $\%OS = 0.3$ %, but the rise time was slowed, $T_r = 2.95$ s.

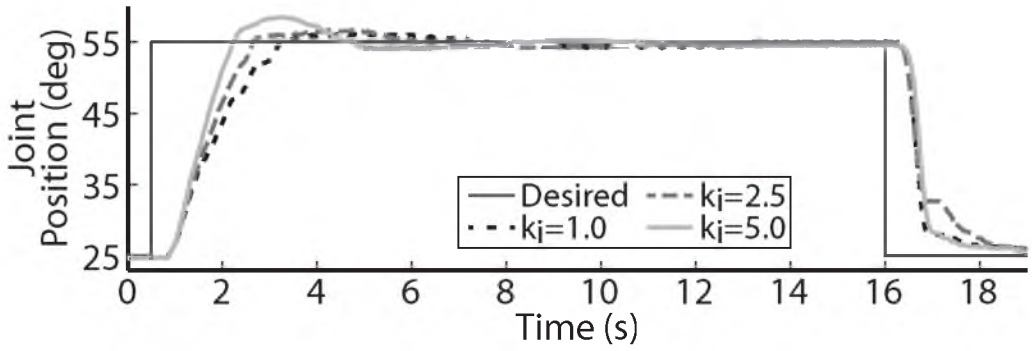

Figure 4.5: PIV-Controller Gain Tuning.

The joint position response to proportional-plus-velocity-plus-integral (PIV) control with a 0.4-Nm loading torque. Changes in the closed-loop system response are shown for increases in the integrator gain, k_i [µs/(deg.·s)], with the proportional gain set at $k_p = 8.0$ µs/deg. and the velocity gain set at $k_v = 10.0$ µs/(deg./s). As the integrator gain was increased, the initial system response became faster, $T_r = 1.95$ s, but there was an increase in overshoot, $\%OS = 11.4$ %.

was turned off when the error was less than zero (descending motion). This resulted in the settling time decreasing from 6.98 s to 6.02 s without affecting any other response metrics. The integrator was then made leaky to deal with integrator windup, i.e., only the 8 most recently acquired error values were numerically integrated, and only when the error was greater than zero. The tuned PIV closed-loop system response is demonstrated in Fig. 4.6 with the following response characteristics: T_r = 2.28 s, T_p = 4.22 s, T_s = 4.5 s, $\%OS$ = 2.4 %, and near-zero SSE, using the following controller gains: k_p = 8.0 µs/deg., k_v = 10.0 µs/(deg./s), k_i = 5.0 µs/(deg.·s). During desired descending motion, i.e., when the error was less than zero, the system was controlled by only two strongly opposing parts, the proportional and velocity control terms. The proportional control strongly turns down the stimulus pulse durations, causing rapid muscle relaxation and descending movement. However, the velocity control then acts to dampen this rapid motion by increasing the stimulus pulse durations. This control led to the evoked stepped descending motion seen in Fig. 4.6.

Controller Robustness

Using the tuned PIV controller gains, the robustness of the controlled response to various step sizes and loading torques was tested along with the ability of the controller to reject disturbance torques. As well, the reliability of the controlled response over experimental sessions was tested using the same six electrodes and controller gains. The PIV-controlled response for a 30-deg. desired step with increasing loading torques is displayed in Fig. 4.7. At very low loading torque of 0.2 Nm, the PIV-controlled response showed T_r = 1.92 s, T_p = 4.97 s, T_s = 7.44 s, $\%OS$ = 7.6 %. As the loading torque increased to 0.6 Nm, the controlled response took longer, T_r = 2.3 s, T_p = 4.7 s, T_s = 8.4 s, and had more overshoot, $\%OS$ = 15.63 %.

The PIV-controlled response for several desired step sizes against a loading torque of 0.4 Nm, and with a starting position of 25 deg., is presented in Fig. 4.8. The system response to a desired step size of 15 deg., 30 deg., and 45 deg. was similar: T_r = 2.07 ± 0.12 s (mean ± standard deviation), T_p = 3.66 ± 0.32 s, T_s = 6.67 ± 0.15 s, $\%OS$ = 13.96 ± 0.26 %. For the 60-deg. desired step, the system response had similar rise characteristics, T_r = 1.77 s, $\%OS$ = 10.4 %, but was slow in settling, T_s = 11.01 s.

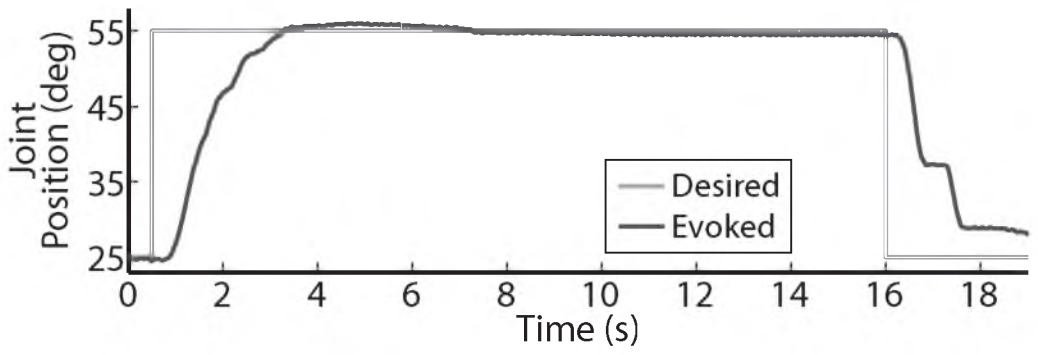

Figure 4.6: Fully-Tuned PIV-Controlled Step Response.

The joint position response to the tuned PIV controller, $k_p = 8.0$ µs/deg., $k_v = 10.0$ µs/(deg./s), and $k_i = 5.0$ µs/(deg.·s), with included integrator improvements, and against a 0.4-Nm loading torque. Removing the integrator when the error was less than zero and making the integrator leaky reduced the settling time to $T_s = 4.5$ s and the overshoot to $\%OS = 2.4$ %, while keeping $T_r = 2.28$ s, $T_p = 4.22$ s.

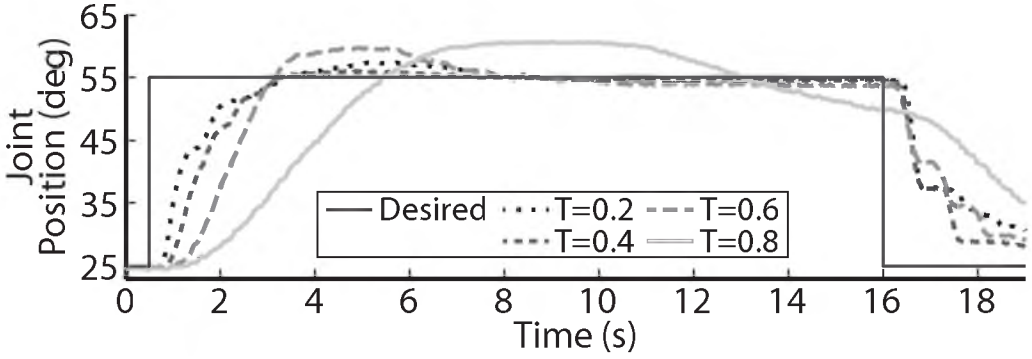

Figure 4.7: Robustness of the PIV-Controlled Step Response when Loading Torque Changes.

The PIV-controlled response to increasing oppositional loading torques (T, measured in Nm). As more load was applied to the ankle, the system required more windup to evoke enough force to generate motion. This windup resulted in delayed response and more overshoot, even with employed antiwindup strategies. At the highest loading tested, 0.8 Nm, the system was unable to settle to a steady-state value because the activated muscle fibers began fatiguing and the maximal stimulation level was reached.

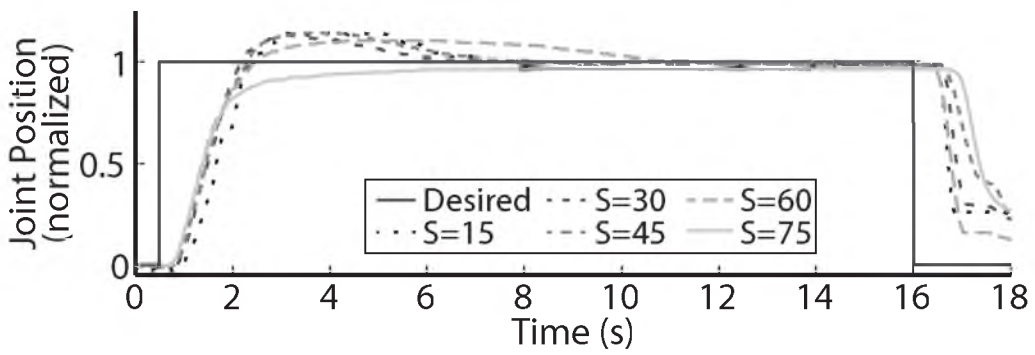

Figure 4.8: Robustness of the PIV-Controlled Step Response when Step Size Changes.

The normalized PIV-controlled response to various sizes of the desired step in joint position (S, measured in deg.) against a 0.4-Nm loading torque. The system started at 25 deg. and the controlled response was similar across different achievable step sizes. The system had difficulty achieving a 25-deg. to 100-deg. step, even with maximal stimulation.

The closed-loop system was unable to achieve a 75-deg. desired step (25 deg. to 100 deg.), even with maximal stimulation.

The closed-loop controller was successful in responding to applied disturbance torques, as demonstrated in Fig. 4.9. The system response was initially allowed to settle against a loading torque of 0.4 Nm and then the loading torque was increased to 0.6 Nm at t = 16 s. The increased load was maintained for 15 s and then the loading torque was decreased from 0.6 Nm to 0.4 Nm. When the load was initially applied,the system settled in 1.88 s with near-zero overshoot. When the load was removed, the system settled in 5.56 s, also with near-zero overshoot.

Using the same six electrodes and PIV controller gains, the closed-loop controlled response remained consistent over time, as shown in Fig. 4.10. When tested with a 30-deg. step in joint position against a 0.4-Nm load, the initial response, the response 5 hours later during the same experiment, and the response during a subsequent experiment 19 days later were similar, $T_r = 2.07 \pm 0.19$ s, $T_p = 4.13 \pm 0.16$ s, $T_s = 6.68 \pm 0.45$ s, $\%OS = 3.65 \pm 1.55$ %.

The PIV controller was tested to the limit where activated muscle fibers showed strong fatigue, as presented in Fig. 4.11. The fatigue-resistance of aIFMS has been well shown [14, 18], but it is not fatigue-preventing. Over time, as activated muscle fibers fatigued, the overall evoked joint torque was not enough to hold the desired joint position. As shown in Fig. 4.11b, the controller responded by increasing the delivered stimulation intensities to the six electrodes so that the desired joint position was maintained until the activated muscle fibers were no longer able to evoke enough joint torque to resist the 0.4-Nm loading torque, even with maximal stimulation.

Time-varying Trajectories

The closed-loop PIV controller was able to evoke time-varying ramped joint-angle trajectories with slopes ranging from 2 deg./s to 64 deg./s against a 0.4-Nm loading, as presented in Table 4.1. The controlled response was smooth and accurate for slower ramp speeds, such as the 4-deg./s trajectory shown in Fig. 4.12a, with small amplitude error and short time delay for both the ramp-up ($E_a = 0.21 \pm 1.02$ deg., T_d = 1.25 s) and the ramp-down phases (E_a = -0.24 $\pm$ 0.98 deg., T_d = 1.45 s).

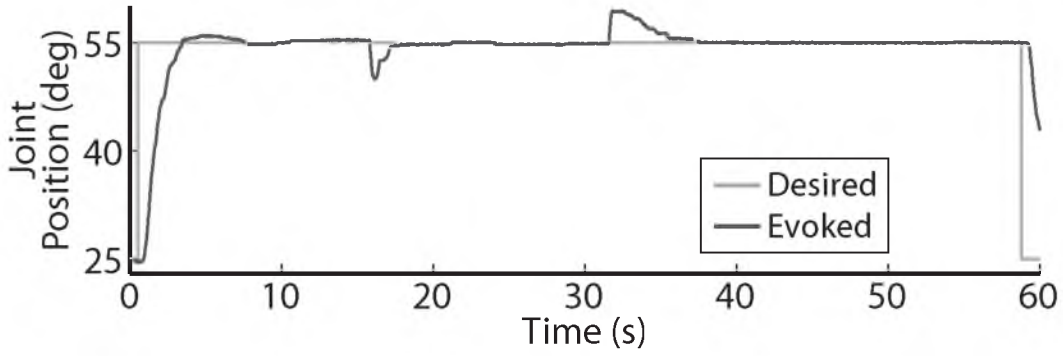

Figure 4.9: Robustness of the PIV-Controlled Step Response when External Disturbance Torques Are Applied.

The PIV controller was successful in responding to disturbance torques. The initial loading torque of 0.4 Nm was increased to 0.60 Nm at $t = 16$ s, held for 15 s, and then lowered back to 0.4 Nm at $t = 31$ s. The controller was able to drive the response back to steady-state when the disturbance torque was added and removed.

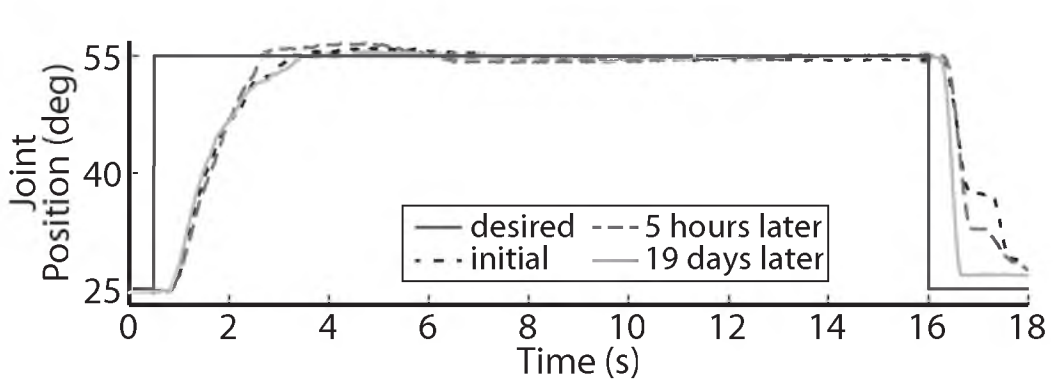

Figure 4.10: Reliability of the PIV-Controlled Step Response over Time.

Using the same six electrodes and PIV controller gains, the closed-loop system response remained consistent over time during a single experiment and over experimental days.

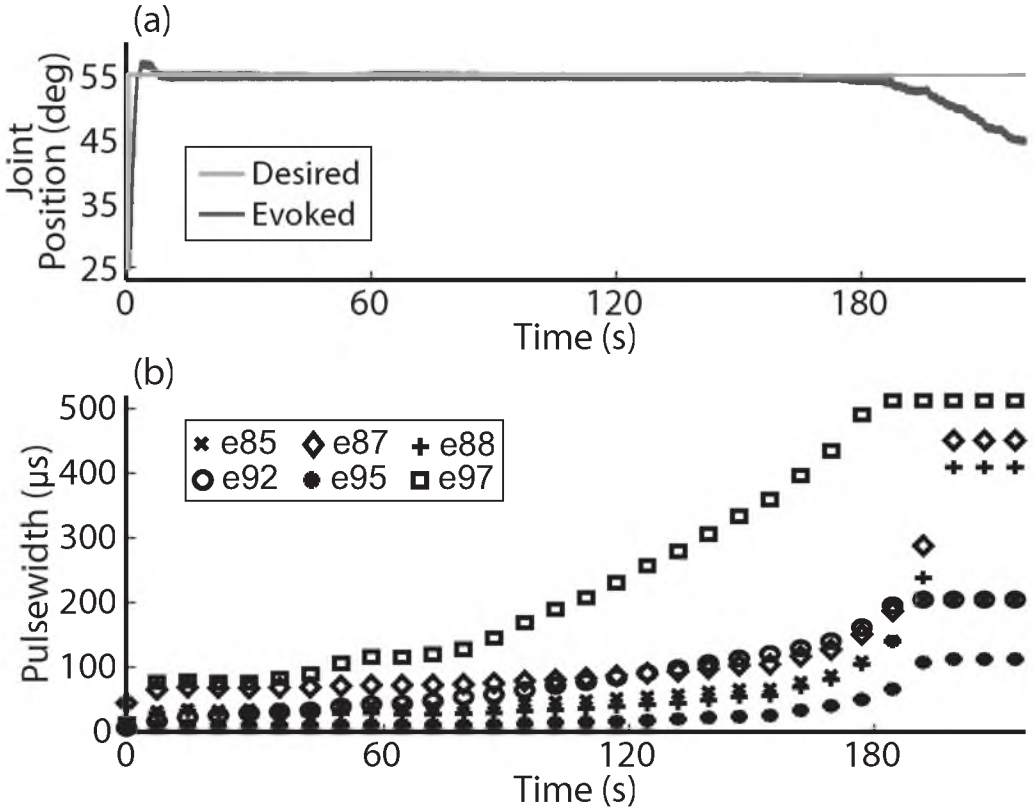

Figure 4.11: Modulation of Electrode Stimuli to Achieve and Hold a Desired Joint Position.

The PIV closed-loop controller successfully modulated per-electrode stimulation intensities (pulsewidth) to compensate for the effects of fatigue. Results are shown for a 30-deg. step in joint position, with 3-minutes of stimulation against a 0.4-Nm loading torque. (a) The activated muscle fibers began to fatigue and the controller compensated by increasing the stimulation intensity delivered via all six electrodes (b) to hold the desired joint position. Eventually, the activated muscle fibers were unable to evoke enough joint torque to hold the desired joint position against the loading torque, even with maximal stimulation.

Table 4.1: Error and Time Delay Across Ramped Motion Trials

Ramp Slope (deg./s)	Error Amplitude (deg., $\mu \pm SD$)	Time Delay (s)
+2	0.46 ± 0.81	0.74
+4	0.21 ± 1.02	1.25
+8	0.44 ± 1.25	1.25
+16	0.10 ± 1.28	1.30
+32	0.11 ± 2.33	1.31
+64	-0.12 ± 4.27	1.27
-2	-0.85 ± 0.49	1.07
-4	-0.24 ± 0.98	1.45
-8	-0.18 ± 2.07	1.44
-16	-0.59 ± 2.45	1.39
-32	-1.01 ± 2.53	1.29
-64	-0.24 ± 6.06	1.35

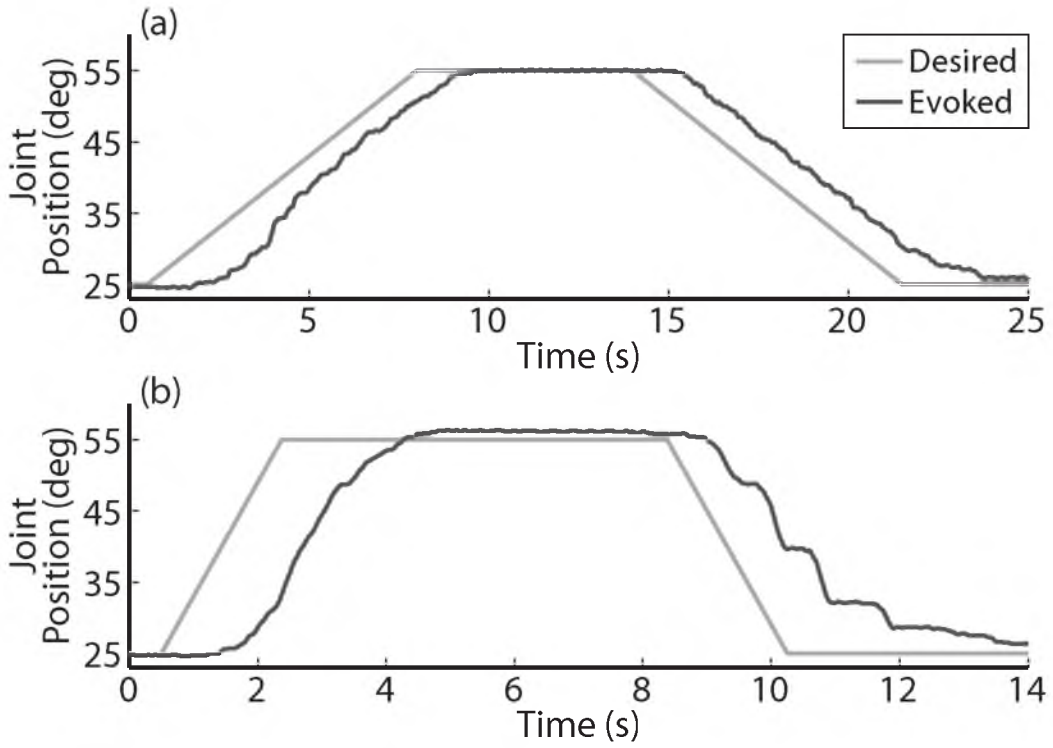

Figure 4.12: PIV-Controlled Ramped Joint Motion.

The PIV closed-loop controller evoked time-varying ramps in joint position. Results are shown for a 4-deg./s ramp in joint-angle (a) and a 16-deg./s ramp in joint-angle (b), against a 0.4-Nm loading torque. (a) The controller was able to evoke accurate and smooth joint position trajectories for slower moving desired ramp trajectories, with minimal time delay (T_d = 0.75 s). (b) Although the time delay did not increase for the faster desired ramp trajectory (T_d = 1.27 s), the error increased and the descending eccentric motion became stepped, similar to earlier desired step trajectories.

The time delay remained at approximately 1.3 s when the speed of the desired ramp trajectories increased, as shown in Table 4.1. However, the error of the controlled response increased and the smoothness of the evoked motion decreased, as shown in Table 4.1 and Fig. 4.12b. When the desired ramp speed reached 16 deg./s, the profile of the evoked response resembled that of desired steps (Fig. 4.6), with a rapid rise and slower settling phase for the ramp-up and a more stepped response for the ramp-down.

The closed-loop PIV controller was also able to evoke time-varying sinusoidal joint-angle trajectories with frequencies ranging from 0.05 Hz to 0.4 Hz against a 0.4-Nm loading torque, as displayed in Table 4.2. The controller accurately evoked a 0.05-Hz, 35-deg. to 60-deg. sinusoidal joint-angle trajectory with small time and phase delay (T_d = 1.46 s, Φ_d = 26.4 deg.), as shown in Fig. 4.13a, using stimulation pulsewidths shown in Fig. 4.13b. The desired sinusoidal trajectories started 10 deg. from the torque-loaded 25-deg. starting position because during stimulation, the activated muscles and associated tendons stiffen, making it difficult for the low torque loading to rapidly force the joint back to the 25-deg. starting position, which can be seen by the flat valleys of the evoked response in Fig. 4.13a. The controller had difficulty evoking the full magnitude of the sinusoidal joint motion when the desired frequency increased, as shown in Fig. 4.14 and Table 4.2, and although the time delays decreased, the associated phase delay increased. This increased phase delay was expected because there will always be fixed inherent system delays, such as neuromuscular delays of approximately 35 ms from stimulation to peak response and 100-ms delay due to the controller sampling one stimulation cycle backwards in time.

Discussion

The results presented in this paper demonstrate that tracking of desired step, ramp, and sinusoidal joint-angle trajectories can be successfully achieved with real-time joint-angle feedback control of aIFMS. This demonstration is important because although prior experiments evoked precise time-varying isometric muscle force trajectories [17], many real-world motions involve the generation of dynamic nonisometric

Table 4.2: Time Delay, Phase Delay, and Evoked Magnitude Across Sinusoidal Motion Trials

Desired Frequency(Hz)	Time Delay (s)	Phase Delay (deg.)	Evoked Peak-Peak Magnitude (deg.)
0.05	1.46	26.4	25.12
0.1	1.22	43.9	22.09
0.2	0.99	69.4	15.62
0.4	0.79	113.8	8.78

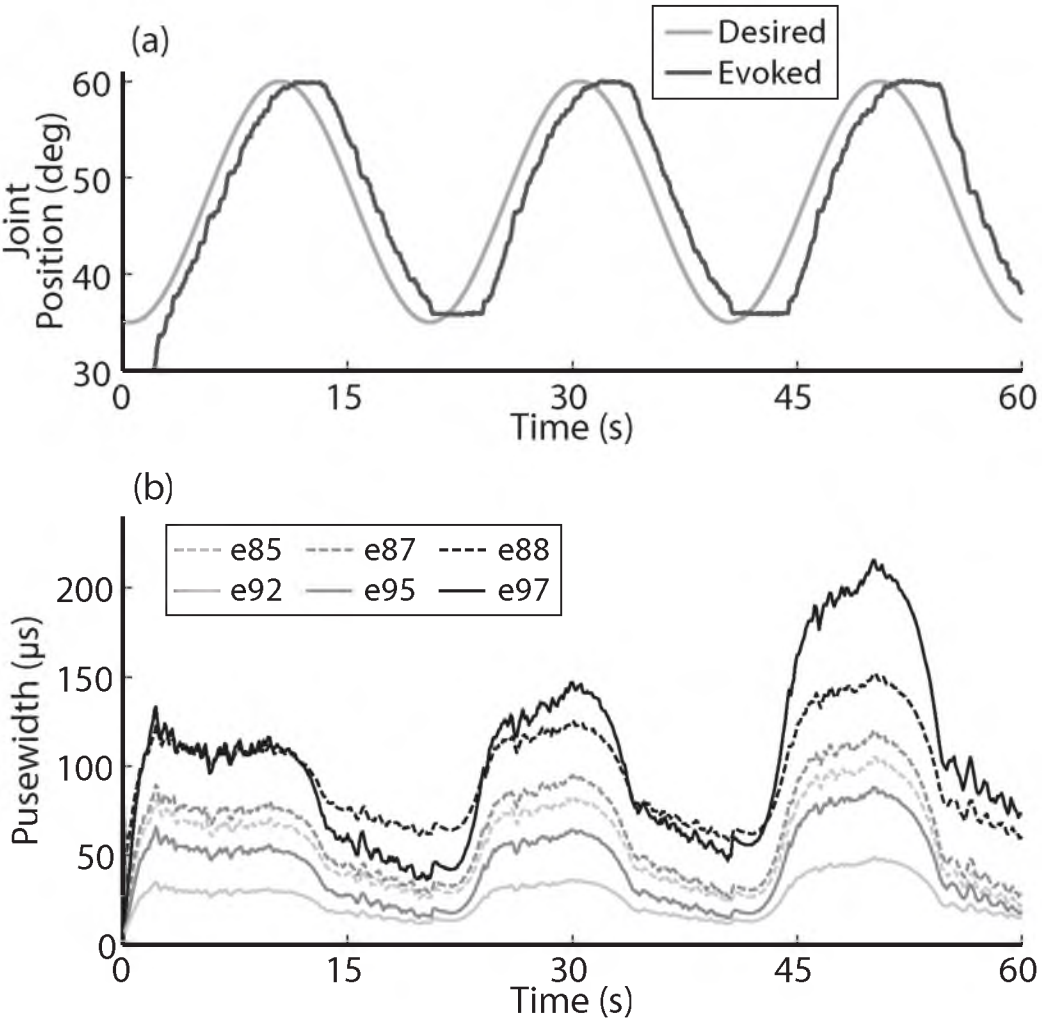

Figure 4.13: PIV-Controlled 0.05-Hz Sinusoidal Joint Motion.

The PIV closed-loop controller-evoked time-varying periodic joint trajectories. Results are shown for a 0.05-Hz joint-angle trajectory (a), along with the required stimulation pulsewidths for each utilized electrode (b). The controller was able to evoke accurate and smooth joint position trajectories for slower moving desired trajectories, with minimal time and phase delay ($T_d = 1.46$ s, $\Phi_d = 26.4$ deg.). During the descending phase, the controller was able to evoke smoothly graded eccentric motion, similar to desired ramp trajectories.

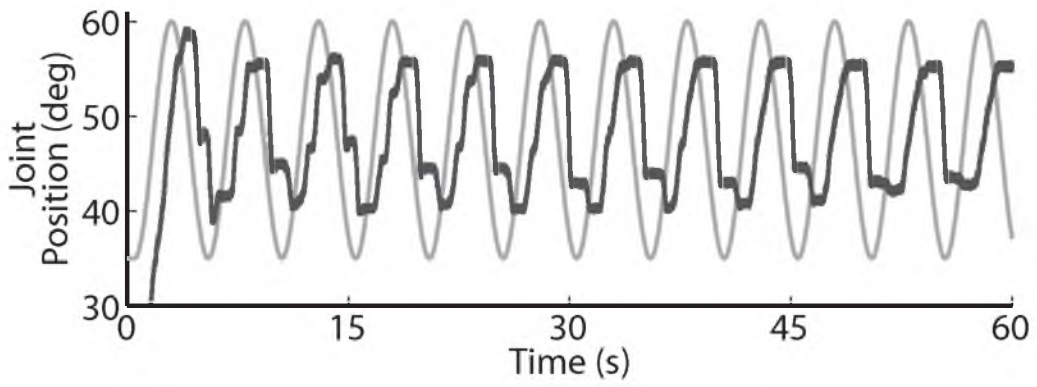

Figure 4.14: PIV-Controlled 0.2-Hz Sinusoidal Joint Motion.

For faster moving periodic trajectories, such as the 0.2-Hz sinusoid shown, the controller had difficulty evoking the desired amplitude and sinusoidal profile and the descending motion became more stepped.

muscle forces that are complicated by nonlinear dependencies of muscle force on muscle length and velocity. Because of these complexities, it was necessary to adapt the proportional-only controller used in [17] to the proportional-integral-velocity controller with integrator antiwindup used in this study. The set of desired trajectories were used to evaluate the controller but they also have real-world relevance, because lower-limb neuroprostheses will need to be able to robustly evoke controlled stances (ramped and stepped motion) and gait (periodic motion).

It is critically important for a clinically-viable FNS-based neuroprosthesis that the closed-loop controlled response be robust to a change in loading torque and/or desired motion, to be resistive to external disturbances and muscle fatigue, and to be consistent over time. With increased loading torque, the system required more muscle fibers to be activated to evoke enough joint torque to initiate motion. In terms of the PIV controller, this led to more integrator windup before enough stimulation was delivered to generate motion (Fig. 4.7), which can lead to large transient overshoot (Fig. 4.5). To reduce the overshoot, the integrator was made leaky, i.e., early acquired error values were dropped from the numerical error integration over time, in effect turning the integrator into a lag compensator (Fig. 4.6). This successfully reduced the transient overshoot while allowing early integration windup in the controller to recruit the necessary muscle fibers. The leaky integrator was also useful for evoking smooth time-varying joint trajectories (Fig. 4.12a, Fig. 4.13a). There will always be some delay in the closed-loop response because the controller is looking backwards in time, which would likely lead to large integrator windup and less smooth evoked motion.

The controller-evoked results were similar across different desired step sizes (Fig. 4.8), but the system was unable to achieve a 25-deg. to 100-deg. step although this is not outside the movement range for feline ankles [35]. This may be because of electrode limitations. The USEA was not characterized until after it was chronically implanted, and the few electrodes that selectively activated ankle plantar-flexion muscles were found to be only on the far two columns on the caudal side of the array. Because of this, only a small subset of approximately 10 electrodes was viable for

these experiments, as opposed to near 30 in prior studies, and these electrodes evoked lesser torques than seen in prior studies.

The controller was also able to handle externally applied disturbance torques (Fig. 4.9). When the disturbance torque was added, the controller was able to rapidly drive the system back to steady-state with near-zero overshoot. However, when the resistance torque was removed, the controlled response took longer to return to steady-state. The controlled results for a 30-deg. step remained consistent over 19 days without having to change the controller gains (Fig. 4.10). Such stable controller gains would reduce the need for daily controller tuning or rule-based control for specific motions.

Although aIFMS is fatigue-resistant [14, 18], all activated muscle fibers will eventually fatigue. The PIV-controller was successful in compensating for the fatigue of activated muscle fibers by rapidly increasing stimulation to recruit more muscle fibers and hold a desired joint position (Fig. 4.11). Eventually, all activated muscle fibers showed strong fatigue against the 0.4-Nm load and the controller was unable to recruit more muscle fibers after reaching maximal stimulation. This could create problems for continuous high-force generation during experimental sessions, and safety measures should be created that recognize increasing error even with rapidly increasing stimulation.

By using the velocity of the evoked joint-angle trajectory to create damping, as opposed to the derivative of the error which is often used [36], the controller avoided a large error derivative that occurs at the discontinuities in desired position for step trajectories. This strategy resulted in smoother evoked step-up motion. However, the large velocity gain did cause a more stepped downward motion, which was seen in many of the results. When there was a large negative error, e.g. during a step-down phase, the controller rapidly decreased the intensity of stimulation delivered via the USEA electrodes, attempting to allow rapid muscle fiber relaxation and descending motion. In response to this, because of the large velocity gain, and the fact that the integrator is turned off during descending motion, the controller attempted to dampen and slow this rapid descent by activating more muscle fibers, causing

the downward motion to manifest a stepped descending trajectory. This may be compensated for in future work by the addition of antagonist muscle control.

One of the major limitations of current clinical FNS-based prostheses is the inability to evoke graded muscle force due to their on/off nature [8]. This makes it difficult for a lower-limb prosthesis to smoothly control a sit-to-stand motion or the eccentric stand-to-sit motion, something a paralyzed individual will require in a lower-limb neuroprosthesis. Towards this goal, our real-time, PIV-controlled aIFMS system was successful in evoking smooth slow-moving, time-varying joint motions with low error and short time delay (Fig. 4.12a, Fig. 4.13a). However, the controller struggled to evoke more rapidly changing desired positions (Fig. 4.12b, Fig. 4.14). In earlier studies using proportional-only control of isometric forces [17], we were able to evoke faster time-varying trajectories up to 2.0 Hz with shorter time delays, but only after increasing and tuning the proportional controller gain. This study was designed to evaluate the PIV controller-evoked responses using only one set of tuned controller gains. It may be possible to evoke higher frequency sinusoidal trajectories with more accuracy and less delay with different PIV controller gains, but this would likely require substantial time to tune for each desired frequency. This is an area that will need to be addressed with future controller designs considering that other researchers have been able to generate up to 0.8-Hz FNS-controlled feline walking [37] and because normal human movement can often have components as fast as 2 Hz [34] with reaction time delays of approximately 200 ms [38].

The closed-loop controller was successful in evoking desired joint motion trajectories, but improvements to the closed-loop response may be achievable by using more sophisticated nonlinear, adaptive, and optimal control strategies, which have been extensively studied for SISO control of FNS-based motor neuroprostheses [39, 40, 41, 42]. Additionally, adding some predictive feedforward control [43, 44, 45] would likely reduce the inherent time delay of the controller, especially for ballistic motion such as during rapid changes in desired position. Although this study investigated real-time control of the per-electrode aIFMS stimulus intensities using a fixed stimulation frequency with fixed interelectrode phasing, it may be possible to improve the evoked responses by adding control over the stimulation frequency

and interelectrode phasing. Because the controller is only able to add unidirectional force, descending motion of the joint is solely dependent on controlling the number of muscle fibers that are allowed to relax and their time-dependent dynamics. Using controlled antagonistic muscles would likely improve the evoked descending motion, but the amount of agonist/antagonist co-contraction would require additional control methodology. All of these improvements will be investigated in future experiments designed for more complex multiple muscle and multiple joint control.

The experiments were conducted 3.5 and 4 months after implantation of the USEA in the sciatic nerve and the same six electrodes were utilized during both experimental sessions. This is an important outcome of these experiments that confirms and extends the successful chronic use of USEAs for stimulation and recording [17, 18, 27, 46]. The ability to have consistently stable electrodes will help minimize the need for continual controller tuning and initialization, which will be important in a clinical application.

Conclusion

This paper demonstrated the first successful closed-loop limb position control using aIFMS delivered via a chronically implanted USEA. The approach presented in the paper, and experiments validating it, represent an important step towards creating the next generation of clinically viable, fatigue-resistant, controlled FNS-based neuroprostheses to aid and restore lost motor function in persons with paralysis.

References

[1] "Spinal cord injury facts and figures at a glance," National Spinal Cord Injury Statistical Center, Tech. Rep., 2012.

[2] K. D. Anderson, "Targeting recovery: Priorities of the spinal cord-injured population," *Journal of Neurotrauma*, vol. 21, no. 10, pp. 1371–1383, Jan. 2004.

[3] D. Prodanov, E. Marani, and J. Holsheimer, "Functional electrical stimulation for sensory and motor functions: Progress and problems," *Biomedical Reviews*, vol. 14, pp. 23–50, 2003.

[4] X. Navarro, T. B. Krueger, N. Lago, S. Micera, T. Stieglitz, and P. Dario, "A critical review of interfaces with the peripheral nervous system for the control of neuroprostheses and hybrid bionic systems," *Journal of the Peripheral Nervous System*, vol. 10, no. 3, pp. 229–258, Sep. 2005.

[5] M. R. Popovic, T. Keller, I. P. I. Pappas, V. Dietz, and M. Morari, "Surface-stimulation technology for grasping and walking neuroprosthesis," *IEEE Engineering in Medicine and Biology Magazine*, vol. 20, no. 1, pp. 82–93, Jan.-Feb. 2001.

[6] R. Brissot, P. Gallien, M.-P. Le Bot, A. Beaubras, e. D. Laisn, J. Beillot, and J. Dassonville, "Clinical experience with functional electrical stimulation-assisted gait with parastep in spinal cord injured patients," *Spine*, vol. 25, no. 4, 2000.

[7] J. T. Mortimer, "Motor prostheses," *Comprehensive Physiology*, pp. 155–187, 1981.

[8] N. Bhadra and P. H. Peckham, "Peripheral nerve stimulation for restoration of motor function," *Journal of Clinical Neurophysiology*, vol. 14, no. 5, 1997.

[9] A. Branner, R. B. Stein, and R. A. Normann, "Selective stimulation of cat sciatic nerve using an array of varying-length microelectrodes," *Journal of Neurophysiology*, vol. 85, no. 4, pp. 1585–1594, Apr. 2001.

[10] B. R. Dowden, A. M. Wilder, S. D. Hiatt, R. A. Normann, N. A. Brown, and G. A. Clark, "Selective and graded recruitment of cat hamstring muscles with intrafascicular stimulation," *IEEE Transactions on Neural Systems and Rehabilitation Engineering*, vol. 17, no. 6, pp. 545–552, Dec. 2009.

[11] P. M. H. Rack and D. R. Westbury, "The effect of length and stimulus rate on tension in the isometric cat soleus muscle," *The Journal of Physiology*, vol. 204, no. 2, pp. 443–460, Oct. 1969.

[12] T. I. H. Brown, Y. Huang, D. L. Morgan, U. Proske, and A. Wise, "A new strategy for controlling the level of activation in artificially stimulated muscle," *IEEE Transactions on Rehabilitation Engineering*, vol. 7, no. 2, pp. 167–173, 1999.

[13] S. Cooper and J. C. Eccles, "The isometric responses of mammalian muscles," *The Journal of Physiology*, vol. 69, no. 4, pp. 377–385, 1930.

[14] D. McDonnall, G. Clark, and R. A. Normann, "Interleaved, multisite electrical stimulation of cat sciatic nerve produces fatigue-resistant, ripple-free motor responses," *IEEE Transactions on Neural Systems and Rehabilitation Engineering*, vol. 12, no. 2, pp. 208–215, Jun. 2004.

[15] A. K. Wise, D. L. Morgan, J. E. Gregory, and U. Proske, "Fatigue in mammalian skeletal muscle stimulated under computer control," *Journal of Applied Physiology*, vol. 90, no. 1, pp. 189–197, Jan. 2001.

[16] K. Yoshida and K. Horch, "Reduced fatigue in electrically stimulated muscle using dual channel intrafascicular electrodes with interleaved stimulation," *Annual Review of Biomedical Engineering*, vol. 21, pp. 709–714, Nov. 1993.

[17] M. A. Frankel, B. R. Dowden, V. J. Mathews, R. A. Normann, G. A. Clark, and S. G. Meek, "Multiple-input single-output closed-loop isometric force control using asynchronous intrafascicular multi-electrode stimulation," *IEEE Transactions on Neural Systems and Rehabilitation Engineering*, vol. 19, no. 3, pp. 325–332, Jun. 2011.

[18] R. A. Normann, B. R. Dowden, M. A. Frankel, A. M. Wilder, S. D. Hiatt, N. M. Ledbetter, D. A. Warren, and G. A. Clark, "Coordinated, multi-joint, fatigue-resistant feline stance produced with intrafascicular hind limb nerve stimulation," *Journal of Neural Engineering*, vol. 9, no. 2, p. 026019, 2012.

[19] J. Bobet, R. B. Stein, and M. N. Oguztoreli, "A linear time-varying model of force generation in skeletal muscle," *IEEE Transactions on Biomedical Engineering*, vol. 40, no. 10, pp. 1000–1006, Oct. 1993.

[20] M. Ferrarin and A. Pedotti, "The relationship between electrical stimulus and joint torque: a dynamic model," *IEEE Transactions on Rehabilitation Engineering*, vol. 8, no. 3, pp. 342–352, Sep. 2000.

[21] R. Riener, J. Quintern, and G. Schmidt, "Biomechanical model of the human knee evaluated by neuromuscular stimulation," *Journal of Biomechanics*, vol. 29, no. 9, pp. 1157–1167, Sep. 1996.

[22] T. Schauer, O. Negard, F. Previdi, K. J. Hunt, M. H. Fraser, E. Ferchland, and J. Raisch, "Online identification and nonlinear control of the electrically stimulated quadriceps muscle," *Control Engineering Practice*, vol. 13, pp. 1207–1219, Sep. 2005.

[23] F. E. Zajac, "Muscle and tendon: properties, models, scaling, and application to biomechanics and motor control," *CRC Critical Reviews in Bioengineering*, vol. 17, no. 4, pp. 359–411, 1989.

[24] F. Parmiggiani and R. B. Stein, "Nonlinear summation of contractions in cat muscles," *Journal of General Physiology*, vol. 78, no. 3, pp. 277–311, Sep. 1981.

[25] D. A. Gordon, R. M. Enoka, and D. G. Stuart, "Motor-unit force potentiation in adult cats during a standard fatigue test," *The Journal of Physiology*, vol. 421, pp. 569–582, Feb. 1990.

[26] Y. Giat, J. Mizrahi, and M. Levy, "A musculotendon model of the fatigue profiles of paralyzed quadriceps muscle under fes," *IEEE Transactions on Biomedical Engineering*, vol. 40, no. 7, pp. 664–674, Jul. 1993.

[27] A. Branner, R. B. Stein, E. Fernandez, Y. Aoyagi, and R. A. Normann, "Long-term stimulation and recording with a penetrating microelectrode array in cat sciatic nerve," *IEEE Transactions on Biomedical Engineering*, vol. 51, no. 1, pp. 146–157, Jan. 2004.

[28] P. J. Rousche and R. A. Normann, "A method for pneumatically inserting an array of penetrating electrodes into cortical tissue," *Annals of Biomedical Engineering*, vol. 20, pp. 413–422, Jul. 1992.

[29] R. A. Normann, D. McDonnall, G. A. Clark, R. B. Stein, and A. Branner, "Physiological activation of the hind limb muscles of the anesthetized cat using the utah slanted electrode array," *Proceedings of the 2005 IEEE IJCNN*, vol. 5, pp. 3101–3108, Aug. 2005.

[30] S. D. Hiatt, A. M. Wilder, K. S. Guillory, B. R. Dowden, R. A. Normann, and G. A. Clark, "1100-channel neural stimulator for functional electrical stimulation using high-electrode-count neural interfaces," *Proceedings of IFESS 2010 in Artificial Organs*, vol. 34, no. 8, Aug. 2010.

[31] B. R. Dowden, M. A. Frankel, R. A. Normann, and G. A. Clark, "Non-invasive method for selection of electrodes and stimulus parameters for fes applications with intrafascicular arrays," *Journal of Neural Engineering*, vol. 9, no. 1, p. 016006, 2012.

[32] A. M. Wilder, S. D. Hiatt, B. R. Dowden, N. A. T. Brown, R. A. Normann, and G. A. Clark, "Automated stimulus-response mapping of high-electrode-count neural implants," *IEEE Transactions on Neural Systems and Rehabilitation Engineering*, vol. 17, no. 5, pp. 504–511, Aug. 2009.

[33] R. I. Close and A. R. Luff, "Dynamic properties of inferior rectus muscle of the rat," *The Journal of Physiology*, vol. 236, pp. 259–270, Jan. 1974.

[34] M. P. Murray, "Gait as a pattern of movement," *American Journal of Physical Medicine and Rehabilitation*, vol. 46, no. 1, pp. 290–333, Feb. 1976.

[35] L. N. MacFadden, "Musculoskeletal modeling for intrafascicular multielectrode stimulation of the feline hindlimb," Ph.D. dissertation, University of Utah, Salt Lake City, 2009.

[36] N. S. Nise, *Control systems engineering*, 4th ed. New York, NY: J. Wiley & Sons, 2004.

[37] K. A. Mazurek, B. J. Holinski, D. G. Everaert, R. B. Stein, R. Etienne-Cummings, and V. K. Mushahwar, "Feed forward and feedback control for over-ground locomotion in anaesthetized cats," *Journal of Neural Engineering*, vol. 9, no. 2, p. 026003, 2012.

[38] A. T. Welford, *Reaction times*. New York, NY: Academic Press, 1980.

[39] H. J. Chizeck, P. E. Crago, and L. S. Kofman, "Robust closed-loop control of isometric muscle force using pulsewidth modulation," *IEEE Transactions on Biomedical Engineering*, vol. 35, no. 7, pp. 510–517, Jul. 1988.

[40] S. Jezernik, R. G. V. Wassinik, and T. Keller, "Sliding mode closed-loop control of fes: controlling the shank movement," *IEEE Transactions on Biomedical Engineering*, vol. 51, no. 2, pp. 263–272, Feb. 2004.

[41] V. Nekoukar and A. Erfanian, "Adaptive terminal sliding mode control of ankle movement using functional electrical stimulation of agonist-antagonist muscles," *Proceedings of IEEE EMBS 2010, Beunos Aires, Argentina*, pp. 5448–5451, 2010.

[42] P. H. Veltink, H. J. Chizeck, P. E. Crago, and A. El-Bialy, "Nonlinear joint angle control for artificially stimulated muscle," *IEEE Transactions on Biomedical Engineering*, vol. 39, no. 4, pp. 368–380, Apr. 1992.

[43] J. J. Abbas and R. J. Triolo, "Experimental evaluation of an adaptive feedforward controller for use in functional neuromuscular stimulation systems," *IEEE Transactions on Rehabilitation Engineering*, vol. 5, no. 1, pp. 12–22, Mar. 1997.

[44] P. E. Crago, N. Lan, P. H. Veltink, J. J. Abbas, and C. Kantor, "New control strategies for neuroprosthetic systems," *Journal of Rehabilitation Research and Development*, vol. 33, no. 2, pp. 158–172, Apr. 1996.

[45] M. A. Frankel, G. A. Clark, S. G. Meek, R. A. Normann, and V. J. Mathews, "Adaptive parameter selection for asynchronous intrafascicular multi-electrode stimulation," *Proceedings of the 2012 IEEE International Conference on Acoustics, Speech and Signal Processing*, pp. 753–756, 2012.

[46] G. A. Clark, N. M. Ledbetter, D. J. Warren, and R. R. Harrison, "Recording sensory and motor information from peripheral nerves with utah slanted electrode arrays," *Proceedings of the 2011 IEEE EMBS*, pp. 4641–4644, 2011.

CHAPTER 5

CONCLUSION

Although there are FNS devices in clinical use that can evoke upper limb grasping and lower limb standing and walking in paralyzed individuals, the movements that are evoked are ungraceful, poorly coordinated, may require significant secondary physical efforts, and are often terminated quickly due to rapid muscle fatigue [1, 2, 3]. Advanced FNS methods, such as the aIFMS used throughout this research, provide new capabilities to evoke very selective, graded, and fatigue-resistant muscle forces in chronic animal experiments that are expected to translate well to human clinical studies in the near future [4, 5, 6, 7]. Controlling the parameters of aIFMS, i.e., the per-electrode stimulus intensities and the interelectrode stimulus phasing, presents unique challenges that were addressed by the research within this dissertation. There were numerous successful outcomes of this research, but there were also limitations to each approach that will need to be addressed in future studies.

Summary of Major Research Findings

In Chapter 2, we developed a linear model of aIFMS isometric force generation using twitch-force recruitment curves and characteristic twitch-force response kinetics. The time-varying aspect of the model was the twitch amplitude and time of stimulation, and a gradient descent adaptive algorithm was employed to determine these stimulation parameters to evoke time-varying isometric force trajectories. A variety of isometric force trajectories ranging from steps, to sinusoids, to more-complex time-varying forces were successfully evoked for short time periods in simulation, and then in animal experiments using stimulation parameters determined from simulation.

In Chapter 3, we designed a novel methodology for determining an appropriate error signal for use in a real-time closed-loop feedback controller for determining the per-electrode stimulus intensities of aIFMS using fixed interelectrode stimulus phas-

ing. Instead of using the error right before adjusting the output stimulus intensities, as is often done in robotic motor control, the controller looks back in time to a point when the peak response is expected for each individual stimulation. The controller used this point in time to determine the error for each individual stimulation and then used that error to proportionally adjust the following cycle's stimulation intensity for the associated electrode. This was all accomplished in real-time. A variety of isometric force trajectories ranging from steps, sinusoids, and more complex time-varying forces were successfully evoked with good response characteristics even in the presence of nonlinear system dynamics, such as potentiation and fatigue.

In Chapter 4, we built on the success of the research in Chapter 3 and adapted the real-time controller to use joint-angle feedback to control ankle position against an imposed joint torque. Dynamic nonisometric muscle forces have additional complexities such as the muscle force dependence on muscle length and velocity [8]. Thus, it proved necessary to extend the proportional-only controller used in Chapter 3 to a proportional-plus-integral-plus-velocity (PIV) controller. Tuning the PIV controller was done using a desired step response in joint position and evoked response improvements were created by altering the integrator. Overshoot associated with integrator windup was reduced by making the integrator numerically leaky, in effect turning it into a lag compensator. Because decreases in joint position were achieved solely by the relaxation of muscle fibers, removing the integrator during decreasing motion helped to reduce oscillations. The PIV controlled response, using initially tuned PIV controller gains, was consistent across changes in step size and changes in joint loading torque, robust to external disturbance torques, and stable over time during an experimental session and across experimental days. The PIV controller was also successful in smoothly evoking concentric ramp-up and eccentric ramp-down trajectories, as well as slow moving sinusoidal motion.

Limitations

During the research conducted in Chapter 2, it proved necessary to add an additional gain factor when going from stimulus intensities determined in simulation to those used experimentally. This was likely due to the fact that the aIFMS

model assumed linear summation of the independently activated motor unit groups, although it has been well shown that contractions of multiple motor unit groups do not combine linearly [9]. Also, potentiation of overlapping motor units can lead to increases in force output [10], though these dynamics are not well modeled. The isometric forces were only evoked for very short time periods in this study. Although aIFMS is fatigue-resistant, it does not prevent the eventual fatigue of the electrically activated muscle fibers. The model used in this study did not account for fatigue, which would be necessary when evoking sustained forces over longer periods of time. The model also utilized a characteristic twitch waveform that was independent of the stimulus intensity. As stimulation levels are increased for each individual electrode, it becomes possible to activate motor unit groups of different types within a targeted muscle or even motor unit groups within a different unintended muscle, and the kinetics of the twitch response will change when motor unit groups of differing types are recruited. There was a substantial amount of time required to tune the adaptation gains for both stimulus intensity and timing, which could be alleviated by automating the gain tuning process.

Although the research in Chapter 3 presented the first closed-loop controller to determine aIFMS stimulus intensities in real-time, there were some limitations that could be improved in future studies. During desired steps in isometric force, the time from step onset to the peak evoked response was approximately 1.0 s, which may not be fast enough when ballistic changes in force are needed. Using the control methodology of Chapter 3 by itself will always lead to responses with inherent delay because the controller always looks one cycle of stimulation backward in time to determine an error signal. This delay could lead to system instabilities for faster moving time-varying desired forces. There was substantial time required to tune the proportional controller gain for each of the various desired isometric force trajectories, which may not be possible in a clinical FNS controller. This study used six electrodes at a 60-Hz composite stimulation frequency. The per-electrode frequency was low enough to be fatigue-resistant, but the 60-Hz composite frequency produced a near, but not fully, fused isometric response. By using more electrodes at the same 10-Hz per-electrode, but a faster composite frequency, a more ripple-free fused response

may be possible. The amount of ripple evoked in this study was due in part to the composite stimulation frequency, as well as the interelectrode phasing. The control method used in this study did not alter the initially determined interelectrode phasing. Closed-loop methods have been developed for reducing the ripple of desired static forces by changing the phasing of stimulation, but these methods rely on a fixed per-electrode stimulus intensity [11, 12]. Improvements to the system response may be achieved by incorporating more sophisticated control and these concepts are discussed in more detail in the Future Work section below.

The work presented in Chapter 4 demonstrated the first successful control of aIFMS to evoke precise limb motion; however, some motions were difficult to achieve. During the step-down phase of step responses, the integrator part of the controller is turned off and the two remaining parts of the controller work in opposition to each other in a manner that is not well timed. When the controller sees a rapid large negative error, such as during a desired step down in position, the proportional part of the controller greatly reduces the level of stimulation, allowing for the relaxation of numerous motor units. This fast falling motion is then in turn opposed by the velocity damping part of the controller which increases the level of stimulation to dampen, i.e., slow down, the rapid descent. This cause-effect type of control led to the more stepped downward motion seen in many of the results. The controller had substantial difficulty in evoking faster moving time-varying joint motions such as during rapid desired ramp and sinusoidal trajectories. The evoked joint motion began to have characteristics similar to those seen for desired step motions when the slope of the ramp trajectory increased to 16 deg/s and beyond. Although the controller was successful in evoking a slow-moving 0.05-Hz sinusoidal trajectory, the faster sinusoidal trajectories were difficult to achieve; the evoked responses were smaller than the desired magnitude and the evoked waveform became more stepped, again similar to step down responses. Unlike the results of Chapter 3, this study did not look at how the evoked responses changed if the PIV controller gains were altered after initial tuning. However, additional PIV tuning for each desired trajectory would be difficult in an experimental setting and would likely not be possible in a clinical FNS controller. Similar to Chapter 3, improvements to the system response may

be possible with more sophisticated control methods, which will be discussed in the Future Work section below.

Future Work

Controller Improvements

The closed-loop experiments used a linear P or PIV controller to determine the stimulus intensities of aIFMS in real-time. Although successful for evoking some isometric force and joint motion trajectories, a number of improvements can be made to the controller that will likely lead to improved responses. A variety of more sophisticated control methodologies could be used to improve these system responses, but detailed physiological modeling of aIFMS will be required. The most important part of this model would be the nonlinear summation of forces evoked from independent groups of motor units and how the level of axonal activation overlap affects that summation. Nonlinear controllers have seen recent success in single electrode FNS controllers [13, 14], but these systems use sliding mode controllers that often require fast system response characteristics that are not present when individual electrodes are stimulated at low per-electrode frequencies, such as during aIFMS. Other nonlinear control methods that rely on well modeled system dynamics, such as a backstepping controller [15], may be useful for aIFMS, and these control methods should be investigated when a good physiological model of aIFMS becomes available. Optimal control methods, such as gain scheduling [16], may be useful for different loading scenarios or faster moving limb movements.

Closed-loop methods that use only error feedback will always suffer from inherent system delays. Normal human motion uses very open-loop predicted force generation for the initial part of most motions and then uses visual and proprioceptive feedback for fine tuning. A number of FNS methods for single electrode stimulation use adaptive model systems to determine stimulation intensity in real-time [17, 18, 19], and some of these methods may be useful for aIFMS. The adaptive feedforward method of Chapter 2 could be altered for use in a real-time closed-loop system. The error between a desired and evoked position, determined by the methods described in Chapter 3 and 4, could be used to adapt the recruitment curve model for each

electrode. This adapted recruitment curve could then be used to predict a necessary stimulation level or stimulation timing to achieve the next desired joint position or muscle force. Inherent feedback controller delays could thus be mitigated by using a feedforward predictive term in the controller.

Human Comparisons

There needs to be a way to evaluate the quality of the controller-evoked responses as the control methods are continually improved. At the moment, we are only able to quantitatively analyze the controller results based on comparison to other controller results. We can say that overshoot is reduced by adding damping, and that steady-state error is reduced by adding integration. We cannot, however, say that we are performing well enough that the evoked motion is viable for clinical utility. The only human response metric that has been studied with reliability is reaction rate, which is approximately 300 ms for the average human [20]. We do not have good control metrics for simple movements that could be used to evaluate stance, such as what would be an acceptable or desired rise time, settling time, overshoot, etc., or to evaluate gait, such as how accurate does tracking need to be before the movement becomes unstable. Having these metrics could prove useful for deciding when a controller is performing poorly, adequately, or above desired specifications.

Toward this goal, some very preliminary work has been done that used the controlled torque loading device created during the research presented in Chapter 4. Seated subjects were asked to push the foot plate with two fingers against an applied torque, similar to the study of Chapter 4. a desired position and the measured position of the foot plate were shown on a nearby oscilloscope as two traces of different color. At a random point in time, the desired position trace began to follow either a stepped, ramped, or complex periodic trajectory. The subjects were asked to push (rotate) the foot plate and track the desired position trajectory in real-time. The results of the human subjects were compared against the controller-evoked responses shown in Chapter 4.

The time from step onset to when the initial response occurred, i.e., the reaction time, was similar between the controller-evoked responses and the responses of the

human subjects, as shown in Fig. 5.1. However, it did take longer for the controller-evoked response to settle for both the desired step up and step down trajectories. For a desired ramp in position, the smoothness of the controller-evoked response was similar to the human subjects, but there was a larger delay, as shown in Fig. 5.2. This can be attributed to the fact that the human subjects knew that there were only three possible trajectory types, and they were able to quickly realize that it was a ramped trajectory. Using this knowledge, they rapidly caught up with the desired trajectory and were then able to track it with much less delay than the controller-evoked response. This prediction was also visible for the complex periodic trajectory, as shown in Fig. 5.3. The subjects that tried harder to predict the desired position had less delay in their response, but substantially more error when they overshot the peaks or valley in the desired response.

These preliminary results suggest at some very important outcomes, although the methodology of how to do these experiments can be greatly improved. First, our controller-evoked step responses were not dramatically different from what a normal human can do, especially when looking at reaction rates. Second, as expected, humans clearly use a large feedforward predictive component in their movement and this should be strongly considered for future FNS controller designs.

In conclusion, the novel aIFMS control methods presented in this dissertation provide a foundation for developing robust FNS control methods that will be used in the next generation of neuroprostheses. These FNS-based neuroprostheses will be able to evoke coordinated and sustained movements using paralyzed muscles, such as for grasping, reaching, stance, and gait. This will improve paralyzed individuals mental and physical health, as well as returning autonomy to them for simple tasks like drinking a beer in the evening, taking off one's clothes, and getting in bed for the night.

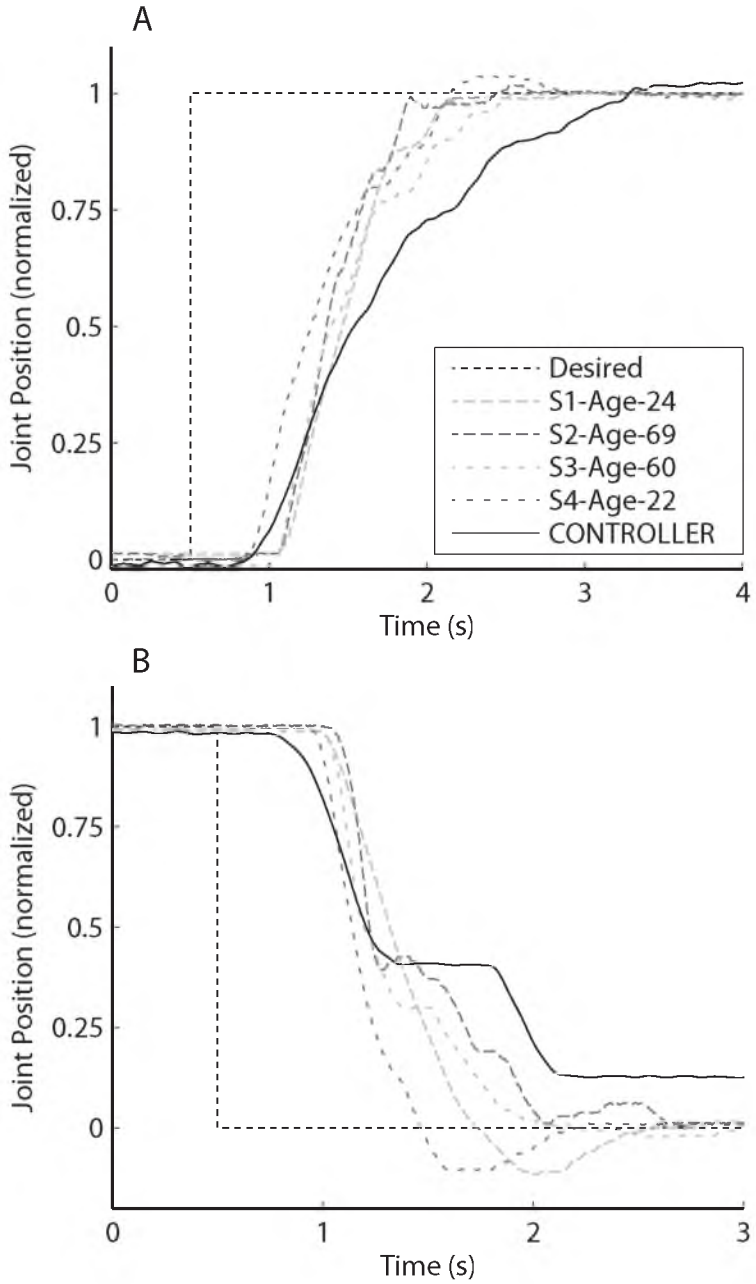

Figure 5.1: Human Comparison - Steps in Position.

A comparison of human performance and controller-evoked motion for desired positive steps in position (A) and desired negative steps in position (B). The controller-evoked response was similar to human performance in initial response delay, but there was more time required for the controller-evoked response to settle.

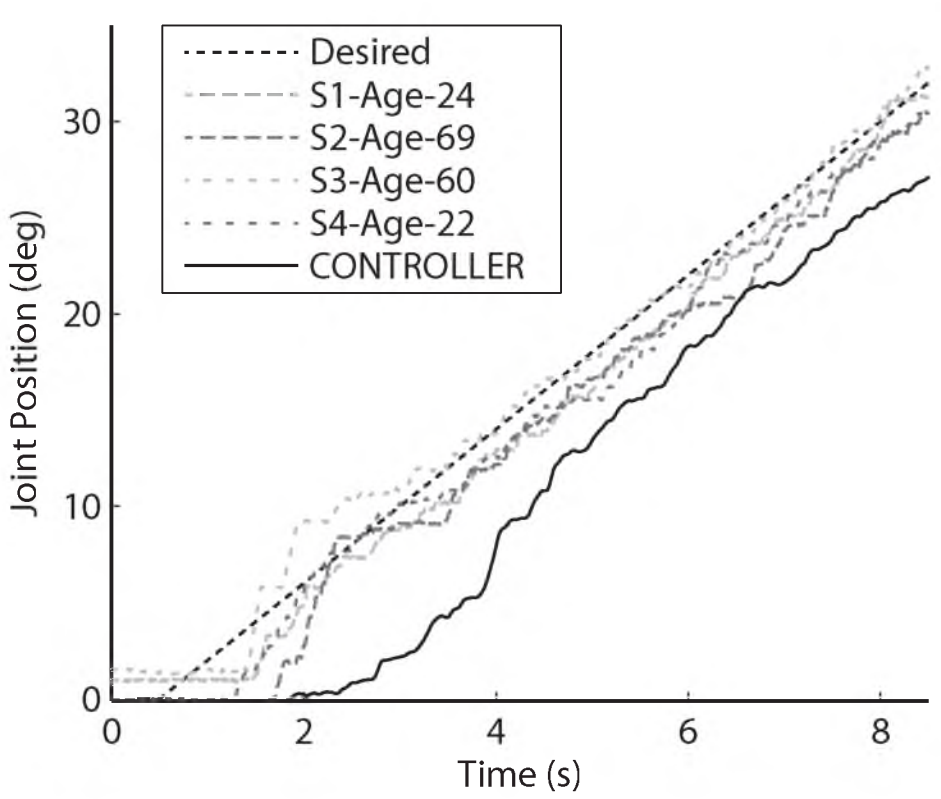

Figure 5.2: Human Comparison - Ramps in Position.

A comparison of human performance and controller-evoked motion for desired ramps in joint position. The smoothness of controller-evoked response was similar to human performance but there was a larger delay.

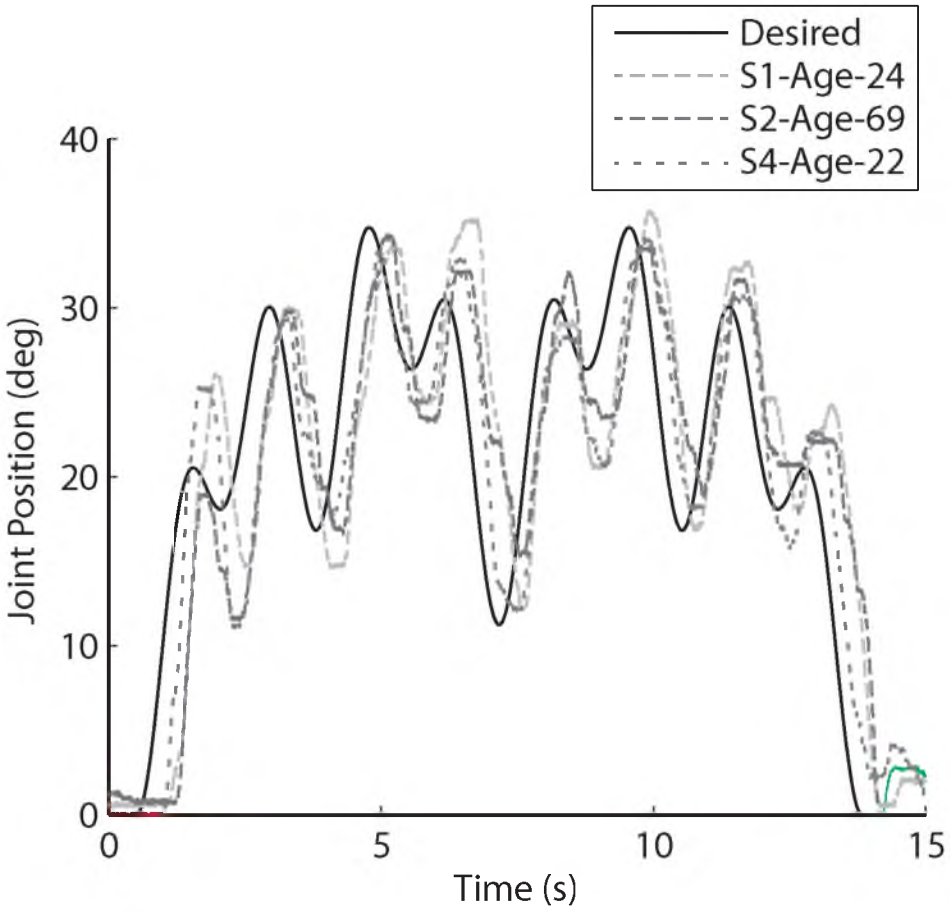

Figure 5.3: Human Comparison - Complex Periodic Motion.

A comparison of three human subjects for a desired complex periodic trajectory. The subjects that attempted to predict the motion have less delay time, but substantially more error.

References

[1] N. Bhadra and P. H. Peckham, "Peripheral nerve stimulation for restoration of motor function," *Journal of Clinical Neurophysiology*, vol. 14, no. 5, 1997.

[2] K. J. Klose, P. L. Jacobs, J. G. Broton, R. S. Guest, B. M. Needham-Shropshire, N. Lebwohl, M. S. Nash, and B. A. Green, "Evaluation of a training program for persons with sci paraplegia using the parastep1 ambulation system: Part 1. ambulation performance and anthropometric measures," *Archives of Physical Medicine and Rehabilitation*, vol. 78, no. 8, pp. 789–793, 1997.

[3] D. Popovic, A. Stojanovic, A. Pjanovic, S. Radosavljevic, M. Popovic, S. Jovic, and D. Vulovic, "Clinical evaluation of the bionic glove," *Archives of Physical Medicine and Rehabilitation*, vol. 80, no. 3, pp. 299–304, 1999.

[4] A. Branner, R. B. Stein, E. Fernandez, Y. Aoyagi, and R. A. Normann, "Long-term stimulation and recording with a penetrating microelectrode array in cat sciatic nerve," *IEEE Transactions on Biomedical Engineering*, vol. 51, no. 1, pp. 146–157, Jan. 2004.

[5] A. Branner, R. B. Stein, and R. A. Normann, "Selective stimulation of cat sciatic nerve using an array of varying-length microelectrodes," *Journal of Neurophysiology*, vol. 85, no. 4, pp. 1585–1594, Apr. 2001.

[6] D. McDonnall, G. Clark, and R. A. Normann, "Interleaved, multisite electrical stimulation of cat sciatic nerve produces fatigue-resistant, ripple-free motor responses," *IEEE Transactions on Neural Systems and Rehabilitation Engineering*, vol. 12, no. 2, pp. 208–215, Jun. 2004.

[7] R. A. Normann, B. R. Dowden, M. A. Frankel, A. M. Wilder, S. D. Hiatt, N. M. Ledbetter, D. A. Warren, and G. A. Clark, "Coordinated, multi-joint, fatigue-resistant feline stance produced with intrafascicular hind limb nerve stimulation," *Journal of Neural Engineering*, vol. 9, no. 2, p. 026019, 2012.

[8] W. K. Durfee and K. I. Palmer, "Estimation of force-activation, force-length, and force-velocity properties in isolated, electrically stimulated muscle," *IEEE Transactions on Biomedical Engineering*, vol. 41, no. 3, pp. 205–216, Mar. 1994.

[9] F. Parmiggiani and R. B. Stein, "Nonlinear summation of contractions in cat muscles," *Journal of General Physiology*, vol. 78, no. 3, pp. 277–311, Sep. 1981.

[10] D. A. Gordon, R. M. Enoka, and D. G. Stuart, "Motor-unit force potentiation in adult cats during a standard fatigue test," *The Journal of Physiology*, vol. 421, pp. 569–582, Feb. 1990.

[11] A. M. Wilder, R. A. Normann, and G. A. Clark, "Optimization of a tremor-reducing algorithm for asynchronous stimulation of independent motor-unit groups," *Proceedings of IFESS 2010 in Artificial Organs*, vol. 34, no. 8, Aug. 2010.

[12] A. K. Wise, D. L. Morgan, J. E. Gregory, and U. Proske, "Fatigue in mammalian skeletal muscle stimulated under computer control," *Journal of Applied Physiology*, vol. 90, no. 1, pp. 189–197, Jan. 2001.

[13] S. Jezernik, R. G. V. Wassinik, and T. Keller, "Sliding mode closed-loop control of fes: controlling the shank movement," *IEEE Transactions on Biomedical Engineering*, vol. 51, no. 2, pp. 263–272, Feb. 2004.

[14] V. Nekoukar and A. Erfanian, "Adaptive terminal sliding mode control of ankle movement using functional electrical stimulation of agonist-antagonist muscles," *Proceedings of IEEE EMBS 2010, Beunos Aires, Argentina*, pp. 5448–5451, 2010.

[15] J. Slotine and W. Li, *Applied nonlinear control*. Upper Saddle River, NJ: Prentice Hall, 2002.

[16] F. L. Lewis and V. L. Syrmos, *Optimal control*, 2nd ed. New York, NY: J. Wiley & Sons, 1995.

[17] J. J. Abbas and H. J. Chizeck, "Neural network control of functional neuromuscular stimulation systems: computer simulation studies," *IEEE Transactions on Biomedical Engineering*, vol. 42, no. 11, pp. 1117–1127, Nov. 1995.

[18] L. A. Bernotas, P. E. Crago, and H. J. Chizeck, "Adaptive control of electrically stimulated muscle," *IEEE Transactions on Biomedical Engineering*, vol. 34, no. 2, pp. 140–147, Feb. 1987.

[19] J. Riess and J. J. Abbas, "Adaptive control of cyclic movements as muscles fatigue using functional neuromuscular stimulation," *IEEE Transactions on Neural Systems and Rehabilitation Engineering*, vol. 9, no. 3, pp. 326–330, Sep. 2001.

[20] A. T. Welford, *Reaction times*. New York, NY: Academic Press, 1980.